PUBLICATIONS OF THE ASTRONOMICAL SOCIETY OF THE PACIFIC, **123**:288–332, 2011 March

IMACS: The Inamori-Magellan Areal Camera and Spectrograph on Magellan-Baade

ALAN DRESSLER,[1] BRUCE BIGELOW,[2] TYSON HARE,[1] BRIAN SUTIN,[3] IAN THOMPSON,[1] GREG BURLEY,[1] HARLAND EPPS,[2] AUGUSTUS OEMLER, JR.,[1] ALAN BAGISH,[1] CHRISTOPH BIRK,[1] KEN CLARDY,[1] STEVE GUNNELS,[4] DANIEL KELSON,[1] STEPHEN SHECTMAN,[1] AND DAVID OSIP[5]

Received 2010 November 4; accepted 2010 December 27; published 2011 February 28

ABSTRACT. The Inamori-Magellan Areal Camera and Spectrograph (IMACS) is a wide-field, multipurpose imaging spectrograph on the Magellan-Baade telescope at Las Campanas Observatory. IMACS has two channels—f/2 and f/4, each with an $8\text{K} \times 8\text{K}$ pixel mosaic of CCD detectors, that service the widest range of capabilities of any major spectrograph. These include wide-field imaging at two scales, $0.20''$ pixel^{-1} and $0.11''$ pixel^{-1}, single-object and multislit spectroscopy, integral-field spectroscopy with two $5'' \times 7''$ areas sampled at $0.20''$ pixel^{-1} (Durham IFU), a multiobject echelle (MOE) capable of $N \sim 10$ simultaneous full-wavelength $R \approx 20,000$ spectra, the Maryland-Magellan Tunable Filter (MMTF), and an image-slicing reformatter for dense-pack multislit work (GISMO). Spectral resolutions of $8 < R < 5000$ are available through a combination of prisms, grisms, and gratings, and most modes are instantly available in any given IMACS configuration. IMACS has a spectroscopic efficiency over 50% in f/2 multislit mode (instrument only) and, by the AΩ figure of merit (telescope primary surface area times instrument field of view), IMACS scores 5.7 m^2 deg^2, compared with 3.1 for VIMOS on VLT3 and with 2.0 for DEIMOS on Keck2. IMACS is the most versatile, and—for wide-field optical spectroscopy—the most powerful spectrograph on the planet.

Online material: color figures

1. INTRODUCTION

IMACS is a facility instrument of the Magellan-Baade 6.5 m Telescope at the Carnegie Institution's Las Campanas Observatory. It is an internally baffled, imaging spectrograph whose f/2 mode of all-transmissive optics delivers a field of almost $\frac{1}{2}^\circ$ diameter—the largest of its kind. Using the same collimator with an all-transmissive f/4 camera and reflection gratings produces a $\frac{1}{4}^\circ \times \frac{1}{4}^\circ$ field for higher-resolution imaging and spectroscopy. Bigelow and Dressler (2003) provides an abbreviated description of the design and construction IMACS, and its science capabilities and performance were reviewed in preliminary form in Dressler et al. (2006).

IMACS was designed at the Carnegie Observatories and constructed mainly at its shops, using a combination of private and public funds. The instrument was shipped to Chile and mounted on the Magellan-Baade 6.5 m telescope in 2003 August. Commissioning began in 2003 October; IMACS was phased into regular operation in 2004 January (Osip et al. 2004). IMACS became regularly available in 2004 April, and through 2010 August, it has been the most-used instrument on the Baade telescope, accounting for 67% of the nights available for astronomy. IMACS is available to members of the Magellan Consortium and their collaborators and to the full US astronomical community through the Telescope System Instrumentation Program (TSIP).

The purpose of this article is to provide a detailed description of IMACS and report its performance. The presentation is divided into two major sections, the first describing the elements, modes, operation, software, performance and applications of the instrument, the second describing the design, construction, and maintenance of the mechanical, electronic, optical, computer, and detector systems. In broad terms, the first section is aimed at astronomers and the second at engineers, with the customary overlap of those interests. Specifically, for the first section, § 2 is a brief history and basic description of IMACS, §§ 3 and 4

[1] Carnegie Observatories, 813 Santa Barbara Street, Pasadena, CA 91101-1292; dressler@obs.carnegiescience.edu, thare@obs.carnegiescience.edu, ian@obs.carnegiescience.edu, greg.burley@gmail.comoemler@obs.carnegiescience.edu, bagish@obs.carnegiescience.edu, birk@obs.carnegiescience.edu, clardy@obs.carnegiescience.edu, kelson@obs.carnegiescience.edu, shec@obs.carnegiescience.edu.

[2] UCO Lick Observatory, University of California, Santa Cruz, CA 95064; bigelow@ucolick.org, epps@ucolick.org.

[3] Hamilton Sundstrand Space Systems International 2771 North Garey Avenue, Pomona, CA; Brian.Sutin@hs.utc.com.

[4] Paragon Engineering, 2277 Joy Lane, Westcliffe, CO 81252; paragon_engineering@yahoo.com.

[5] Las Campanas Observatory, Carnegie Observatories, Casslla 601, La Serena, Chile; dosip@lco.cl.

provide a more detailed description, § 5 describes its multiple capabilities and modes, and § 6 analyzes the performance of IMACS as an imager and spectrograph in a variety of relevant aspects. For the second section, § 7 discusses in detail the design, fabrication, and assembly of IMACS at a system and subsystem level, followed by shorter descriptions of the mosaic CCD cameras in § 8, lab testing in § 9, and shipping, installation, and operation in § 10.

A complete IMACS User Manual is available on the World Wide Web[6] as part of full documentation and links to tools for using IMACS.[7]

Because these sites contain more detailed information specific to observing with IMACS than can be given here, this article contains numerous references to the IMACS User Manual or these tools. Our purpose here is to give information on the capabilities and unique features of IMACS and information that will be helpful to astronomers who are considering using IMACS for their programs and to engineers who are interested in the particular solutions that were found to difficult and sometimes unique challenges.

2. A BRIEF HISTORY AND DESCRIPTION OF IMACS

2.1. History

IMACS grew with the design of the first Magellan telescope, specifically the choice of the configuration for the secondary mirror and the ports at which instruments would be placed. In collaboration with the Steward Observatory of the University of Arizona, Carnegie chose a 6.5 m borosilicate mirror produced by the Steward Observatory Mirror Laboratory, one that matched the primary mirror for the MMT upgrade. This, in turn, suggested the adoption of its large f/5 secondary mirror for wide-field instruments at the Cassegrain focus. However, Carnegie astronomers were concerned that the swapping of instruments would be limited by the large baffles required for the f/5 focus, which were incompatible with sensitive infrared observations. Instead, the choice for the Baade telescope was an f/11 secondary at the Gregorian focus feeding a rotatable tertiary, just above the primary mirror, that would direct the beam to stations at two Nasmyth platforms and three auxiliary Nasmyth ports.[8] The idea for a wide-field spectrograph fed by the f/11 beam at the Nasmyth focus came from an optical design by Stephen Shectman for a refracting all-spherical ADC + corrector and collimator that would produce a 30′ diameter field with virtually no degradation of the FWHM $< 0.10''$ images expected for the telescope. In a sense, the Gregorian secondary and the wide-field corrector became the first elements in the wide-field spectrograph that was to become IMACS.

Field size was the primary driver of the ambitious f/2 camera, but this was far from the only goal in planning IMACS. This was to be not only the premier multiobject spectrograph but the primary low-to-medium dispersion optical spectrograph at the Observatory, even for single-object observations. It was therefore essential that IMACS be able to adequately sample the best images the Magellan telescopes produce, better than FWHM $\lesssim 0.30''$. Seeing of this quality is not common, but it is not rare either. This requirement led to a second channel of IMACS—the f/4 camera with its $0.11''$ pixel^{-1} scale. A wide range of dispersions, with multiple configurations, was considered essential, and an efficient way of acquiring single objects (without using the CCD detectors) was a high priority. The usual requirements—high spatial and spectral stability, high efficiency, and simplicity of operation were added to the mix. As the design developed, it also became clear that the telescope focal plane at the entrance to IMACS, and its 150 mm pupil, could be made easily accessible. Sufficient space allowed a number of additional capabilities, for example, a tunable filter and echelle mode in the pupil and an integral field unit (IFU) and small-field image reformatter at the telescope focus; these opportunities also drove many aspects of the final design. More detail on the design and fabrication of IMACS follows in §§ 7—10.

Figure 1 is a picture of IMACS mounted at the west Nasmyth platform of the Magellan-Baade telescope.

2.2. Basic Description

IMACS has two basic operating modes. A single 150 mm (6.0 inch) beam refractive collimator feeds either (1) an f/4

FIG. 1.—IMACS on the west Nasmyth platform of the Magellan-Baade telescope. Tyson Hare installs a multislit mask into the mask server (at the telescope focal surface). The spectrograph structure is covered by insulated aluminum panels with butted vinyl seals. The cable wrap is the black structure seen at the back.

[6] See http://www.lco.cl/telescopes-information/magellan/instruments/imacs/user-manual/the-imacs-user-manual.

[7] See http://www.lco.cl/telescopes-information/magellan/instruments/imacs/.

[8] An f/5 system equivalent to the one at MMT was eventually implemented at the Magellan-Clay telescope.

all-spherical refractive camera delivering $0.11''$ pixel^{-1}, or (2) a double-aspheric, oil-coupled multiplet f/2 refractive camera sampled at $0.20''$ pixel^{-1}. The detector for the f/2 focus is an $8\text{K} \times 8\text{K}$ mosaic of eight E2V $2\text{K} \times 4\text{K}$ 15 μm CCDs. The detector for the f/4 focus is an $8\text{K} \times 8\text{K}$ mosaic of eight SITe $2\text{K} \times 4\text{K}$ 15 μm CCDs, but replacement of the SITe CCDs by E2V CCDs will be accomplished in 2011. The cameras are dedicated to these foci, although interchangeable in an emergency.

The f/4 camera uses 154 mm reflecting gratings (presently six in number) to make spectroscopic observations at resolutions $R = 600$–5000 (resolutions are for 1.0 arcsec slit on blaze). Individual values are tabulated in the IMACS User Manual. The f/2 camera uses 154 mm grisms (presently four in number) to achieve resolutions of $R = 400$–1200 over the full $27'$ diameter field; there are also two prism modes $R \approx 8$–100 and $R \approx 25$–50, red to blue.

The f/4 camera was designed to deliver images of FWHM $\lesssim 0.20''$ over its $15' \times 15'$ field. It performs to design specifications and, in combination with the telescope optics and collimator, has delivered FWHM $\leq 0.45''$ images across the entire field, in excellent seeing of FWHM $\approx 0.30''$.

The f/2 camera was designed to deliver images of FWHM $\lesssim 0.40''$. It achieves this over more than 80% of its $27'$ diameter circular field, with a slow degradation to as much as FWHM $= 0.55''$ at the edge of top and bottom chords. In combination with the telescope the f/2 camera has delivered images of FWHM $= 0.40''$ for over half of the field, degrading to $0.60''$ FWHM at the extreme edge, in excellent seeing of FWHM $\approx 0.35''$.

IMACS was designed for, and is mostly used for, multislit spectroscopy. This occurs mainly in f/2 mode, using 30 inch diameter, spherical-shell, stainless steel slit masks into which hundreds, or even thousands, of small slits are cut with a commercial laser system. Slit masks are also used for echelle dispersion spectroscopy (MOE, described subsequently) in f/4 mode and the small-field reformatter GISMO (Gladders Image-Slicing Multislit Option), also operated at f/4, which uses its own slit masks, to target hundreds of stars or galaxies packed within an area approximately $4' \times 4'$.

IMACS spectroscopic capability also includes an IFU built by Durham University with two apertures of 1000 optical fibers each. Each aperture samples $5'' \times 7''$ in f/2 mode, or $4'' \times 5''$ at f/4, and can use the full range of dispersers for that camera.

Conventional imaging can be done at either focus with an extensive range of filters, including Bessel and Sloan filter sets and an assortment of narrowband filters. The Maryland-Magellan Tunable Filter (MMTF) is a Fabry-Perot etalon with a monochromatic spot diameter ranging from $7'$ to $11'$ over bandpasses tunable from 5 Å–15 Å. The filter is tunable over a range $5000 \text{ Å} < \lambda < 9200 \text{ Å}$, the actual wavelengths depending on blocking filters.

3. THE COMPONENTS OF IMACS

3.1. Two Optical Channels

Although IMACS has two optical channels, it is unlike classical double spectrographs that are divided into two separate wavelength regimes—IMACS is divided by imaging scales and spectral dispersions. Only one mode is used at a time, but both are kept at the ready, and the changeover is rapid. The all-spherical f/4.2 long camera fully (abbreviated f/4 in this article) illuminates a $15.4' \times 15.4'$ field at $0.11''$ per CCD pixel, sampling that is fine enough to exploit the best seeing conditions produced by the Baade telescope, $\sim 0.30''$ FWHM. For imaging and spectroscopy, the wavelength coverage is $3650 \text{ Å} < \lambda < 10,000 \text{ Å}$. The f/2.3 short camera (abbreviated f/2 in this article) delivers a straight-through reimaging mode with a $27.5'$ diameter field sampled at $0.20''$ pixel^{-1}—we believe this is the largest field of any direct-imaging spectrograph. The wavelength coverage of the f/2 camera is $3900 \text{ Å} < \lambda < 10,500 \text{ Å}$ and the scale is $0.20''$ pixel^{-1}, again matched to the CCD detectors for critical sampling.

The observer's choice of camera usually comes down to a matter of spatial and spectral resolution. The f/2 mode of IMACS covers a much greater area of sky, but critically samples only seeing FWHM $\gtrsim 0.40''$ and offers relatively low spectral dispersion, $R < 1200$. These characteristics are well suited to programs concerned with galaxy evolution or cosmology, for example. The f/4 mode covers a smaller field (but comparable with VIMOS and more than twice that of DEIMOS), but at a finer spatial scale that can take advantage of the best seeing the telescope can deliver. The f/4 offers a large range of spectral dispersions, up to the $R \approx 20,000$ echelle mode (MOE). These characteristics are well suited for stellar population work: for example, the stars in nearby dwarf galaxies or the Galactic bulge, or the globular clusters of galaxies of the local supercluster. Specific examples of science done in f/2 and f/4 modes are given in § 5.

3.2. Two 8K × 8K Mosaic CCD Cameras

Each optical channel has a dedicated mosaic CCD camera. The original Mosaic-1 at f/4 uses SITe CCDs; the more recently built Mosaic-2 uses E2V CCDs, which are significantly more sensitive, as shown in § 6.7. The Mosaic-1 camera reads out in 1×1 mode in 93 s at typical noise of 4–5 e^- pixel^{-1}. The Mosaic-2 camera reads out in about 80 s at typical noise of 3–4 e^- pixel^{-1}. Readouts in 2×2 pixel binning are several times faster, of course, and there is a SNAP 4×4 readout, frequently used in tests and setups, that returns the full array in ~ 25 s. A new Mosaic3 camera with E2V detector covering from blue to red with high quantum efficiency is under construction, through the support of the National Science Foundation (NSF) TSIP program. It will replace Mosaic-1 at the f/4 focus.

Figure 2 shows the format that each camera produces on the eight-chip detector array. The f/4 field fills the mosaic array. The

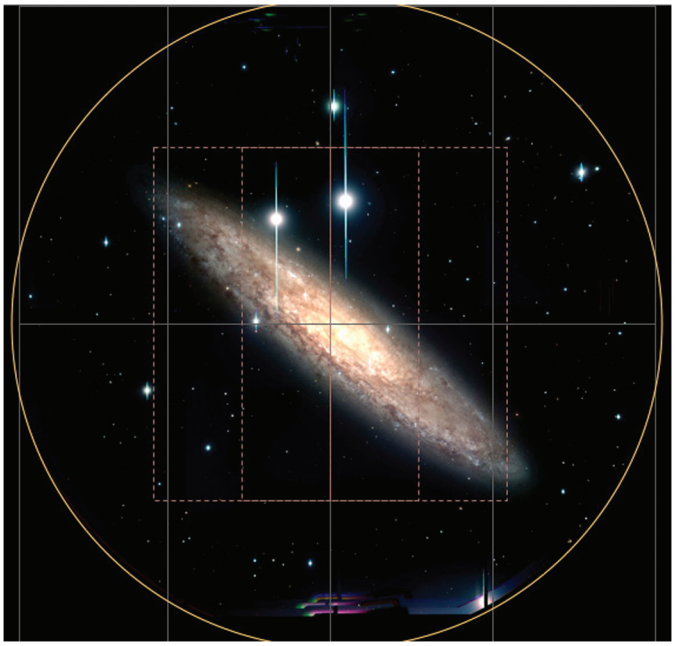

FIG. 2.—Illumination of the mosaic CCD array. The dashed lines shows the outline of the CCD mosaic in f/4 mode, with its fully illuminated $15.4' \times 15.4'$ field. The solid lines show the projection of the CCD mosaic in f/2, which measures 28′ across (including chip gaps). The outer circle is the full but partially vignetted field of 30′ diameter. This IMACS first light picture is a composite B, V, & R image of the galaxy NGC253.

f/2 field underfills the array: it becomes vignetted beyond the $R = 12'$ radius, amounting to 9% light loss at $R = 15'$. The light is baffled beyond this, so the corners of the mosaic are not illuminated (see the IMACS User Manual). The field area sampled by the f/2 camera is 670 arcmin^2 or 0.186° (656 arcmin^2 if the chip gaps are excluded).

Both CCD cameras are cooled by cryo-pumps and are kept continually at-the-ready.

3.3. IMACS Body Plan

Figure 3 is a schematic layout of IMACS, showing the placement of the optical elements and location of the major mechanical components.

Two large 2.5 m (100 inch) steel weldment wheels form the basic structure of IMACS—their rims are ground surfaces that are the bearing on which the instrument rotates, on self-steering rollers (see § 7). The forward wheel (toward the telescope) separates the front and middle compartments and is the mounting surface for the guiders, multislit-mask server, and calibration sources. The aft wheel separates the middle and back compartments and carries the optical bench on which the collimator and both cameras are mounted. The collimator and f/4 camera are contained in the center compartment, between the wheels, and the f/2 camera is housed in the third compartment, behind the aft wheel and in front of the cable wrap at the back end of the instrument. The three major optical elements—collimator, f/2 camera, and f/4 camera—are all mounted from a box (the main optics support structure [MOSS]—basically, the spectrograph) that attaches to the aft wheel. The shutter of each camera is mounted on the camera barrel, as is the part of the filter server that receives the filter. (The main mechanisms of the filter servers are attached to the MOSS as described in §§ 7.3.3 and 7.5.3.) The disperser server is attached to the aft wheel; however, a selected disperser element is transferred to the MOSS to disconnect it from the wheel and other structural elements.

Light from the telescope's tertiary mirror passes horizontally from the hole in Nasmyth rotator, entering the forward compartment, a cylinder approximately 2 m diameter and 0.6 m deep. This compartment is sealed from the telescope by an open/close hatch and from the rest of the instrument by the field lens, which is mounted in a hole in the forward wheel. From this point the slowly converging beam passes within a baffle to the first element of the collimator.

Removable, insulated aluminum panels edged with rubber C-moldings seal the instrument to dust, shield external light, and provide temperature stability with a time constant of approximately 12–24 hr.

3.4. Optomechanical Elements

The optomechanical elements of IMACS make it possible to carry out a very diverse program of observations during a single night, with numerous choices of slit masks, filters, and dispersers. Nevertheless, the graphical user interface (GUI) that controls these devices is simply arranged and easy for an observer to understand and control. The guiders provide signals that fine-tune the drives of the telescope (their traditional function), but they also provide data to trim the turning of the Nasmyth rotator and adjust the primary mirror supports, telescope alignment, and focus.

Commands to change the states of the mechanical functions are executed simultaneously, not sequentially, which significantly reduces reconfiguration time and encourages the observer to make as many changes as are necessary to execute the program carefully and thoroughly, with as little constraint as possible coming from IMACS itself.

3.4.1. The Mask Server

The mask server is jukebox-style: it has six slots for large, dish-shaped multislit masks mounted in hoop frames with squared-off wings, and it carries baffles for f/4 observing and for using the slit-viewing mode, described subsequently. When requested, the GISMO reformatting unit for dense-pack spectroscopy is installed in the mask server, taking up all six slots. The Durham IFU, when installed, takes up three slots.

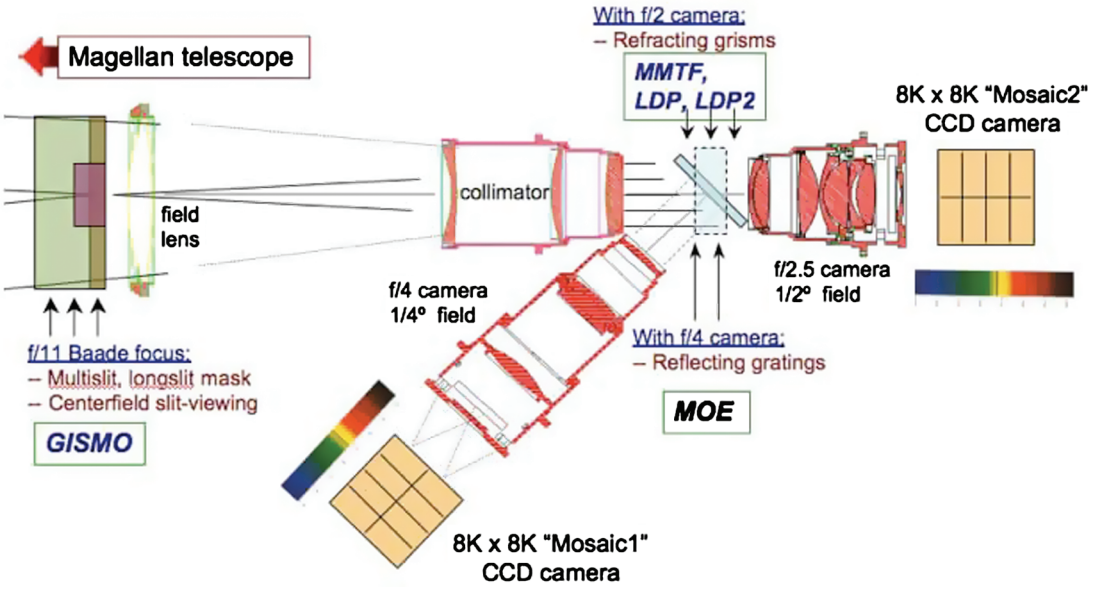

FIG. 3.—Optical and component layout of IMACS.

3.4.2. Guiders

Two of the three guiders sweep 40° arcs above and below the field. The principal guider images a star chosen from an arc segment ∼105″ wide, centered at a radius of 15′ from the field center. The Shack-Hartmann guider forms a pupil image of another similarly selected star, where multiple lenslets produce an array of images whose centroids are monitored continuously, through an observation, for the Shack-Hartmann test. This is used to adjust the primary mirror support system and collimation and focus, through motion of the secondary mirror.

The third guider, the center-field guider deploys to the center field, where it can be used to view in reflection the on-axis light of the telescope, used to acquire a set star to zero the telescope position. The center-field guider also includes a Shack-Hartmann unit that is operated on-axis, engaged by remotely swapping the optics in front of the detector.

The center-field guider includes a science function. It deploys a reflective mask (containing five slits of increasing width, each 17″ long, and a 7″ diameter hole) to a position close to the field center, where it can be used for simple single-object observations by acquiring the target in real-time direct viewing. Guiding can be accomplished by centering the light that falls outside the aperture, or—for long exposures—with a serendipitous star in the field.

The optics barrels for these cameras deliver images to standard 1024×1024 pixel frame-transfer E2V CCDs. The detector packages, built at Carnegie Observatories, send their output to the Magellan Telescope Control System (TCS) for processing. A field of $105'' \times 105''$ is accessed by each camera, at a scale of $\approx 0.20''$ per rebinned pixel.

The excellent stability and rigidity of the guiders in discussed in §§ 6.4 and 7.5.1.

3.4.3. Filters and Shutters

Just in front of the mosaic CCD cameras, the f/2 and f/4 cameras are each slotted to accept a shutter and filter server. The identical filter servers are jukebox-style with 15 positions for 165 mm × 165 mm filters, up to 12 mm thick. The basic complement of filters includes Bessel B, V, R, and CTIO-I and a panchromatic spectroscopic filter (necessary to equalize optical path length) for each camera, and one Sloan g, r, i, z set. Many wideband blocking filters, and several narrowband filters, are available as well—there are plenty of vacant positions for these or for user-provided filters. The design and construction of the filter servers is described in § 7.5.3. An inventory of present filters with transmission curves can be found online.[9]

The IMACS shutters are capable of short, accurate exposures. They are driven by linear motors, with closed-loop feedback. Each shutter has a pair of blades that alternatively open and close the exposure. Because the time trajectories of each blade are closely matched, exposures as short as 1.0 s have been shown to be accurate to better than 2% over the entire field. Design and construction of the shutters is described in § 7.4.5.

3.4.4. The Disperser Server

The largest and most complex IMACS component is the disperser server. This is a large chain-driven wheel that installs

[9] See http://www.lco.cl/telescopes-information/magellan/operations-homepage/instruments/IMACS/imacs-filters/imacs-filters-1.

gratings and grisms in the parallel beam delivered by the collimator. There are five locations for dispersers, an open aperture position for direct imaging with the f/2 camera, and an overcoated-silver mirror for f/4 imaging. Grating tilt mechanisms (GTMs) allow the observer to change the wavelength range remotely, and a GTM can be taken in and out without changing the grating angle. Tilt settings for gratings repeat to $\sim 0.01°$, which is typically a few angstroms. (Grisms and prisms have a fixed wavelength interval.) Swapping between units takes a minute or less. When reinstalled, the position of a grism unit typically repeats to the equivalent of a few pixels on the detector (they are transmissive elements), but shifts of 10–20 pixels are not uncommon for the much heavier GTM units. Holders for narrowband filters are provided—these perform better at the spectrograph pupil rather than the converging beam location of the filter servers. The MMTF (tunable filter) or MOE (echelle) can be mounted in place of one of the standard dispersers.

Configuration of the disperser wheel, the filter servers, and the mask server is carried out during the day, but the large selection of transposable elements, including the swap from f/2 to f/4, allows for very diverse programs to be executed during a single night.

3.5. Calibration Hardware

IMACS observations include imaging flat fields, spectroscopic flat fields, and arc-lamp exposures. The preferred method of taking all calibration exposures is to use the lamp-illuminated opaque screen that deploys in front of the Magellan-Baade secondary mirror. Because the Gregorian focus makes a pupil in front of the secondary, simple illumination of this surface fills the IMACS optics in the same way as light from infinity reflected off the primary and secondary mirrors. The available lamps include high- and low-level quartz-halogen (continuum), He, Ne, and Ar. Some observers also choose to make twilight flats or dark-sky superflats to match and remove the fringes in far-red imaging exposures. As part of the same package, but viewed directly (instead of illuminating the screen), is a thorium lamp used for the high-dispersion echelle mode.

IMACS includes internal calibration sources in its forward compartment, which reflect off of the backside of the instrument hatch—a 30 inch $\times$ 30 inch roll-up movie screen. Because these do not illuminate the instrument in the same way as the telescope, these are intended as daytime calibrations and for engineering tasks, when the telescope itself cannot be accessed. The lamps include multilevel quartz-halogen and arc lamps—Ar, Ne, Xe, Ne + Hg, and Kr.

4. CONTROLS, USER INTERFACE, AND SOFTWARE TOOLS

4.1. Computers

IMACS operation is controlled by a Mac Mini running the Mac-OS X operating system using X11 libraries. This computer resides in the Baade Control Room. Information is entered and actions taken thorough the use of GUIs that have been developed by Christoph Birk at the Carnegie Observatories.

The mosaic array CCD cameras are controlled by an independent, dedicated PC running the Linux operating system, quartered in the Baade Equipment Room. Data are transferred from the cameras to this computer via fiber optics and then transferred over the local network to the camera GUI running on the Mac Mini, which writes the data to the local disk.

The observer has immediate access to both channels of IMACS, f/2 and f/4. The single User GUI that controls the instrument displays options for all devices, highlighting those relevant to the present mode. The individual camera GUIs allow the user to observe with one camera while, for example, taking dark or bias frames with the other.

4.2. User Interface

The style and format of the IMACS GUIs resemble that of most other instruments at the Magellan telescopes, so observers familiar with one instrument find the IMACS controls familiar, though there are many more options than with the other instruments.

The observer chooses the elements of the observation—the slit mask or open for imaging, which filter, which disperser—from pull-down menus in the IMACS GUI, shown in the top of Figure 4.

The observer uses the camera GUIs, shown in the bottom of Figure 4, to enter object identification, choose exposure type (object, nod-and-shuffle, MMTF, bias, or dark flat), CCD binning, and exposure time. There is provision for looping: that is, repeating exposures automatically. There are options for selecting the full mosaic array or any combination of the CCDs. The observer can also set up subrasters anywhere on the chip: these can be read out more rapidly. A common use is for the slit-mask alignment procedure, when subrasters covering the alignment star boxes are used in preference to a 1×1 binning of the full $8\text{K} \times 8\text{K}$ frame. The special observing sequences for nod-and-shuffle (see § 5.3) or MMTF (§ 5.5.2) observations are configured via dialog-boxes that open when these exposure types (ExpType popup menu) are selected.

4.3. Display Tool and Subrasters

Figure 5 shows the display tool dedicated to the mosaic camera—the Quick Look Tool, which displays the data when one of the mosaic CCD cameras is read out. Because of the challenge of displaying the raw data of eight detectors, with their different biases and sensitivity variations, a number of automatic and manual scaling options are provided. Also shown in Figure 5 is the magnifier tool that allows the observer to inspect, at four magnifications, any location on the full mosaic array. The magnifier also provides pixel coordinates and value, mean and

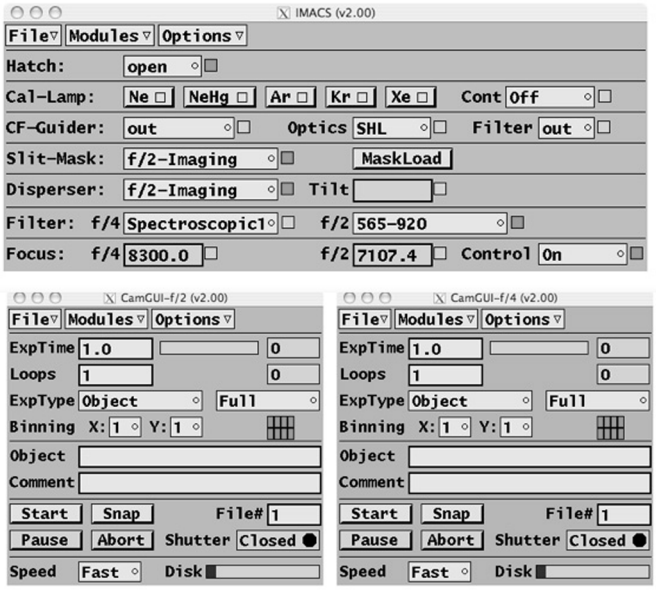

FIG. 4.—*Top*: The IMACS GUI. *Bottom*: Camera GUIs.

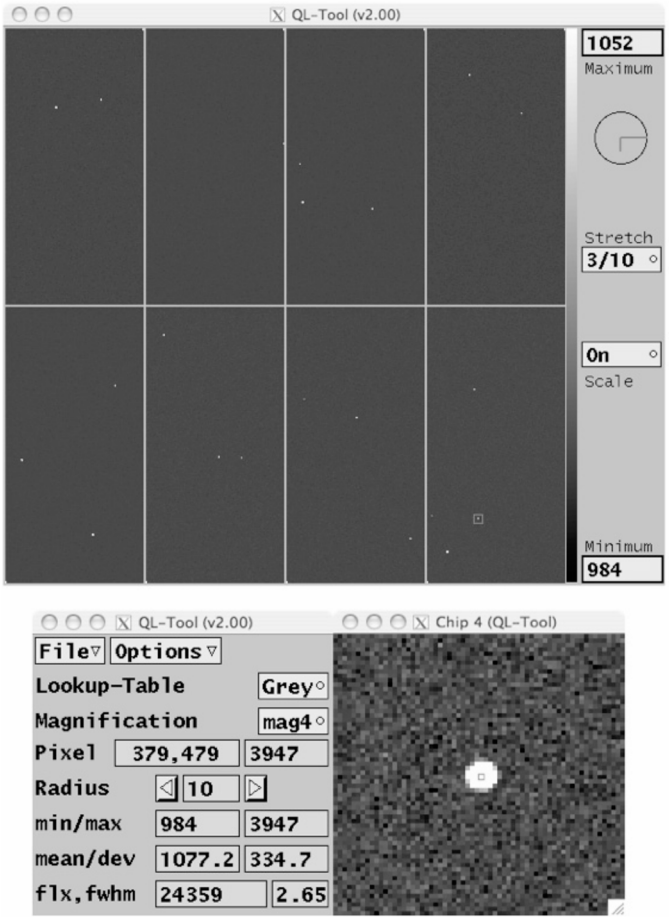

FIG. 5.—*Top*: The Quick Look Tool displays the data as the mosaic camera is read out, or any stored frame. *Bottom*: The Magnifier Tool allows the observer to inspect any small area on the array.

standard deviation in an area, total counts, and FWHM of an object selected with the cursor.

Observers use the Quick Look Tool to monitor data during observations. They typically use another window on the data taking computer to run IRAF, SAOimage DS9, or some similar software package, for closer inspection and manipulation of the data.

The Quick Look Tool includes efficient commands for defining subrasters. By choosing this option on the camera GUI, the user can define up to 16 subrasters per CCD, using the Quick Look Tool to mark areas of the full mosaic array.

4.4. Documentation, Observing Tools, and Cookbooks

Important documents, catalogs of photometric standards, an atlas of spectral arc lines for various IMACS setups, and instructions on how to submit multislit-mask files for cutting are available online.[10] There are helpful scripts for observers: for example, a script that asks for a grating choice and a central wavelength and returns the tilt angle, wavelength range, and an exposure-time calculator for direct imaging. There are also a number of purpose-written software tools—called Observing Cookbooks—that facilitate observing with IMACS. These include instructions for: aligning multislit masks; setting up N&S observations—single or multislit; moving a single object to a specified location on a long slit (at an arbitrary position angle on the sky); observing in the center-field slit-viewing mode; and setting up an observation with the IFU. The more complex modes—MOE, MMTF, and GISMO—require more than a cookbook; links are provided to their operation manuals.

4.5. COSMOS Data-Reduction Software Package

The COSMOS data-reduction package[11] is a powerful and efficient software package that was developed by A. Oemler to deal with the challenge of processing hundreds to thousands of spectra per multislit exposure. COSMOS takes advantage of the accuracy of the optical model described previously, and the optical/mechanical stability of IMACS, to create a reliable spectral map of each slit on a mask. This map connects locations in the two-dimensional space of wavelength and location along the slit to the two-dimensional space of CCD coordinates. After spectral arcs obtained near the time of observation are used for fine-tuning, the spectral map is usually accurate to about one-tenth of a CCD pixel.

[10] See http://www.lco.cl/telescopes-information/magellan/instruments/imacs/.

[11] See http://www.obs.carnegiescience.edu/Code/cosmos.

The spectral map is used for all data reduction up to and including the extraction of the final, summed, cosmic-ray cleaned spectra. From a computational standpoint, this is an efficient way to process the large data sets, but more important for the integrity of the data, all operations are done in the CCD pixel coordinate system, without resampling (interpolating) pixel values. This improves, in particular, the accuracy of sky subtraction near strong night-sky lines, which is done using Kelson's (2003) algorithm. All processes needed to reduce a set of observations of one field can be pipelined so that user intervention is not required from the initial setup to the final step, when individual object exposures are combined. Except for a few support programs written in Tk/Perl, the entire software package is written in the C programming language. Reduction of a set of five exposures of a mask containing a few hundred slits, together with the accompanying flat fields and comparison arcs, typically takes about 20 minutes on an average machine. (2 GHz MacBook Pro).

COSMOS can be used for all multiobject spectroscopy with IMACS, including MOE, GISMO, and prism reductions (described subsequently).[12]

5. MODES OF IMACS

5.1. Multislit Masks

The principal use of IMACS is multislit spectroscopy. The multislit masks for IMACS begin as 26.5 inch diameter disks of 0.010 inch sheet stainless steel into which an approximately spherical shape with a sagitta of ~40 mm is impressed in order to match the f/11 focal surface. The telescope coordinate system is sufficiently well mapped that users are only asked to supply astrometrically accurate positions for their targets: it is not necessary (nor even recommended) to take images of the target field with IMACS in order to prepare a multislit mask (e.g., GMOS; Hook et al. 2003).

A software package maskgen, written and maintained by Ken Clardy at Carnegie Observatories, is provided for designing these masks. The program has a wealth of options, but is particularly well suited to large data catalogs that are to be sampled more-or-less randomly. Particularly in the case of multiple tiers of spectra (when the spectral length is less than half of the detector width in the dispersion direction), the maskgen software resolves conflicts of overlapping spectra in order to maximize yield, taking prioritization into account if that information is included in the catalog. The object list also includes stars in the field of 17–19 mag for use in mask alignment: typically, 10–15 small boxes are cut into the mask for this purpose The output files from the mask-making program are used to produce machine-code scripts for a commercial laser computer numeric control milling machine (at Magellan) that cuts the slits into the curved surface and, in the same operation, mounting holes for the precision pins on the mask frames, to maintain the accurate metrology of the setup. The programs and necessary star catalogs are available at each of the Magellan Partner institutions and online.[13]

External users have the option of accessing the guide star catalogs through transparent Web-based interface to the catalogs on the Carnegie Observatories's computer systems. Observers are asked to submit finished mask designs six weeks before the first night of their program. A charge of $200 per mask covers the cost of production and amortization of the laser milling machine.

Details about use of the multislit masks at the telescope are found in § 6 on Performance.

5.2. Examples of Multislit Spectroscopy

Efficient multiobject slit spectroscopy over a wide-field, with a broad range of spectral dispersions, is the most-used mode of IMACS. A typical application at f/2 is to use slits ~10″ in length and width 1.0″, corresponding to a spectral resolution FWHM = 10 Å ($R = 650$ at 6500 Å) with the 200 lines mm^{-1} grism. Full spectral coverage for this setup would be 4000–10,000 Å or 3000 detector pixels, so there is space along the 8192 pixels in the dispersion direction for two rows of spectra, on average. A blocking filter that reduces the covered area, for example the WB4800-7800, can raise this to three rows of spectra. For such an application about 80% of the 27′ diameter circular field can be used to obtain complete spectra, since the dispersed spectra make full use of the square format of the CCD mosaic.

With the f/4 camera, the higher dispersions of the reflecting gratings means that spectra normally take up more than half of the detector in the dispersion direction, so a single row of slits is more appropriate if a broad wavelength range is required. For example, with the 600 lines mm^{-1} 5000 Å blaze grating, a 0.8″ wide slit delivers FWHM = 2.75 Å ($R = 2000$ at 5500 Å). If the program requires, for example, 2000 Å of spectral coverage, this occupies ~5300 of the 8192 detector pixels. The difference in pixels corresponds to ~5′ of sky coverage, in other words, for objects selected over a $5' \times 15'$ sky area, the full 2000 Å of spectrum will fall on the detector.

An example f/2 program is the IMACS Cluster Building Survey by A. Dressler and collaborators, which uses the parameters described previously. Figure 6 (*top*) is a sky map showing the positions of 1370 galaxy redshifts that were accumulated for five different multislit masks, the first with ~400 slits and the last only ~200 on remaining targets. This field contains a rich cluster at $z = 0.42$, but over the projected 10 Mpc diameter of the f/2 field most of the targets are actually foreground or background to the cluster. Figure 6 (*bottom*) plots the redshifts measured in this field. A principal objective of this program is to study galaxy evolution in the cluster environment and the field

[12] As of this writing, MOE data must be reduced one order at a time, but we intend to fully pipeline the reduction of these data.

[13] See http://users.obs.carnegiescience.edu/clardy/imacs/maskmaking.html.

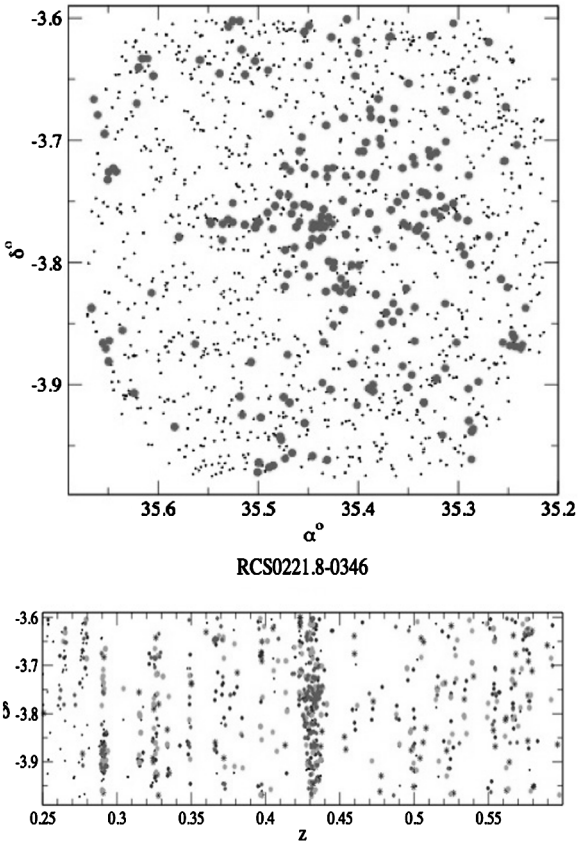

FIG. 6.—*Top*: Sky map of 1370 redshifts in the field of a rich galaxy cluster at $z = 0.42$, accumulated over five IMACS multislit-mask exposures. *Bottom*: The space distribution in redshift—declination space (square pie diagram).

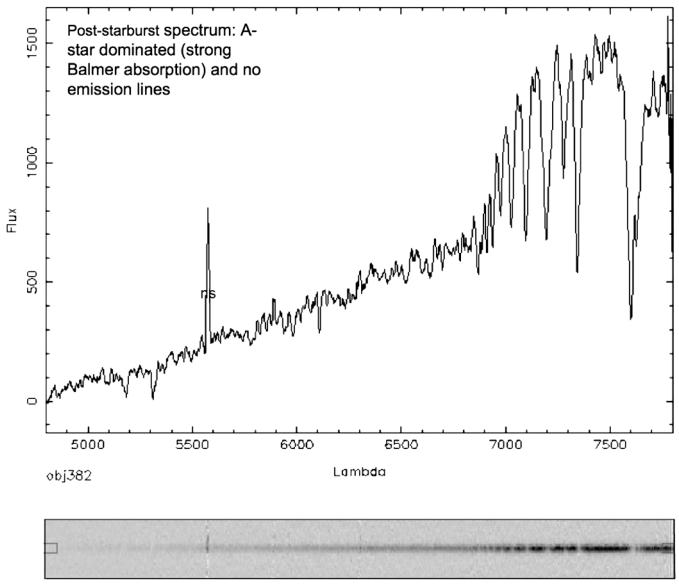

FIG. 7.—*Top*: Spectrum of a strong poststarburst galaxy at redshift $z = 0.75$. *Bottom*: Two-dimensional, sky-subtracted image of the spectrum produced in the COSMOS data-reduction package.

galaxies at the same epoch—high signal-to-noise ratio (S/N) spectra are required to measure not only redshifts but diagnostic features of stellar populations, like the strong starburst spectrum at $z = 0.75$ shown in Figure 7. In this example the total exposure time was 3.3 hr per mask (with the original Mosaic-1 CCD camera), accumulated with five integrations of 40 minutes' duration.

Figure 8 shows a even deeper probe of field galaxies at $z \sim 1$ from Patrick J. McCarthy, part of the Gemini Deep Deep Survey (Abraham et al. 2004). The redshifts for these faint galaxies, $23.0 < I < 23.5$ (or $R \gtrsim 24$), come from absorption-line spectra, more challenging than emission-line redshifts. These observations were made even more difficult by the fact that the Ca II H and K absorption lines appear beyond $\lambda > 8000$ Å, a region of strong OH airglow, and that these observations were made at low spectral resolution ($R \sim 500$). A combination of excellent sky subtraction using the nod-and-shuffle technique (§ 5.3) and excellent seeing aided in obtaining these challenging observations. The spectra shown here were obtained in a 3.5 hr observation with the original Mosaic-1 camera (SITe CCDs) in 2005. A similar observation with the Mosaic-2 camera (E2V) now in use at f/2 would require less than 2 hr.

In 2010 IMACS was used to obtain spectra that confirmed the photometric redshift of the most distant cluster of galaxies found to date, $z = 1.62$ (Papovich et al. 2010). The [O II] doublet $\lambda\lambda 3726, 3729$ was detected in seven galaxy spectra at a wavelength of $\lambda \sim 9800$ Å.

5.2.1. Prism Spectroscopy and Examples

A powerful addition to IMACS capabilities came from outside the Carnegie Observatories and was not part of the original plan for the instrument. Scott Burles proposed and fabricated a zero-deviation prism for the IMACS beam, called a low-dispersion prism (LDP), that delivers very low-resolution spectroscopy—$R \approx 60$ in the visible declining to $R \approx 8$ in the far red, specifically for obtaining large numbers of galaxy redshifts to look for baryon oscillations in the distribution of galaxies at moderate redshift (the Prism Multiobject Survey [PRIMUS] project.[14] Because the number of pixels per spectrum is small, thousands of objects can be observed simultaneously with the multislit masks and wide field of the IMACS f/2 camera. Figure 9 shows an LDP observation by Daniel Kelson on a field containing a rich cluster at redshift $z \sim 0.8$, for which 3412 objects were targeted with a single multislit mask.

Such very low resolution spectra offer an improved way of measuring redshifts in the tens of thousands. The prevalent method of accomplishing this has been to obtain so-called photometric redshifts by acquiring photometric images in ~10

[14] See http://cmb.as.arizona.edu/~eisenste/primus/Home.html.

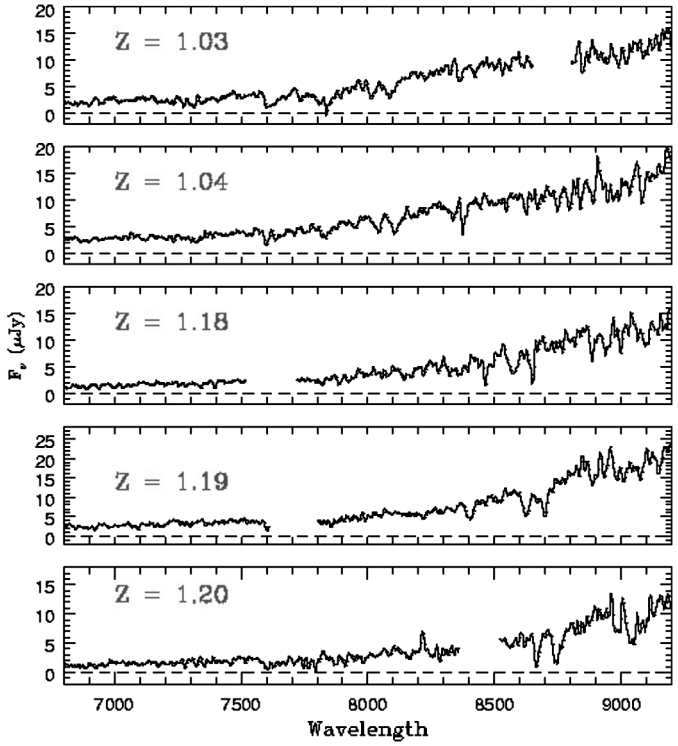

FIG. 8.—Absorption-line spectra of $z > 1$ galaxies ($23.5 < I < 24.0$) from the GDDS sample of McCarthy and collaborators.

intermediate-band images and fitting model spectral energy distributions (SEDs) to these discrete points. As successful as this has been, redshifts done this way are limited in accuracy to a few percent and there is a nonnegligible possibility of aliasing, especially when the number of bands is smaller than 10. The LDP produces continuous energy distributions that can be fit to SED models, as illustrated in Figure 10. These are LDP spectra taken by D. Kelson of galaxies in the outskirts of a rich cluster at redshift $z = 0.83$, from 3 hr of nod-and-shuffle observations, to which multicomponent stellar population templates have been fit. By comparing the redshifts done by this spectrophotometric technique to those obtained with $R \sim 500$ spectroscopy, D. Kelson (2010, private communication) has shown that redshifts can be measured to an accuracy of $\sim 1\%$. The data are useful for more than redshift, however, since they do provide much information on the stellar makeup of the galaxies. Even at this very low dispersion, strong emission lines are detected—another advantage over photometric techniques.

The very low resolution of LDP at the red end of the spectrum makes it difficult to calibrate the spectral energy distributions with high accuracy and makes sky subtraction more difficult as well. A significant improvement is the new multielement prism, the uniform-dispersion prism (UDP), designed by Stephen Shectman, that uses eight alternating wedges of two different glasses to reduce the difference in dispersion between the blue and red ends. As shown in Figure 9, the dispersion delivered by the UDP levels out at $R \sim 25$ beyond $\lambda > 7500$ Å, a distinct improvement over the LDP.

5.2.2. GISMO

A unique capability of IMACS is GISMO, invented by Mike Gladders and built with funds from an NSF Advanced Technologies and Instrumentation (ATI) grant to Dressler and Gladders. GISMO addresses a vexing limitation to multiobject spectroscopy— obtaining spectra for objects at high target density, more than a few per square arcminute. For example, we show in Figure 11 an area of $\sim 4' \times 4'$ covering the core of a distant galaxy cluster that is rich in targets. However, only a number of targets N, of the order of field diameter divided by slit length, can be observed, because the spectra of additional objects will overlap; that is, the separation of the objects in wavelength in the spectrograph format is smaller than the length of each spectrum. In theory, fiber-fed spectrographs are better at this application, but in practice, mechanical constraints limit the density of fibers in an area, and a number of factors (for example, sampled fiber area and precision of sky subtraction) generally favor slit spectroscopy for the faintest targets.

GISMO offers a solution to this problem. It places 16 small slicing mirrors at the IMACS focal surface that each intercept an area approximately $0.5' \times 2'$ of sky. The mirrors redirect the 16 areas through reimaging lenses and folding mirrors so that they reimage—with scale and focal-surface curvature conserved, over the full IMACS f/4 (or f/2) field. These new images are filtered through a slit mask (different from the normal IMACS multislit mask and containing multiple setups) so that only the light from selected targets enters the spectrograph. The densely packed targets shown in Figure 11 now each own enough pixel space, spread over the full mosaic array CCD camera, that their spectra will not overlap. In the example of Figure 11, all the targets shown enclosed by the red slits are observed, compared with the single row that was available previously. The multiplexing advantage is typically 5–8.

Also shown in Figure 11 (*bottom*) is an actual reimaged slice of sky from one GISMO observation. The image quality is slightly degraded in the outermost segments, but images FWHM $< 0.6''$—with most better than $0.5''$—are produced over the field. The loss of efficiency due to the GISMO reimaging optics is $\sim 20\%$, but the multiplexing gain is enormous in comparison.

More about GISMO capabilities and how to use it can be found at the IMACS Web page at Magellan.[15]

5.2.3. MOE

MOE is a cross-dispersed grating that installs in the IMACS disperser wheel and works with the f/4 camera. The design of

[15] See http://www.lco.cl/telescopes-information/magellan/instruments/imacs/gismo/gismoquickmanual.pdf.

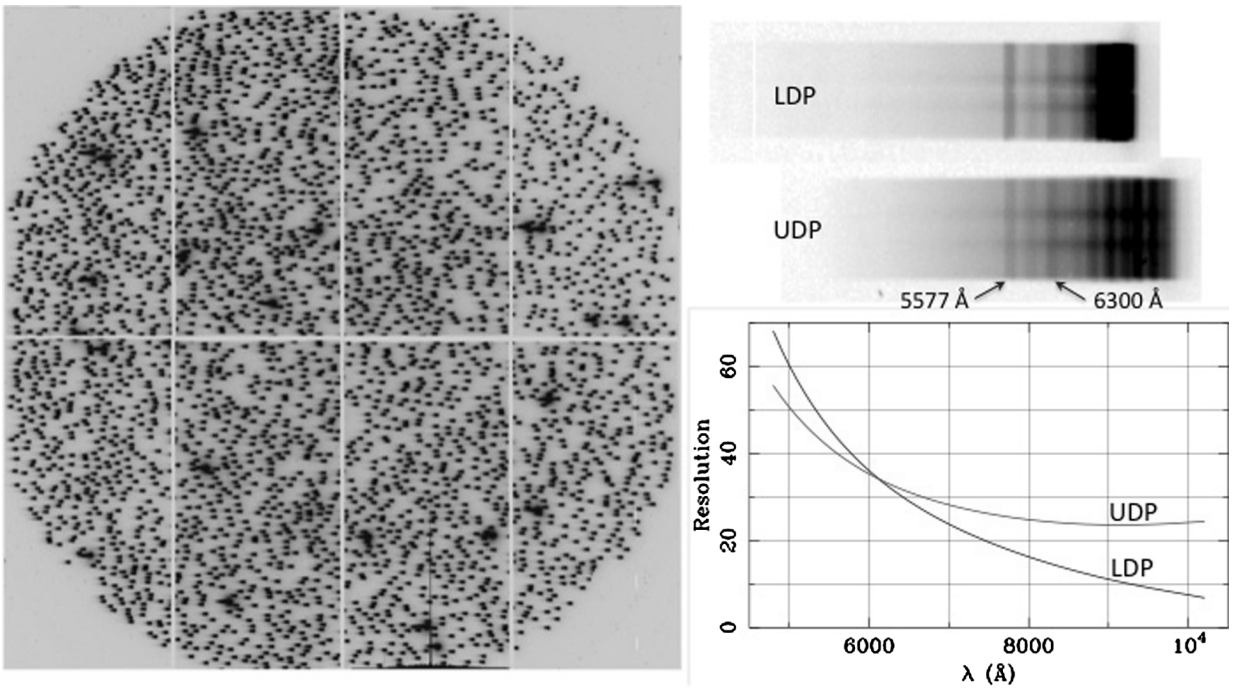

FIG. 9.—*Left*: Multislit mask with very low dispersion prism spectra for of 3412 objects in the field of a rich cluster at $z = 0.83$ studied by D. Kelson (2010 private communication). *Top right*: Example LDP spectrum—nod and shuffle produces doubled object and sky spectra. Below the LDP spectrum is one with UDP, showing the more uniform dispersion of the UDP, compared with the LDP. *Bottom right*: Comparison of the dispersion profiles of the two prisms. Night-sky emission lines 5577 Å and 6300 Å are marked in the UDP spectrum. Atmospheric OH absorption is evident in the UDP sky spectrum out ∼10, 000 Å, where the UDP dispersion is a factor of ∼3 greater than the LDP.

MOE was based on the highly successful ESI on Keck, adapted for IMACS by Sutin and McWilliam (2003), and built in collaboration with the IMACS team. Like ESI, MOE uses an echelle-grating and cross-dispersing prism in the instrument beam to produce spectra of nine orders at moderately high resolution, $R \approx 20,000$, from 3600 Å $< \lambda <$ 9100 Å. Unlike ESI, MOE can take advantage of the IMACS wide-field and large detectors to multiplex such observations for ∼10 targets over the full $15' \times 15'$ field for f/4. This is for full-wavelength coverage: with a blocking filter to limit the wavelength range, up to $N \sim 100$ targets can be observed simultaneously.

Due to a mistake in the manufactured grating blaze, MOE is not operating at its designed efficiency, which was expected to peak at ∼10% (including telescope and detector). Although the multiplexing factor makes up for this deficiency to some extent, it is hoped that a new grating will be available in 2011 to bring MOE up to its design specifications.

The top of Figure 12 shows multiple four-order spectra obtained in the field of the Carina dwarf galaxy, a section of which is enlarged to show the multiple orders. The bottom of Figure 12 shows a comparison of spectra taken by MOE and UVES (Ultraviolet and Visual Echelle Spectrograph) (VLT) of the same star, the UVES spectrum at higher resolution, but from an observation with only 10 targets, compared with 20 for MOE.

MOE is an ideal instrument for chemical abundance work in target-rich fields, for example, the Galactic bulge or Local Group dwarf galaxies, and is being used to measure the velocity dispersions of the faint dwarf galaxies discovered in the Sloan Digital Sky Survey. It is also a powerful tool for studying, for example, the kinematics of planetary nebulae, or the chemical abundance of globular clusters, in galaxies of the Local Supercluster.

5.3. Nod-and-Shuffle Mode

Nod-and-shuffle (N&S) spectroscopy (Glazebrook & Bland-Hawthorn 2001) is a highly regarded method of taking multislit data, especially for very faint objects at wavelengths beyond 7500 Å where atmospheric airglow is bright and composed of many discrete lines and bands. Using the telescope to move the spectra between alternating ends of their slits, each time shuffling the charge on the CCDs back and forth a compensating amount, results in excellent sky subtraction, even at relatively low spectral dispersion. The use of short slits contributes to a larger multiplexing factor, and the excellent sky subtraction makes possible the study of objects whose brightness is a small fraction of that of the night sky. The maskgen program produces slit masks specifically designed for N&S observations, and the IMACS mosaic cameras are able to clock charge in the spatial (long CCD axis) direction. N&S is the default orientation of

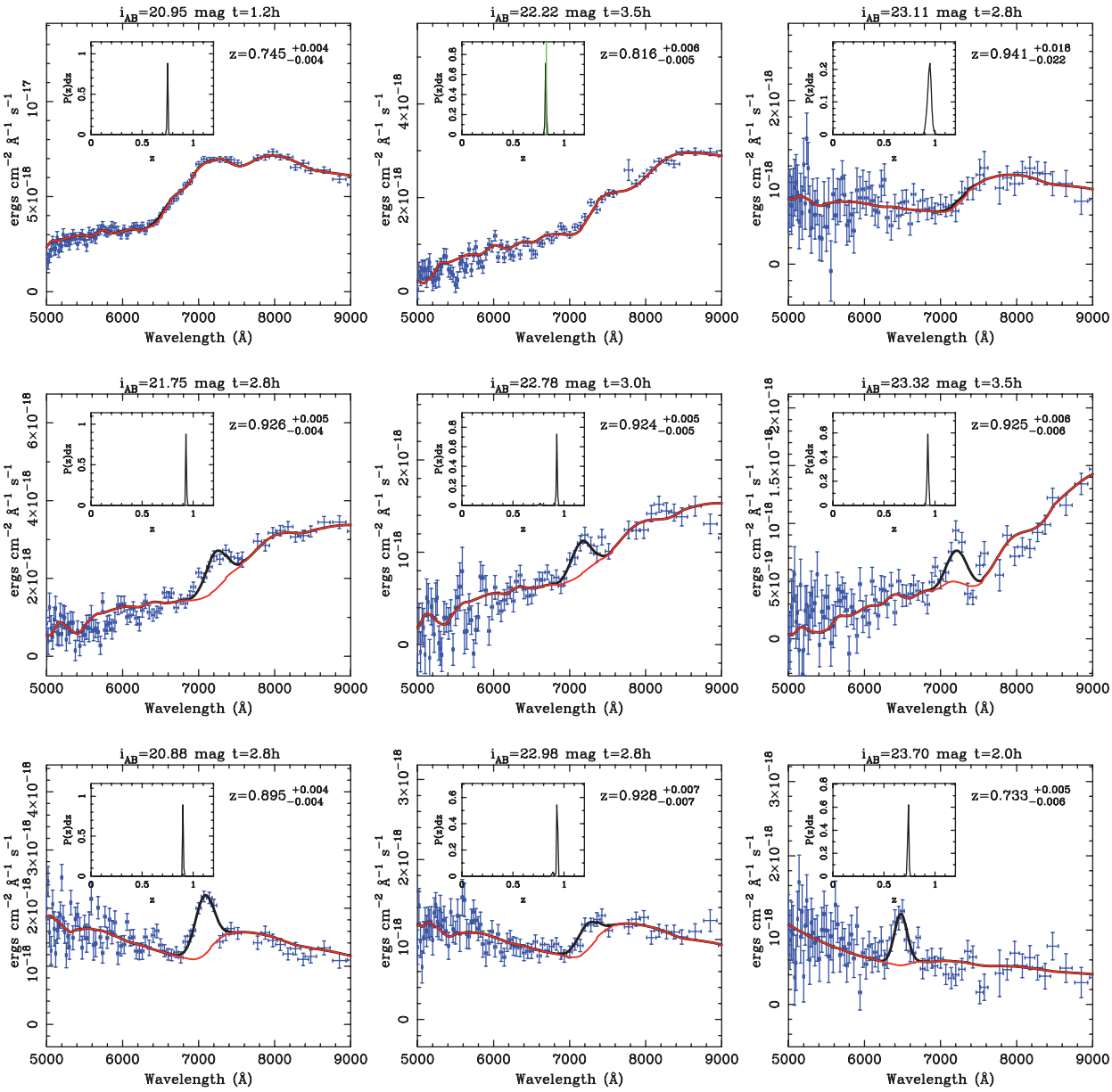

FIG. 10.—Examples of spectrophotometric observations of $z \sim 1$ galaxies from LDP observations (D. Kelson 2010, private communication). In each example the observed prism spectra is the blue line and the fit to multicomponent stellar population templates is the red line. The small inset box shows the autocorrelation determination of the redshift, which is clearly very well constrained by the data and model fits.

the f/4 camera (but not the default mode, while N&S is accomplished at f/2 by rotating a grism by 90°.[16] The default orientation for the f/2 camera has the spectral dispersion along the long axis of the CCDs to take advantage of fewer chip gaps.

Guiding is done differently with N&S. The nod is fixed by moving the target (a software cross) on the image on the principal guider back and forth, and the telescope is moved the same amount (called a coordinated offset). However, the Shack-Hartman (SH) guider has a real aperture, not a software cursor, so it would have to be physically moved to require the SH star. To avoid accumulating guider-position errors, we choose to leave the Shack-Hartmann guider in its place and turn it off during alternate exposures. The 50% duty cycle does not seem to have any measurable consequences, compared with regular operation.

We have found that the N&S method is difficult to apply perfectly over the large IMACS field; since the slits are very

[16]Because the exposure time is cut in half for each part of the exposed CCD, in comparison with conventional spectroscopy, it is important that the sky level in electrons is well above the square of the read noise.

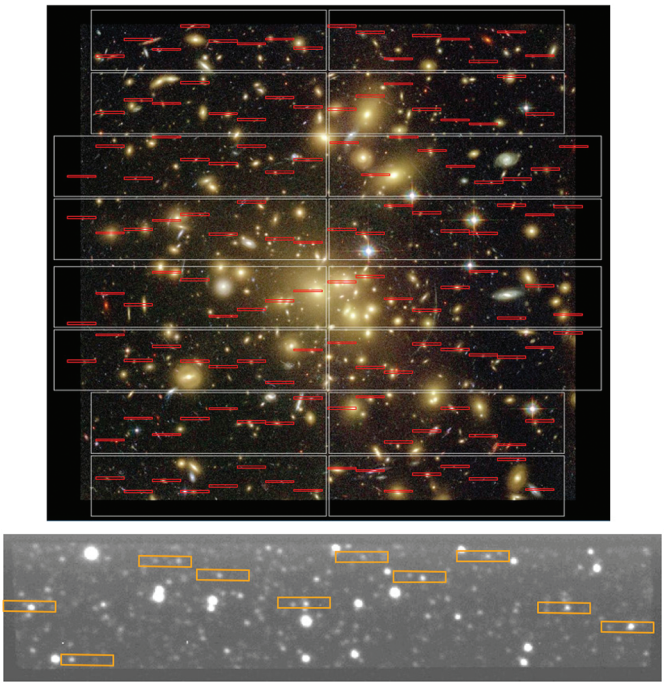

FIG. 11.—*Top*: Layout of the 16 slices of GISMO mapped onto the approximately $4' \times 4'$ central field of IMACS, superposed on an image of a distant rich cluster of galaxies. GISMO allows all the red slits to cover targets in this field, despite the fact that their spectra would overlap in normal multislit spectroscopy. *Bottom*: An actual reimaged segment of a $0.5' \times 2'$ slice. The orange boxes represent $10''$ long slits.

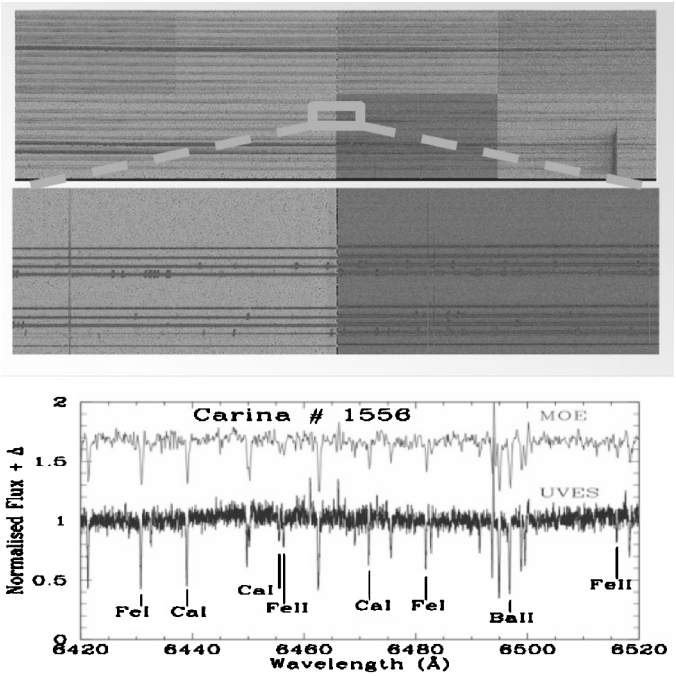

FIG. 12.—*Top*: Multiple high-resolution spectra obtained with MOE. Each trace in the top area has four orders, covering about 1500 Å total. A high magnification enlargement shows two of the four-order spectra. *Bottom*: Comparison of a MOE spectrum and VLT-UVES spectrum for star 1556 in the Carina dwarf galaxy. The UVES spectrum has higher dispersion, $R \approx 40,000$, compared with $R \approx 20,000$ for MOE, but the S/N is within a factor of 2. MOE targeted 20 objects, as compared with the 10 of the UVES observation.

short and spacings are critical, uniformly high quality for the final spectra is challenging. Nevertheless, the advantages of N&S when observing in the far red with faint objects and at low dispersion—especially the prism mode (§ 5.2.1)—make N&S the method of choice for these applications. Fortunately, the conventional staring mode produces very good sky subtraction, allowing this to be the preferred mode for most applications. The COSMOS pipeline (discussed subsequently), which includes a sophisticated sky-subtraction algorithm written by D. Kelson (2003), does an excellent job, even for objects that are very quite small fraction of the night-sky brightness.

5.4. Single-Object and Long-Slit Spectroscopy

A set of long slits of various widths have been cut into standard multislit-mask blanks for single-object and long-slit spectroscopy. These can be used to take spectra of one or multiple (aligned) objects, or for spectra of extended objects up to $25'$ in length in f/2 mode, or $15'$ in f/4 mode.

Single-object spectroscopy can also be accomplished with the slit-viewing unit of the center-field guider, as mentioned previously, which carries a stepped width slit of five segments, each $17''$ in length. This mode is primarily intended for brighter targets that can be readily seen in real-time images from the center-field guider's CCD camera and is also used for spectroscopic calibrations of flux-standard stars.

5.5. Imaging with IMACS

The two cameras in IMACS give the observer considerable flexibility for wide-field imaging. The f/4 system has a $15' \times 15'$ field that is fully illuminated (ideal for tiling an area of sky), and the $0.11''$ pixels critically sample even the best seeing that Baade offers: FWHM $\sim 0.25''$. Projects have included the search for planetary nebulae in and between Virgo-cluster galaxies and measurement of the their globular cluster luminosity functions and color distributions.

The f/2 camera has the much wider field (0.18 deg^2) and, at present, the more sensitive CCD camera, making it better suited to extremely deep searches. The $0.20''$ pixels critically sample seeing that is better than the Magellan median of $0.65''$ FWHM (optical red). The Mosaic-2 camera is particularly sensitive in the red, so this imaging mode has been used, for example, to make photometric catalogs of galaxies at high redshift, or to obtain deep exposures of faint dwarf galaxies in the Local Group.

A wide selection of broadband filters is available, and the large number of filter slots means that very complex programs can be planned. In addition to broadband imaging, both cameras have been used with narrowband filters, which are placed at the spectrograph pupil in order to deliver a fixed bandpass over the wide field. This can also be accomplished with the tunable filter MMTF, described subsequently.

5.5.1. Durham IFU

The IMACS-Durham Integral-Field Unit is a 2×1000 fiber reformatter that samples two areas of the sky, each $5'' \times 7''$ (f/2 mode) and $4'' \times 5''$ (f/4 mode) and spreads them linearly over the full focal-surface/mosaic CCD detector, deconstructing the object into 2000 (1200) spectra with $0.2''$ 2D sampling. The design is derived from the IFU built by Durham University for Gemini North GMOS (Allington-Smith et al. 2002). The design built for IMACS is described in detail online[17] and in Schmol et al. (2004). The IMACS IFU is well suited to spectroscopy of complex galactic objects such as small nebulae or star-forming regions and the kinematics and distribution of stellar populations in intermediate-to-high redshift galaxies. The examples shown in Figure 13 are from the Sloan Lens Advanced Camera for Surveys (ACS; Bolton et al. 2006), in which candidate gravitational lenses were selected from the Sloan Digital Sky Survey on the strength of multiple redshifts. The images in the left column show *Hubble Space Telescope* ACS images from which a smooth model of the galaxy has been subtracted, revealing the lensed image of the background object that contributes the higher-redshift emission lines in the spectra. The IMACS IFU spectroscopy accomplishes the same thing, albeit at lower spatial resolution, by separating the light over the 2D area into a continuum component (*right*)—the lens—and an emission-line component (*center*)—the lensed background galaxy.

Despite its power and efficiency (only a $\sim 30\%$ loss, compared with conventional slit spectroscopy), the Durham IFU is the least-used mode on IMACS. It installs into the slit mask server, occupying only three of the six slots available for masks, so the IFU can also be used as part of a diverse scientific program.

5.5.2. MMTF

The MMTF was built as a collaboration between the University of Maryland and Carnegie Observatories, with substantial support from the NSF ATI program. The project was led by P.I. S. Veilleux, with C.I.s B. Weiner and D. Rupke. The MMTF is a higher-capability version of a Taurus Tunable Filter.[18] It installs in the disperser server in place of a reflection grating, so it can be swapped into the parallel beam at short notice, while still allowing a full program of other IMACS capabilities.

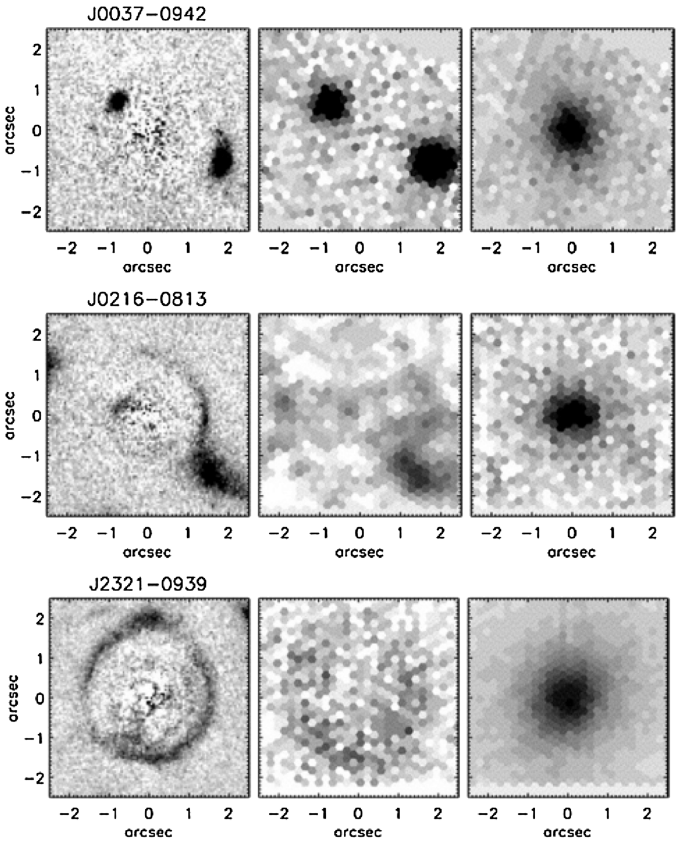

FIG. 13.—Three candidate gravitational lenses observed with the Durham IFU for The Sloan Lens ACS Survey. The three images on the left are *HST* ACS observations of candidate lenses for which a smooth galaxy component has been subtracted. The IMACS IFU data come from single IFU exposures of the same fields, divided into an emission line (*middle*) and a continuum image (*right*). The strong differences show that the emission line comes from a background galaxy lensed by the foreground galaxy seen in the continuum image.

The MMTF consists of a 150 mm diameter Fabry-Perot Etalon whose controller is remotely managed by the IMACS computer. It provides for narrowband (5–12 Å) imaging over the $27'$ diameter of the IMACS f/2 field. The full monochromatic spot diameter is $10'$ at 6600 Å and the MMTF tunes over the wavelength region 5000–9200 Å. A growing set of filters is available, necessary to block higher orders of the target emission line(s). The charge-shifting capability of the mosaic CCD cameras, included to enable nod-and-shuffle slit spectroscopy, allows MMTF to work in a charge-shuffle and band-switching mode that offers the best subtraction of sky backgrounds and drifts of the etalon. With these features the MMTF reaches flux levels of $F \sim 5 \times 10^{-17}$ ergs s^{-1} cm^{-2}.

A sophisticated user interface allows observers with little previous experience to use the MMTF. With the addition of easy-to-apply software for adjusting and operating the MMTF,

[17] See http://www.dur.ac.uk/cfai/projects/oldprojects/imacs-ifu/.

[18] Built by J. Bland-Hawthorne and H. Jones for the Anglo Australian Telescope; see http://www.aao.gov.au/local/www/jbh/ttf.

the initial period of scheduling the MMTF in campaign mode—with a member of the MMTF team monitoring the tunable filter's performance and offering assistance—has given way to operation of the MMTF in an essentially routine manner.

The example shown in Figure 14 is a nearby galaxy imaged in both narrowband Hα and [N II] emission and broadband continuum at the same approximate wavelength. These lines are effective in measuring the star-formation rate and the metal abundance and excitation of gas in the galaxy, but the broad tuning window of the MMTF would allow for imaging in [O III] and [S III], for example, without the need for custom filters. For higher-redshift objects this feature becomes particularly important, for example, as in the extensive study by McDonald et al. (2010) of cooling gas in the cores of 23 rich clusters of galaxies.

A complete description of the MMTF, its operating characteristics, and performance data can be found online[19] and in Veilleux et al. (2010).

6. PERFORMANCE

6.1. Aligning Slit Masks

As described previously, multislit spectroscopy requires considerable preparation, but observations are easy to set up and perform—hardly more difficult than the procedures required for a single object. In the process of designing a mask, the maskgen software requires the user to choose stars for the principal and SH guiders. The field-center coordinates, position angle on the sky, and guide star coordinates are copied to an observing catalog, which is passed to the telescope operator (TO) and into the telescope control system (TCS). As the telescope slews to the target position, the IMACS guiders move to predicted positions for acquiring the guide stars. When the target is reached, the principal and Shack-Hartmann guide stars will typically be displaced by 2–5″ because of pointing errors in the telescope altitude, azimuth, and Nasmyth rotator angle. The slit-mask alignment process begins by taking advantage of the excellent metrology of the IMACS guiders: the observed positions of the guide stars are compared with the predicted positions in the guider fields and offsets are made to the telescope altitude, azimuth, and rotator angle (without moving the guiders). If the astrometry of the alignment stars is known to arcsecond precision or better, this procedure will usually bring the alignment stars of the slit mask within their target boxes (typically $5'' \times 5''$) on the first setting, before any alignment procedures using the mosaic CCD camera have been attempted.

As soon as this centering process is complete, the TO will start the telescope guiding and setup and start the Shack-Hartmann test. In preparation for the night's observing, the observer has generated for each slit mask a file containing the positions, in

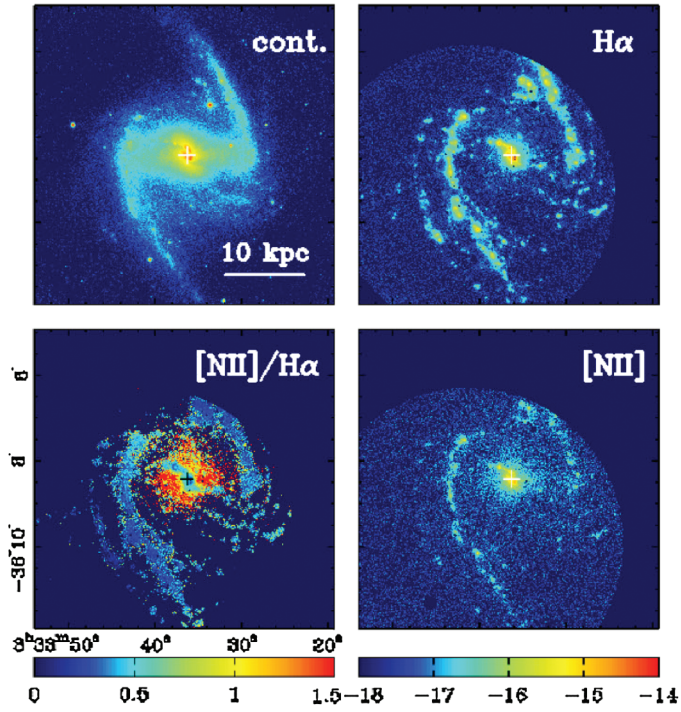

FIG. 14.—Narrowband images of the galaxy NGC 1365 made with the MMTF. The tunable filter allows the user to observe specific spectral features in galaxies and nebulae over a wide range of redshift without the difficulty of obtaining individual filters for each case. The Hα and [N II] emission are diagnostics for star-formation rate, metal abundance, and gaseous excitation.

CCD pixel coordinates, of the alignment star boxes, using a picture of the slit mask and a homemade IRAF script called `icbox`. This procedure also produces a subraster file that allows the mosaic camera to make an exposure sampling only the sections of the array where alignment stars are expected. An R-band exposure of ~30 s is made; when completed, another script `ialign` displays—one by one—the subrasters on a DS9 window, marking automatically the brightest object within the subraster. (The observer accepts this identification or marks another object.) When completed, `ialign` computes offsets in right ascension, declination, and rotator angle that are passed to the TCS, which executes a coordinated offset, in which the guiders determine where the new pointing will be. The commanded telescope moves are just approximations, while the final positions are achieved through guiding to the target.[20] Next, the slit mask is inserted and another subraster picture is taken, through the mask, which shows the realized box positions (which may differ slightly from the setup picture done prior to observing) and the alignment stars in their new positions. The script `ifalign` steps through the boxes and finds the star centroids and box boundaries and calculates a second coordinated offset. The result

[19] See http://www.astro.umd.edu/~veilleux/mmtf/.

[20] In particular, the new position for the principal guide star is determined simply by moving the software cursor, so this is done with an error of less than 0.1″.

of this will be right ascension and declination residuals of a few tenths of an arcsecond and an angular misalignment of less than 0.005°.

Further iterations are sometimes needed, but should not be if the proper alignment stars are identified and the positions are accurate. As soon as the observer is satisfied, the disperser and filter are selected and inserted, the exposure time and object name are entered, and the exposure begins. Elapsed time from the end of the last observation until the new observation begins, including the telescope slew, is typically 10 minutes or less.

Alignment is maintained by guiding the telescope in altitude and azimuth using the principal guide star and guiding the rotator by including the centroid position of the SH pattern of star images, which is computed every 30 s. Because of little flexure between the mechanical components and the telescope focal surface, rotator guiding allows the multislit setup to hold for several hours.

Setups for single objects, or for long slit work (up to $24'$ with the f/2 camera and $15'$ for the f/4), are very similar, if the mosaic camera array is used to acquire and reposition the object. Scripts are available for this too and—unless the area covered is substantial—guiding the Nasmyth rotator is not critical. A more rapid method of spectroscopy for single objects, mentioned previously, is to use the center-field slit-viewing guider. Particularly, if the objects are easily seen in reflection off the slit, setups can be very rapid. There are five slit segments, each $17''$ in length, with widths of 0.25, 0.50, 0.75, 1.0, and $1.5''$, to match the seeing, maximize S/N, or for more-accurate spectrophotometry.

6.2. Repeatability in Multislit-Mask Insertion

A recent modification of the slit-mask server has much improved slit-mask repeatability, bringing it down from several arcseconds to, typically, one arcsecond—the specification in the original design. This is more than adequate with the software tools for alignment described previously. The improvement was accomplished by adding a second clamp that, once the air cylinder has pulled the mask against the hard stops, pulls and locks the mask on the same side but some 20 inches higher up on the mask frame. This prevents small rotation of the mask due to gravity as IMACS rotates, and it has prevented slight cocking of the mask insertion position at some gravity angles. Tests of the upgraded system in March 2009 showed the alignment box positions of slit masks repeated to better than 3 pixels ($<0.8''$) as the mask was repeatedly inserted at different angles, and no motion was detected when a clamped mask was rotated and repeatedly imaged.

6.3. Object Placement in Multislit Spectroscopy

Fabricating a slit mask for a half-degree field of view with a physical size of 0.7 m is challenging. As a test of how well a full field of objects with excellent astrometry can be placed in slits and the mask aligned on the sky, we took Sloan Digital Sky Survey positions for more than 500 stars in the Galactic globular cluster Pal 5. The positions of 18 stars were used for alignment boxes $6'' \times 6''$, with 503 stars spread over the field as targets, imaged through $4'' \times 4''$ holes. This test alignment experiment, shown in Figures 15 and 16, produced median residuals of $0.12''$, which is quite acceptable, but also a long tail to larger values, including many $\sim 0.3''$ residuals in the upper right and lower left corners of the field. These values are uncomfortably large. Various tests were made to track down the problem. The first suspect was systematic errors in laser cutting slits in the mask, but a test of cutting a pair of pinhole-grid masks with a 90° rotation showed that the mill table was performing according to specifications and well below the larger displacements. The problem might arise from the telescope optics, but because of the correlations of residuals on scales of $\sim 5'$, the primary, secondary, and tertiary mirrors are not a likely clause. The ADC/corrector is constructed to cancel atmospheric dispersion by wavelength for less than 2.0 air masses, but not atmospheric refraction, which is on the scale of the systematic displacements we see. There could be some nonuniformities in the pair of crossed prisms that, in order to cancel dispersion, generate deflections of several-tenths of an arcsecond, but tests involving independent motions of the prisms did not show any clear generation of such offsets. Recent experience with cutting a heavily perforated slit mask (100 long slits that removed 10% of the stainless steel) showed a substantial warping of the shape of the mask, with large-scale residuals of $\sim 0.5''$. Because of this we now suspect that variations in the figure of slit-mask blanks, as delivered or altered by the laser cutting, are the likely explanation for the larger correlated residuals seen in the Pal 5 test. There is no obvious cure to the problem, but it suggests that slit-widths of less than $1.0''$ should be avoided unless strictly required by the observing program.

6.4. Holding Objects on Slits

A critical issue for a multislit spectrograph is the possibility of flexure between the guiders and the slit mask itself, which is held at the focal surface of the telescope. To the extent that there is flexure, the guiding of the telescope will fail to keep the objects centered on the slits. A common cause of this problem is flexure in cantilevered arms that allow the guider optics to reach into the field. A priority for the IMACS design was to minimize this problem, and this was achieved. As described in § 7.4.1, the rigid connection between the slit-mask mechanism and the principal and Shack-Hartmann guiders means that the flexure between slit mask and guider is less than $0.5''$ for a full rotation of the instrument. This was first verified in the lab during testing and then at the telescope. For 2–3 hr of tracking on a field there is negligible drift of the objects from their setup positions.

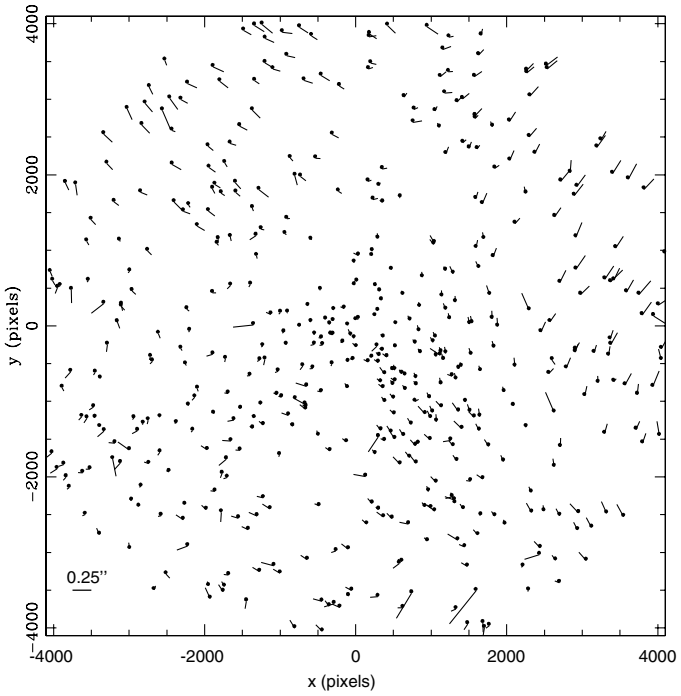

FIG. 15.—The distribution of residuals of target stars from the centers of their boxes, magnified by a factor of 100. A vector of 0.25″ is shown for scale, at lower left. Large displacements are seen in the upper left of the field and, to a lesser extent, to the lower right, correlated on scales of ∼2000 pixels or 5–10′.

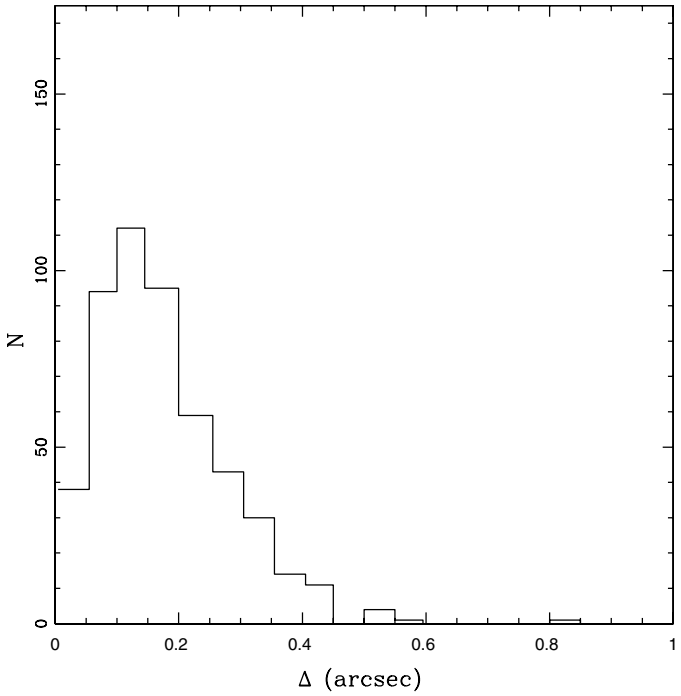

FIG. 16.—Distribution of the displacements of 503 stars from their box centers, the data of Figure 15. The median residual of 0.12″ is acceptable for IMACS multislit observations, but the long tail of residuals up to 0.6″ is not.

6.5. Flexure between Focal Surface and Detector

The amount of flexure in the optical train that causes the drift across the detector—even if the guider succeeds in holding objects at a fixed location in the focal surface of the telescope—is another critical issue that limits performance, by reducing the exposure time over which a direct image or spectrum will remain as sharp as the optical system can deliver. Once the physical size constraints for optics, dispersers, and the instrument itself were set, this requirement drove the IMACS design more than any other single issue. As described in §§ 7.2 and 7.3, IMACS was designed to be a kinematic structure (no overconstraints), the main optical components were mounted at their centers of gravity, and unavoidable cantilevers were kept as short and stiff as possible. Detailed finite element models were made for all critical components of IMACS. The result of this considerable effort was remarkable and unprecedented for an instrument of the size of IMACS: an object held at the focal surface of the telescope moves on the mosaic detector, for either the f/2 or f/4 optical train, $\sim 0.3'' \times \sim 0.6''$ for a full rotation of IMACS.

Not anticipating that the flexure could be reduced to this degree by purely mechanical means, we fitted each mosaic array camera with a Physik Instrumente piezo stage that carries the detectors and allows for ± 7 pixels of translation in x and y, described in § 8, and made provision to implement both open-loop (lookup table) and closed-loop (image monitoring) correction as IMACS rotates. We have in fact implemented the open-loop correction and reduced the flexure for a full rotation to about $\sim 0.3''$. For practical purposes, flexure over any single IMACS observation is nil.

6.6. Fringing with the SITe and E2V CCD Detectors

Both MOSAIC cameras in IMACS exhibit some amount of fringing in the 0.75–1.0 μm wavelength region, an effect that arises from alternating constructive/destructive interference in the first, relatively transparent (in the infrared) layer of the CCD. The E2V devices are deep-depletion CCDs, which means that this layer is relatively thick, which should minimize the effect. However, the amplitude of fringing is similar in the two cameras. The Mosaic-2 camera is only $\sim 1\%$ up to ~ 7000 Å, but increases steadily to a maximum of $\sim 10\%$ further to the red. The SITe CCDs are of the more conventional type, thinned in a proprietary process. Similar to Mosaic-2, the fringing of Mosaic1 also becomes noticeable at $\lambda > 7500$ Å and reaches a maximum peak-to-peak amplitude of 6–7% at 8500–9000 Å. Even at these amplitudes, fringing is a minor issue in data reduction, demanding no great wavelength stability in spectroscopic flat fields (that is, a careful matching the pixel wavelength for the flats and the observations is not required). The weak fringe pattern seen in direct imaging can be removed by dithering and stacking sky exposures to make a so-called

superflat and treating the fringe pattern as an AC component that needs to be scaled and subtracted from the data frames.

6.7. Throughput in Imaging and Spectroscopic Modes

The throughput of the f/2 and f/4 optical trains of IMACS, including the three telescope mirrors and ADC/corrector, has been monitored through observations of Hamuy spectroscopic flux-standard stars taking through a 7″ diameter circular aperture carried in the center-field slit-viewing guider. Equal-length sky exposures were made at the time of the observations. Data were processed using the IRAF routines `standard` and `sensfunc` and converted to values of quantum efficiency with a script written by Mark Phillips.

The throughput curves are shown in Figure 17 for the spectroscopic mode of f/2 and in Figure 18 for f/4, for a variety of grisms and gratings. The curves show the typical performance between primary and tertiary mirror cleanings and washings (a 2 yr cycle). Throughputs in imaging mode are generally given in magnitude zero points (see preceding discussion and the IMACS User Manual), but can be inferred from Figures 17 and 18 by assuming grism efficiencies of ~75–80% and grating efficiencies of 70–75%.

The performance of other low-to-medium dispersion spectrographs on other large telescopes is conventionally given in terms of spectrograph throughput only, not including telescope optics. In order to back out the Baade optics, a mean value of 85% reflectivity has been assumed for the three mirrors. (M2, downward looking, tends to be higher than M1 and M3, and values start at ~92% at recoating and drop 75–80% at the end of a cycle.) An attenuation of ~5% is assigned to the ADC/corrector, although arguably this is as much a part of IMACS as the telescope, since it is required by IMACS alone. All these factors combine to a typical throughput of ~60% for the optics feeding IMACS, which means that the throughput of IMACS itself peaks at well over 50% for the f/2 side and ~40% for the f/4 side, the principal difference being the higher quantum efficiency of the E2V CCDs, compared with SITe CCDs. The latter is comparable with that of the GMOS spectrograph (Hook et al. 2003), a spectrograph with an order-of-magnitude-smaller field, and also comparable or higher than DEIMOS and VIMOS, the other wide-field spectrographs on 6–10 m class telescopes, which have only reported fragmentary results at the time of their commissioning.

6.8. Autofocus

The Magellan Shack-Hartmann system, which continually monitors optical performance at each of the telescope ports, accurately adjusts telescope focus during the night. Thus, the focusing of the telescope during an IMACS multislit observation, for example, is assured by this system.

What remains is to keep IMACS itself focused: that is, to make sure that images at the focal surface will be in focus

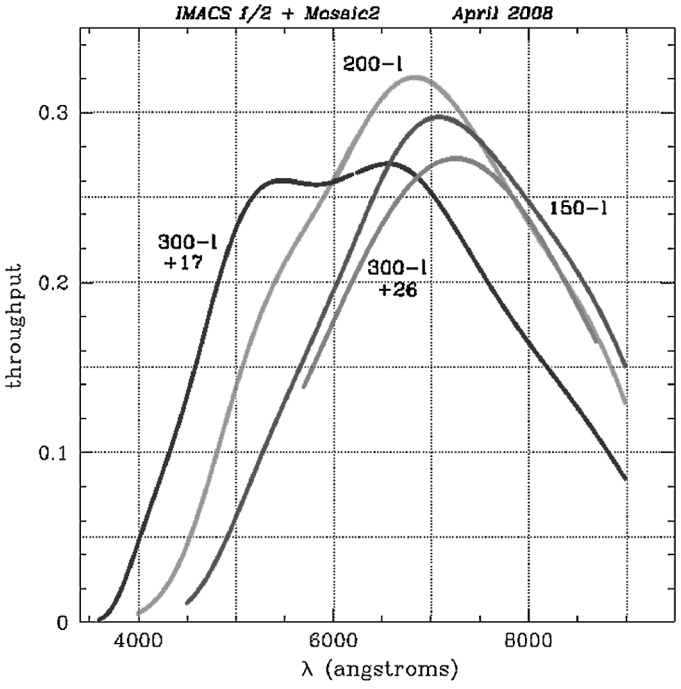

FIG. 17.—The throughput of the f/2 optical train, including Baade telescope mirrors and the ADC/corrector. The attenuation of the atmosphere is not included—the curves are for zero air mass.

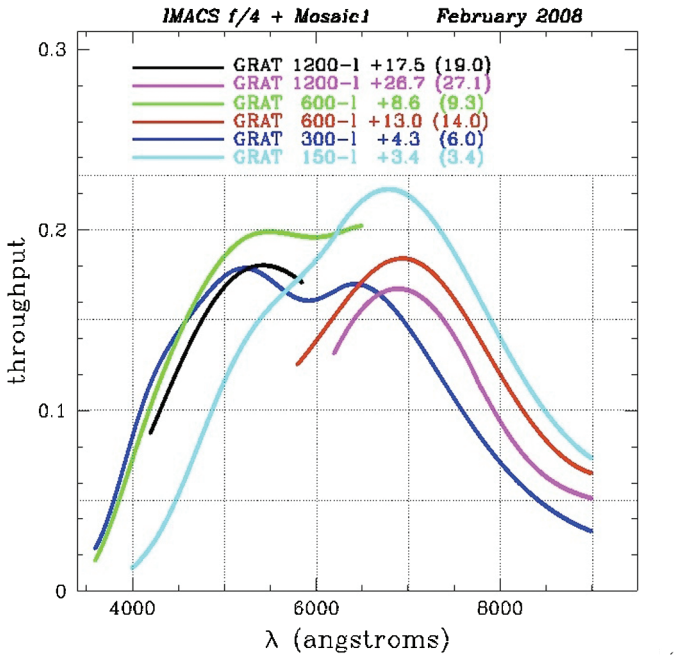

FIG. 18.—The throughput of the f/2 optical train, including Baade telescope mirrors and the ADC/corrector. The attenuation of the atmosphere is not included—the curves are for zero air mass.

on the detectors. This internal focus is affected by changing temperature within IMACS, in response to ambient conditions, and by the introduction of different optical elements, such as filters, which also vary the optical path length. An early design goal of IMACS was to have this be done as automatically as possible, with little-or-no intervention required from the observer. In order to help deal with temperature variations, a large number of temperature sensors were installed throughout the instrument, on optics and structure, which provide a constant data stream that is monitored and logged. When combined with simple equations that predict expected changes in focus for the collimator and cameras, the IMACS operating system sends continuous updates to the mosaic CCD cameras, each of which is equipped with a flexure that allows the CCD package to be moved in piston only to adjust the focus (see § 8 on the mosaic CCD cameras). In practice, the focus offsets of all filters used in IMACS are measured relative to the Bessel-R filter, and these are automatically included in the calculation when a filter is selected.

Over the years of IMACS operation, we have found that the predicted season-to-season variation of the focus, corresponding to full temperate range of approximately 0°C to 20°C, are in fact correlated with the focus actually determined with a pinhole mask, but not well enough (with too much scatter) to operate IMACS throughout the year using only the autofocus feature. However, over a period of days or even weeks, the differential changes in focus do track the predicted focus quite well. Therefore, common practice is to remeasure the focus at the beginning for each new observer and adjust the master offset as necessary at that time. Then, during observations throughout the night(s) of the run, the autofocus feature successfully adjusts the focus in response to temperature fluctuations and, of course, the differences from filter to filter. Observers can turn off the autofocus feature, but they are strongly advised not to.

6.9. Point-Spread Function and Scattered Light

The point-spread function for the f/2 and f/4 channels (Fig. 19) was determined by co-adding ~20 well-exposed images from through a pinhole mask with ~0.30″ diameter apertures. The IRAF subroutine `qphot` was used to measure the light within apertures of increasing size. Both cameras produce images with well-defined cores—0.35″ for the f/2 channel and 0.30″ for f/4. However, as is typical for optical trains with many refractive and/or reflective elements, a small fraction of the light scatters to much larger radii. In both IMACS channels, f/2 and f/4, 2% of the light scatters outside a diameter of 1.5″, with 1% scattered beyond ~3.5″.

In long spectroscopic exposures with many hundreds of slits (summing to a comparatively large area of sky), scattering of 1–2% of the total light passing through the slits can be seen as a diffuse background over the field. We assume that this is the result of the overlapping of individual cases of wide-angle scattering of the point-spread function, as seen in Figure 19.

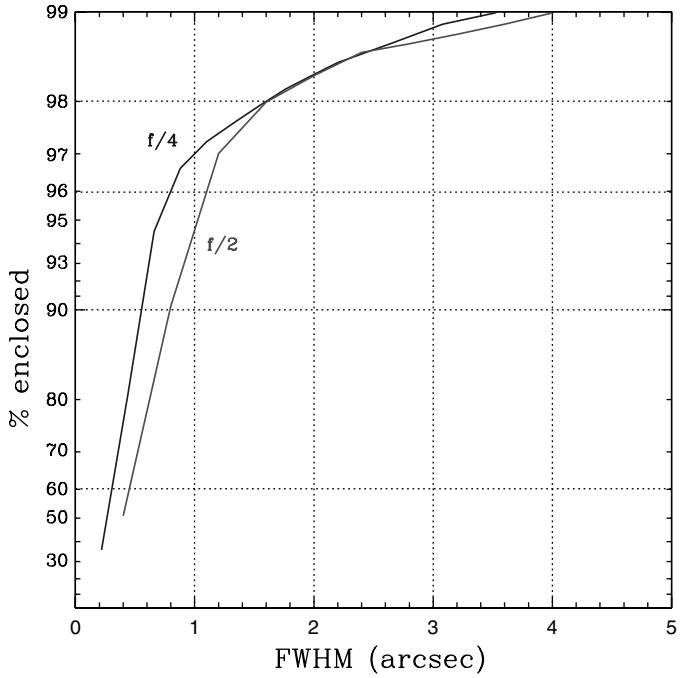

FIG. 19.—The point-spread function for the f/2 and f/4 channels of IMACS. The data show the wings in the light profile of 0.30″ FWHM (f/4) and 0.35″ FWHM (f/2). For both channels, 2% of the light scatters to a diameter greater than 1.5″, with 1% outside of a 3.5″ diameter.

Generally this is removed in the process of sky subtraction, but strictly speaking, there may be small errors introduced in spectrophotometric measurements.

6.10. Ghost Images

Harland Epp's optical designs for the f/2 and f/4 cameras included the minimization of ghost images. In addition, the mechanical design process paid particular attention to the attenuation of light that scattering off the walls of the optics cells; our solution was to insert sets of thin, concentric rings rings separated by spacers in key sections of the cell walls (see § 7.3). These measures appear to have been largely successful. For example, a 6 mag star imaged at a position near the center of the f/2 field produced only one significant ghost containing ~2% of this light level, split between a 40″ diameter disk with an 80″ halo. This ghost is basically round when the star is close to on-axis, but becomes trifoil-shaped as the star is moved outward in the field. Accurate photometry would not be possible on a long exposure within this ghost image or, of course, around an equally large region $r < 100''$ of scattered light around the star itself, but aside from these comparatively small regions, the full image is relatively uncontaminated.

In the case of multislit spectroscopy, with a sufficiently large number of slits, faint ghost images of the brightest night-sky lines from one spectrum (in particular, λ5577) fall on the spectra of others objects. These present problems for data reduction that are much like those associated with the zero-order image of one

spectrum falling on the first order image of another. Generally, such problems can be ignored because the loss of spectrum is so small, however, it is possible in a case-by-case basis to remove such contamination if the importance of the spectrum warrants the effort.

Since IMACS is used primarily for spectroscopy, many fewer deep, direct images have been taken, particularly in fields of low Galactic latitude. With that qualification, there have been no reports of significant glint—light from bright stars outside of the IMACS field, which is baffled inside the telescope at 30′ diameter.

6.11. Reliability

The overall reliability of IMACS has been very good: an average of 1.0% of observing time (with a dispersion of 0.6%) has been lost to instrument failures in the 10 scheduled semesters of 2006–2010. Most of this time has been lost to mechanical malfunctions, as described subsequently.

It is best to start with what has proven to be completely reliable. The mosaic CCD cameras have operated more-or-less without fault, although there has been a little time lost due to problems with the CryoTiger systems that provide cooling for the CCDs. Keeping this system running properly is an ongoing concern. In the first few years some time was lost because of leaks in the fittings of the glycol circulation system that cools the CCD electronics, but this problem appears to have been solved.

Computers, software, and firmware have also performed with great reliability, with occasional problems with cabling and communications devices. Because IMACS is always connected, it does not suffer from the usual ills of instruments that must be continually cabled and uncabled, but there are so many cables for IMACS, running through a challenging cable wrap, that the few incidents per year are not surprising. These have generally not resulted in lost observing time, although some number of hours per year has been lost due to communication errors between the DSP (CCD controller) and data-acquisition computer.

The IMACS shutters and three guiders have been reliable, with little time lost, although there were incidents with both devices in 2007–2008 that cost some hours on a few nights. These problems have been corrected with improvements in the mechanics of the shutters and in the encoders of the guiders.

Most of the ∼1% of observing time lost each year can be attributed to malfunctions of the mask server, the filter servers, and disperser server, in that order. The special requirements of IMACS necessitated the building of each of these systems with little heritage from previous Carnegie instruments. In particular, robust and reliable filter wheels have been a staple of previous instruments, but the physical constraints and the requirement of many filters made this impossible and instead necessitated a jukebox style, for which we had no experience. The problems associated with the filter servers and mask server, which share many characteristics, relate to trying to guide a loosely constrained filter or mask into a tightly, kinematically constrained location in the optical path. We have been surprised how difficult, from the start of routine operations in 2004, it has been to make these devices truly failure-proof over the full range of orientations with respect to gravity. Improvements were made in 2005–2006 that significantly improved the reliability of each filter server. The mask server, which had worked very well in the first few years, became less reliable over 2007–2008; modifications in the mask frames, guides, and latching components were made during 2009 to fix these problems. Both mask server and filter servers are now more reliable, but their operation has not become trouble-free. From our experience with these devices, future designs would not include a loose-to-tight philosophy, but would seek to control position accurately throughout the operation.

The disperser server, including the grating tilt mechanisms, is the most complex and novel part of IMACS. Because it moves heavy components off of the wheel and onto the spectrograph, completely releasing contact, it was challenging in design and execution. The disperser server rarely fails altogether, but from time-to-time it refuses to install a disperser unless the gravity angle is changed, which wastes time. This problem continues to draw attention now and then, but no fix is apparent.

Our credo is that any time lost due to instrument failure is too much, so we have continued to work toward complete reliability, no doubt unrealistic for an instrument of such size and complexity. The Magellan partners have agreed that a partner institution that has contributed instrumentation will continue to provide technical support for anything more than routine maintenance and minor adjustment. This departs from the practice at most observatories where responsibility for the instrument—after commissioning—passes primarily or fully to the onsite operation. Although such shared responsibility presents some unique challenges, one positive aspect is that a small team of Carnegie support people in Pasadena has been able to continue its attempt to perfect IMACS.

7. THE DESIGN, FABRICATION, AND ASSEMBLY OF IMACS

The majority of IMACS parts were manufactured in Pasadena, California, at the Carnegie Observatories's shops. Exceptions were the main structure, manufactured at Martinez & Turek, Inc., in Rialto, California, and the lenses of the major optical components, most of which were fabricated at TORC Industries in Tucson, Arizona. Assembly and testing were carried out exclusively in the Carnegie shops.

7.1. The Design of IMACS

A rough description of IMACS was sketched out in 1996, but the design began in earnest in 1997. Wide-field imaging and

mulitslit spectroscopy had been identified as core capabilities, with high-resolution imaging and high spectral resolution as secondary, yet still important, goals. The approximate envelope of the spectrograph was already set by the f/11 collimator that had been designed in concert with the Gregorian secondary and ADC/corrector that would feed the wide-field Nasmyth focus. It was clear from the start that the instrument would extend further than the existing Nasmyth platform, into an empty space between it and the enclosure, and that the platform would require structural reinforcement. Furthermore, the radius of the instrument structure, which must rotate with the telescope field of view, would be close to the height of the elevation axis above the platform, if guiders were to be placed on the perimeter of the $1/2^\circ$ diameter science field provided by the corrector. Although the goal was for a fast camera to access this entire field, it was soon clear that this would be a very challenging camera to design and build. Furthermore, a camera made to address the full field would not also be able to take full advantage of the best images the telescope could offer if the full field was addressed. For both these reasons, a slower f/4 camera was envisioned that would be easier to build and offer FWHM $\lesssim 0.2''$ FWHM images over a smaller, though still substantial, field. This camera would be relatively long and mounted at a spectrograph angle of $\sim 45^\circ$ (with the faster camera mounted axially), which further challenged the diameter restrictions of the basic layout.

Another important goal of the mechanical design was for minimum flexure, to be met by balancing the optical components and limiting the moments that would be applied to the optics support structure. A combination of plate weldments and space-frame elements was thought to be best suited to achieving this, as shown in the first paper on IMACS by Bigelow et al. (1998). Figure 4 of that paper shows that IMACS was originally conceived as a cantilevered cylindrical structure attached to the Nasmyth rotator, with some sort of final bearing to take the instrument's end weight. However, early analysis showed that it would be difficult to make such a structure quasi-kinematic. Large support forces carried in this manner would likely result in significant unintended forces from the support rollers that would distort the structure. This led to the idea of a system largely decoupled from the Nasmyth rotator and supported by its own carriage mounted on the Nasmyth platform. The carriage would support the instrument structure with four rollers bearing on the machined rims of the two disks. With Z defined as the elevation axis, the rollers would constrain four degrees of freedom: X and Y translations and rotations about the X and Y axes. To minimize any overconstraint, the rollers were designed to be self-steering, using a castering principal that would prevent the wheels from scuffing due to imperfect alignment. By eliminating this force, the four-roller system would behave quasi-kinematically, with each roller essentially defining a single degree of freedom. The remaining two degrees of freedom (Z translation and rotation), are defined by the telescope Nasmyth rotator via two additional links. Finite element analysis showed great promise for this design solution, since all flexure would be due only to rotation in the gravity field (with no coupling of moments to the telescope structure) and therefore small and repeatable. As described in § 6.5, the success of this design, which essentially eliminated flexure, exceeded our expectations.

Other design goals included the permanent mounting of IMACS on the telescope, with little of the connecting and disconnecting of cables that can contribute significantly to the malfunction of astronomical instrumentation. Mechanical reconfiguration—filters, slit masks, gratings, etc.—should take less than a minute per operation and should be done in parallel rather than sequentially. Of course, the intent was that mechanisms would be robust and nearly trouble-free but, like most devices full of prototypes, this proved elusive. Accommodation was to be made, as much as possible, for users to add to IMACS to augment its capabilities. Despite its complexities, IMACS was intended to be easy to configure and operate—and it is.

7.2. Tooling and Metrology

An important aspect of the IMACS design, fabrication, and assembly strategy was to minimize the number of mechanical and optical alignment adjustments. Providing numerous adjustment features complicates the design process and results in additional parts to fabricate and additional alignment steps to carry out in assembly. By carefully holding tight tolerances in fabrication, and by using simple metrology systems during assembly, we attempted (and, in general, succeeded) to limit the total number of manual alignment and adjustment steps. A few exceptional cases are described subsequently.

The collimator and f/2 and f/4 cameras were all designed to allow one-time manual adjustment of lens spacings only, by controlling the thickness of a small number of flat-ring spacers between lens groups. The spacing adjustments were provided so that the optomechanics could be fabricated in parallel with the lenses. Small fabrication errors in radii of curvature and center thickness for each lens were folded into an as-built version of the optical prescription, with spacings as the only remaining free parameters. In most cases, the initial spacer thicknesses were within the tolerance allowances and no additional spacer changes were required. The primary exception among the main optical systems was the f/2 camera, which utilized two aspheric lenses, both of which were accepted based on mechanical, versus optical, metrology. Focal-plane tilt, coma, and, to a lesser extent, astigmatism in the f/2 focal plane were ultimately corrected (and nearly brought to as-designed image quality) by radial and axial adjustments of the last lens (S09) and by tilting the detector system with respect to the camera optical axis. In this case, better metrology of the aspheres would probably have avoided the need for the compensating adjustments, but the cost of optically qualifying the two aspheres was deemed excessive at the time of their fabrication (optical tests would have essentially doubled the cost of each asphere).

Although the field lens and collimator lens groups were fabricated and mounted separately, the two optical systems work together to reimage the telescope's exit pupil. The tolerance allowance on the spacing between the field lens and the collimator lens assembly was only a few thousandths of an inch and was therefore not controllable within the manufacturing errors of the optomechanics and the instrument structures. In this particular case, a precision metrology device was designed and manufactured by Bal-Tec.[21] The measuring bar consisted of an Invar rod, with a precision-diameter ball attached at each end. One end included a micrometer head, which allowed precise and well-calibrated length changes between the two balls. In this way, the ball-bar could be positioned between the two opposing vertices of the field lens and first collimator lens, and the bar length extended until the end balls were in contact with both lens vertices. A measured spacing error could then be corrected with the ring spacer between the collimator mounting flange and the instrument structure (MOSS). In final assembly, the spacing was measured to be within tolerance, and the collimator barrel spacer was used in the as-designed thickness.

The single largest metrology challenge in IMACS was posed by the instrument structure, in particular, the MOSS. This single large weldment determines the axial alignment of the collimator, both cameras (f/2 and f/4), and the mounting interface for the pupil optics (gratings, grisms, and low-dispersion prisms). The mounting of the MOSS structure in the rear disk of the main instrument structure (the MOSS disk) determines the location of the collimator and f/2 camera axes with respect to the rotational axis of the instrument. A decentering error between the MOSS and MOSS disk would result in vignetting at the pupil that varied with instrument rotator angle. Angular alignment errors between the MOSS and MOSS disk would result in misalignment of the pupil optics and cameras, which would negatively impact final image quality in both cameras. The fully assembled IMACS structure is approximately 2.5 m in diameter and 4 m long, which puts it well outside the metrology capabilities of most telescope instrument facilities. For this reason, the acceptance metrology of the structure was contracted to an independent metrology specialist. An unfortunate consequence of this approach was that fabrication and/or assembly errors in the structure, while possibly evident in the metrology report, were not noticed and resolved until installation of IMACS on the telescope. Modern laser-based metrology systems (laser trackers)—not readily available around 2001—would have made the acceptance metrology of the IMACS structure much more straight-forward and robust.

7.3. The IMACS Structure Assembly

Figure 20 shows the fully assembled IMACS at the Baade telescope with most enclosure panels removed. The key elements of the IMACS structural systems are the carriage, the main structure, and the MOSS, which carries the majority of the optical subsystems. The instrument team adopted specific design criteria for the instrument structures: quasi-kinematic structure and support of optics; design for minimal tilt deflections; design for low hysteresis; avoidance of multiple alignment degrees of freedom; and combination of monocoque and space-frame structures. The detailed design and analysis of the structures, including the carriage, castering roller assemblies, main structure, and main optics support structure, were all carried out by Steve Gunnels of Paragon Engineering (Westcliffe, Colorado). Paragon also provided the design and fabrication of the 31 insulated aluminum-skin panels that together form the instrument thermal enclosure and shield the optical elements from external stray light. The instrument thermal controls and enclosures are also supported by the main structure and hence are discussed in the sections that follow.

7.3.1. Instrument Carriage

Nasmyth-focus instruments on altitude-azimuth telescopes must provide for field rotation about the elevation axis. IMACS accomplishes this by supporting a rotating structure on four rollers, two under each of the two large disks that define the main structure. The rollers are mounted on the instrument carriage.

The carriage provides the primary structural interface between the IMACS instrument and the Magellan-Baade telescope. A monolithic plate weldment, the carriage, and its associated moving parts were fabricated by Rettig Machine, of Redlands, California (see Fig. 21). The carriage bolts at its four corners to the Baade west Nasmyth platform. It provides, via the four-roller assemblies, four of the six constraints that kinematically define the position of the instrument as well as possible with respect to the telescope. The last two degrees of freedom, rotation of the instrument around the elevation axis and translation along that axis, are provided by the Nasmyth instrument rotator through flexured rods designed to constrain one degree of freedom each.

Several of the Magellan facility instruments are mounted directly to an instrument rotator on the telescope optics support structure. In the case of IMACS, the mass (~6000 lb) and resulting moment load applied by the instrument to the telescope instrument rotator would have exceeded its capacity. Similarly, the Magellan Nasmyth platforms were not originally designed with for such a large instrument, and therefore the platform supporting the IMACS instrument was structurally reinforced prior to installation of the instrument. Overconstraints caused by friction, imperfect alignment, or tracking errors at the rollers would tend to distort the main structure and hence contribute to flexural image motion. For this reason, the four-roller assemblies are mounted on pairs of rod flexures, which allow the support roller assemblies to self-align and caster with respect to the mainframe disks. Preload springs balance the roller assembly mass on their flexures to compensate for the effect of gravity acting on the tilted unit. When the direction of rotation of

[21] See http://www.precisionballs.com/.

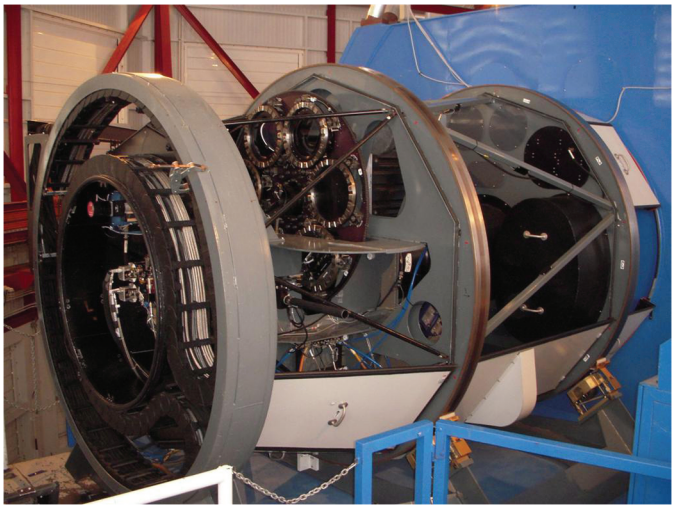

FIG. 20.—IMACS installed at the west Nasmyth platform of Baade, with most of the enclosure panels removed. This photo shows the carriage with its self-steering rollers supporting the rotation IMACS structure assembly. The rotating assembly consists of three sections. (1) Main structure—two monocoque disks (FOSS and MOSS) connected by the gray square-tube main truss. This section encloses the collimator and its baffle and the f/4 train: filter server, shutter, f/4 camera, and Mosaic-1 CCD camera (all far side, not visible). (2) Forward compartment, the short projection from the FOSS disk to the Nasmyth instrument rotator. This section encloses the field lens, the mask server, the three guiders, and the calibration unit. (3) Aft compartment—the secondary truss (*black bars*) supports the cantilevered, rotating portion of the utility wrap at the back of the instrument. In this section is the MOSS box, the weldment to which the collimator and f/2 and f/4 cameras are attached—in other words, the spectrograph. Also visible is the primary structure (wheel) of the disperser server; the gratings and grisms face forward and are identifiable by the index rings used to latch a selected unit to the spectrograph. Also enclosed in the aft compartment are the f/2 train: filter server, shutter, f/2 camera, and detector. The filter server and detector are slightly visible within the utility wrap.

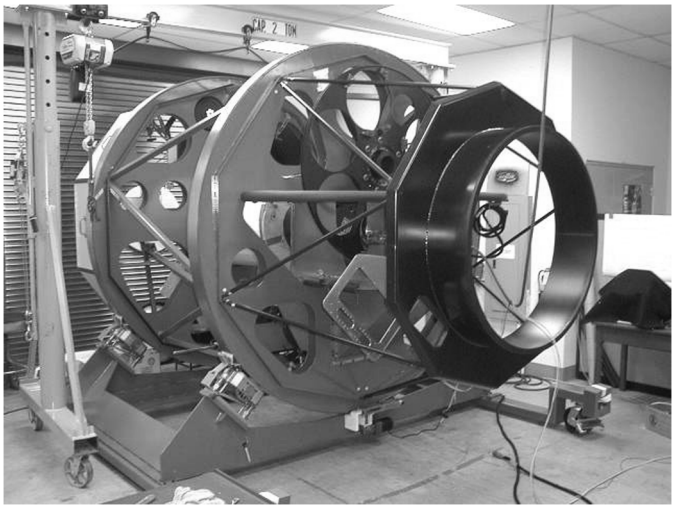

FIG. 21.—An early stage of assembly of IMACS in the Carnegie Observatories shops. This photo shows the carriage, with its self-steering rollers supporting the rotating part of the IMACS structure assembly. The rotating assembly consists of two monocoque disks connected by the main truss, the secondary truss (*black*) supporting the cantilevered rotating portion of the utility wrap, and the MOSS. Also visible in the photo is the primary structure (*wheel*) of the disperser server that carries the spectrograph dispersers and accessories.

IMACS reverses, the rollers translate slightly to affect a toggling between two opposing pivot points for the castering action. A roller assembly (carrier, roller, flexures, and pivot points) is shown in Figure 22. Although not shown, scrapers lined with replaceable plastic blades help to reverse the castering when the rotation of IMACS changes direction, and they also keep the rollers and disk rolling surfaces clean in the presence of dirt and dust in the dome.

7.3.2. Main Structure

The instrument main structure is a single weldment of two large disks joined by a connecting truss (see Figs. 20 and 21). The disks are approximately 2.5 m (100 inches) in diameter and are constructed as light plate weldments. The connecting 10-bay truss is made from 1-3/4 inch (45 mm) square tubing. The low-carbon steel main structure was fabricated by Martinez and Turek, Inc., of Rialto, California. Following final welding operations, the main structure was stress-relieved using vibrational methods. The combination of monocoque (disks) and space-frame (truss) structures provides an extremely stiff, yet lightweight, foundation for mounting of the remainder of the instrument subsystems. The front disk supports the three guiders and their wavefront sensors, the slit-mask server, the calibration system, the field lens, and the forward enclosure panels. The rear disk supports the main optics support structure (see subsequent details), the disperser server, and the instrument utility wrap (via a second 10-bay truss structure). Figure 23 shows the operational IMACS from the back.

The detailed design of the disk and truss structures was optimized using finite element analysis, to insure that image motion (flexure) contributions by the structure were within the allowances defined in the image motion error budget.

7.3.3. Main Optics Support Structure

The MOSS carries the refracting collimator, f/2 camera, and f/4 camera, as well as the fixed matrix ring that defines the installed position of the pupil optical elements (gratings, prisms, grisms, etc.). As with the instrument main structure, the MOSS was constructed by Martinez and Turek, Inc., as a single plate weldment and stress-relieved using vibrational methods. Following final welding and stress relief, the entire MOSS was final-machined in a single setup to ensure that the four mounting interfaces for the optics (collimator, two cameras, and dispersers) were coaxial (as appropriate) and properly aligned with respect to each other. The MOSS attaches to the main structure via bolted joints that were shimmed and pinned in the final

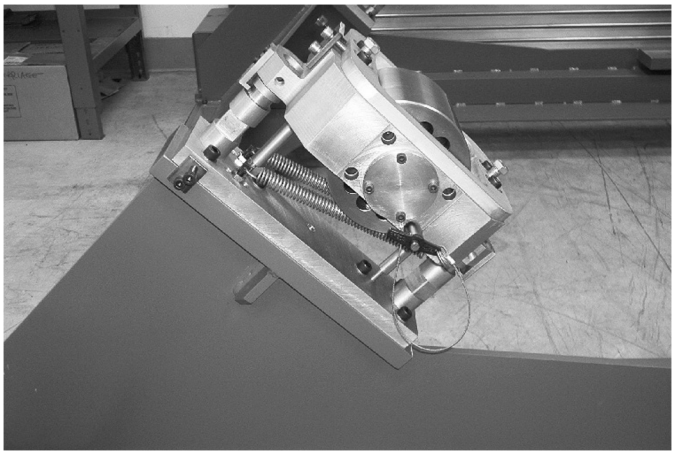

FIG. 22.—A self-steering roller assembly mounted on one corner of the IMACS carriage. The roller that bears against the IMACS disk is held in a rectangular frame that can toggle between two pivot points, causing the roller to act as a trailing caster for both directions of IMACS rotation. The switch between pivots is accomplished by the friction forces between the disk and roller when the rotation direction reverses and by additional frictional forces generated by the roller scrapers.

assembly of the instrument structure by Martinez & Turek.[22] Thus, there were no adjustment features provided for final alignment of the optical subsystems, only spacer rings for as-built adjustment of the individual spacings between the collimator and cameras. The bolted joints allowed the structure to be temporarily disassembled for transport in a single 8 ft × 10 ft × 40 ft commercial shipping container.

7.3.4. Enclosure Panels

The large disks of the IMACS structure are joined by a 10-bay truss of square tubes; a second truss projects back to the cable wrap instrument utility wrap. Various types of skins were considered to provide a thermal and light seal to enclose these elements, including panels linked together with hinges, metal, or plastic sheets to cover several sections at a time, or even the use of a fabric or other flexible material. In the end, we selected removable discrete panels that cover each of the main structure polygons separately. Paragon Engineering designed and fabricated composite panels using aluminum skins separated by a 20 mm sheet of CMI Divinicell foam insulation. PVC edge channels with integral seals (Trim-Lok extrusions) were used around the panels to seal the panels to each other and to the main structure. The front panels provide a light-and-dust seal between the IMACS front-structure (forward optics support structure [FOSS]) disk and the telescope instrument rotator. One of these panels includes a hinged door to provide access

[22] In fact, a manufacturing error left the MOSS box tilted with respect to the optical axis, a situation that was corrected with great difficulty when the alignment of IMACS was underway at the telescope.

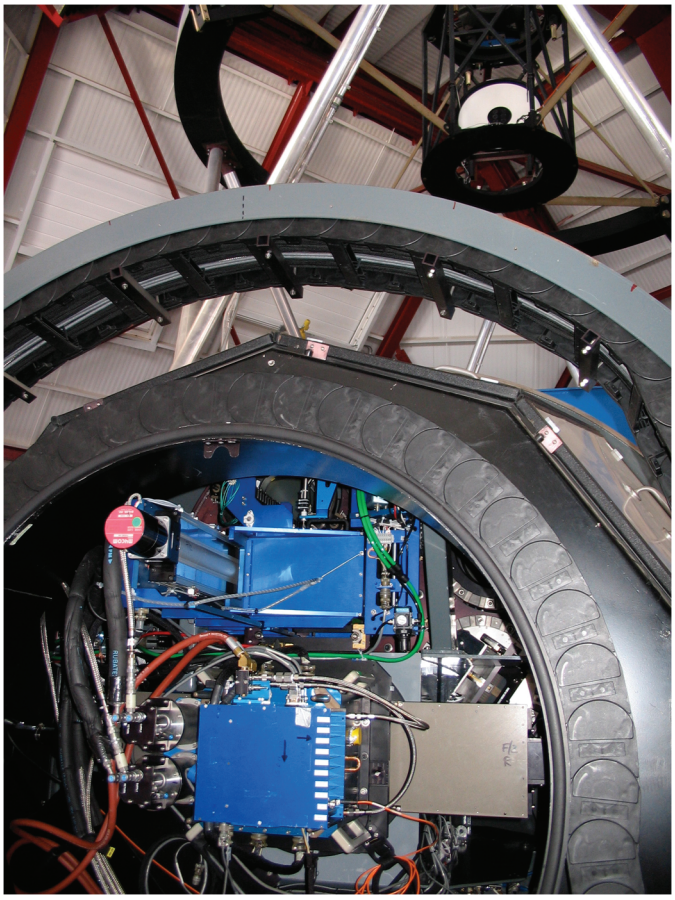

FIG. 23.—Rear view of IMACS, showing some f/2 components. Inside the inner race of the utility wrap is the f/2 filter server (*top*)—motor and stage to the left. The Mosaic-2 CCD camera is behind the blue electronics box in the center, with CryoTiger heads on the left and one side of the f/2 shutter to the right. Two index rings at the back of the dispersers are visible above the shutter. A large circular enclosure panel covers this whole area. Above the outer race of the utility wrap the Baade telescope structure and dome can be seen. The small black ring is the bottom of the cage of Gregorian secondary mirror, visible at top. The white doughnut is the pupil screen that is illuminated for flat-field observations, seen in its retracted position.

to the mask server. The center section panels enclose the volume between the two disks, and the trapezoidal rear panels enclose the conical volume between the MOSS disk and the instrument utility wrap. Center and rear panels also provide light-tight and dust-tight seals for the interior of the instrument. Four panels include extensions to provide clearance around the camera shutter actuators, and a separate small dome of the same materials covers the protrusion of the f/4 Mosaic-1 detector.

Each of the panels carries a set of four quarter-turn fasteners, which can be released with hand tools to remove a panel from the instrument. The best feature of this system has been the completely open access to IMACS—all panels can be quickly removed and reinstalled. The most difficult problems have been maintenance of the latches and seals and some surface damage

to the panels themselves—wear and damage that has accumulated from the hundreds of remove-replace cycles that most of the panels have experienced. Unfortunately, a panel is difficult to repair and requires the fabrication of an entirely new replacement.

The enclosure panels were designed and analyzed to verify that the panel materials and dimensions would meet the thermal stability requirements as defined by thermooptical analyses of the collimator and cameras. In addition to the insulated enclosure panels, the instrument volume is lightly pressurized with filtered dome air to expel dust, and fans circulate air within the enclosure to prevent stratification.

7.4. Optics

The usual parameters of element size, material availability, and transmission played a strong role in choices for optical materials. Another major factor driving the optical design was the large operational temperature range of -4°C to 20°C that is typical of the Las Campanas site. Both the f/2 and f/4 optical trains were designed to include compensation for thermally induced changes in focus and plate scale.

Descriptions of the optical elements can be found in Bigelow & Dressler (2003), along with a discussion of the optomechanical design and implementation. An important choice for optomechanical design was to rely on precision machining and dead reckoning instead of providing adjustments to lens position within each lens cell. Following a complete analysis of the error budget for each element, the optics were potted in their cells with sufficient accuracy to meet the requirements in center, axial position, and tilt. Typical requirements were ± 25 μm for centration and ± 25 μm in tilt over the diameter of each lens.

7.4.1. Optics Mounting

The lens mounts for the IMACS optics face a number of stringent constraints. The mounts must locate and support the lenses over a wide range of gravity orientations and temperatures, while maintaining the optical figures and alignment. The thermal environment dictates operation over a temperature range from -4°C to 20°C and a survivability range from -10°C to 30°C. Science requirements dictate that image motion stability be held to 0.1 pixels over the course of a typical exposure, for all allowed orientations with respect to gravity and the -4°C to 20°C thermal range. In all three optical trains (collimator and f/4 and f/2 cameras), oil coupling, and/or oil lenses add variable hydraulic forces to the list of loads. In order to meet what were often conflicting requirements, elastomeric mounts were chosen for the radial and axial support of all the science-path optics (with the exception of the field lens, described subsequently).

Elastomeric mount here means a room-tempeature vulcanizing (RTV) rubber ring that is cast in place between each lens and its cell. The width, depth, and material properties of the elastomeric ring can be varied for each lens (geometry and material) to meet the support requirements (in terms of radial, axial, and tilt stiffness) while maintaining low-stress support across the range of operating temperatures and orientations. A sequential process was used to design the width and thickness of each RTV ring. First, spreadsheet calculations were used to estimate width and thickness combinations, estimating changes in the effective stiffness and coefficient of thermal expansion of the RTV ring due to constraints on the (free or constrained) surfaces of the ring. Multiple load cases for each design were then optimized with finite element analysis to determine stress and stiffness in appropriate gravity, thermal, and hydraulic load cases. In keeping with our design goal of minimizing the number of parts in the instrument, a minimalist approach was used in the design of the cells and barrels. In particular, we did not design in the capability for individual alignment of each lens or group within a barrel or for each barrel within the instrument. Rather, the cells and barrels designs were kept extremely simple and held to tight fabrication tolerances following the optical design. The only degree of freedom left for compensation at final assembly was lens (or group) spacing, which was adjusted by changing the thickness of flat-ring spacers. The cell and barrel designs were toleranced such that the sum of the fabrication and assembly errors would meet the alignment error budget allowances.

We believe that the precision with which the radii of curvature of all spherical surfaces were known (from manufacture) justified this approach, and after assembly we indeed found evidence that further adjustments were not needed. However, there is good evidence that this method failed to meet specified optical performance in the case of the f/2 camera, where the two aspheric (bur rotationally symmetric) surfaces are located. In this case we believe that the failure of one or both of these elements to match the optical specifications is precisely the problem.

7.4.2. f/2 Camera Aspheres

The final f/2 camera design includes two elements with moderate asphericity on one side. These lenses were produced by Tinsley Laboratories, which used a high-precision mechanical profilometer for surface measurements during the final figuring. According to the report of profilometer measurements, the combined errors of the two aspheres should have contributed negligibly to any degradation of the image quality. However, actual performance of the f/2 camera at the telescope suggested that the specifications for at least one of these aspheric surfaces were not met. At installation, the f/2 focus of IMACS exhibited a tilted focal plane, coma, and astigmatism that increased the image diameters by 0.1″ to 0.3″ over the field. These aberrations were determined from out-of-focus doughnut images across the field fed to analysis programs written by D. Kelson. Subsequent remeasurements of the metrology of the f/2 camera elements showed no significant centering or axial displacement errors, so the likely cause of the aberrations is, we think, the figure of one or perhaps both aspheric surfaces. We compensated

the for tilted focal plane and coma by shimming the mosaic CCD camera and repositioning the field flattener (S09) axially and radially. Some significant astigmatism remains, but the camera performance is now very near the design specification of images FWHM < 2 pixels (0.40″) over more than 80% of the field (see the IMACS User Manual).

7.4.3. Field Lens

Since the field lens is positioned very close to the focus of the telescope, wavefront aberrations have a weak influence on the image quality. Consequently, the project used a comparatively economical grade of Dynasil fused silica, guaranteed to have low numbers of occlusions and bubbles. A favorable opportunity at Contraves-Brashear Systems led to a lower cost of fabrication than had been expected. Since the field lens is 651 mm in diameter, standard interference coatings would have been expensive to apply and difficult to remove in the event of a coating-chamber accident. We instead chose have the field lens dip-coated in SolGel by Clevelend Crystal. Except for one unfortunate scrape that occurred during a maintenance procedure, the fragile coating has held up well over nine years. It has been effectively cleaned by an acetone flush on three occasions.

7.4.4. Focus and Scale Compensation

Thermooptical effects in the f/11 collimator are small, compared with those in the two cameras. Rather than thermally compensating the collimator as a standalone optical system, the collimator temperature effects were folded into the cameras for the purpose of temperature compensation.

For the f/4 camera, compensating for temperature could be effected by adjusting the detector focus. However, since the design is not telecentric, moving the focus also results in an undesirable plate-scale change. This was compensated by moving the largest CaF2 singlet axially, in conjunction with a simultaneous change of detector focus. Since the required motion with temperature was too large for passive compensation (e.g., via a simple high-CTE spacer), the CaF2 singlet cell was articulated with respect to the barrel, using three flexures. Three small DC servo motors from Physik Instrumente were used to actuate this element over a piston range of ∼1 cm. The three actuators also enabled tip/tilt of the CaF2 singlet, which could have been useful for flexure compensation in the f/4 camera, but this capability was never needed. Furthermore, after some years of operation, the IMACS team and users decided that articulating the CaF2 singlet for scale invariance was unimportant, considering the capabilities of the data-reduction routines, and the remaining articulation feature (piston) was disabled.

Due to the large path length in CaF2 in the f/2 camera, the relatively simple temperature compensation scheme used for the f/4 camera was inadequate. In the early optical designs of the f/2 camera, acceptable optical performance was not obtained over the full operating temperature range, even with controlled axial movement of several elements in the camera. However, Epps and Sutin (2003) proposed that, since the large elements in the multiplets needed to be optically coupled using a fluid in any case, this fluid could be used to improve thermal compensation. In general, fluids have very different thermooptical behavior than solids, and this additional degree of freedom gives the optical designer more options. For a horizontal optical system, the pressure head due to the fluid is the same regardless of the size of the gap between the lenses; however, the final lenses required a large amount of fluid that necessitated large reservoirs to account for thermal expansion of the comparatively large volume of couplant. The final design does in fact only require motion of the detector position to compensate for temperature, and this motion does not result in a change of scale. As bonus, use of the liquid lenses allowed Epps to remove one of the three aspheres in the original design, with negligible loss of performance. Cargille LL-5610 was chosen as the oil couplant for the collimator and cameras; samples were sent to the Ohara Corporation's precision measurement laboratory, where the index of the fluid was measured at wavelengths and temperatures covering the full operating range of the instrument.

7.4.5. Optical Coatings

The transmitting and reflecting optics in IMACS provided a wide range of optical coating challenges. In terms of size, the ∼600 mm diameter field lens was the most challenging. The number of coating companies with appropriately sized coating chambers was very limited, the risks associated with heating and cooling such a large lens were substantial, and the consequences of a dielectric coating accident (removing well-adhered dielectric coatings would require regrinding and polishing of the optical surfaces) would be serious for the project in terms of budget and schedule. In the end, we selected the SolGel coating method for the field lens, applied by Cleveland Crystals.[23] Cleveland Crystals also designed and fabricated specialized shipping and handling tools for the coated field lens, which were reused later in the integration, shipping, and final installation phases.

Two different coating designs were required for the f/2 and f/4 cameras, the latter being designed to work further into the ultraviolet, $\lambda \approx 3500$ Å, compared with the ∼3900 Å cutoff of the f/2 camera. The collimator—feeding both—received the f/4 prescription. For the collimator and camera lenses, which ranged in size from 200 mm to 350 mm in diameter, the highest coating risks were associated with the two f/2 camera aspheres and the CaF2 optics. As with the field lens, a dielectric coating failure could easily have required regrinding and repolishing of the affected surface(s), which would seriously impact the

[23] See http://www.clevelandcrystals.com.

project budget and schedule, especially in the case of the aspheres. Dielectric coating processes requiring elevated temperatures posed an extra risk for the many CaF2 lenses, due to thermal shock sensitivity of that material. Based on such considerations, we chose Spectrum Thin Films[24] (STF) to apply the coatings on the remaining IMACS optics, using a low-temperature, ion-beam-assisted process (ion beam sputtering). We discovered some time after the lenses were coated that fluoride compounds were used in the coating prescriptions and that these compounds were extremely sensitive to damage by high humidity and condensation. In the case of the dewar window, which experienced multiple condensation events (due to radiative cooling from the cold detector array), the original coating failed (in both transmission and adhesion) and the lens had to be reground, repolished, and recoated. During the lens repair process, STF developed a high-transmission hydrophobic coating, which was then applied to the repaired dewar window.

The main reflective coating required in the IMACS science optics was for the imaging mirror for the f/4 channel. The imaging mirror resides in the disperser server; when installed at the pupil, it folds the collimated beams into the f/4 camera. Two mirrors were fabricated, one coated with bare aluminum and the other with the SilverStar-protected silver coating by the Denton Coatings Group (now Quantum Coatings, Inc.[25]).

As described in § 9.1, a large freezer was built around IMACS with the primary purpose of testing mechanical functions at subfreezing temperatures. These tests were generally successful, but we found it difficult to keep the enclosure dry enough to prevent some condensation on the optical elements. The result of one particularly wet incident seemed to be the slight fogging of some of the exposed surfaces that had been antireflection coated by STF, who subsequently informed us that these coatings were subject to hydroscopic damage. With respect to final performance, our goal was to achieve a cumulative loss of $<10\%$ in throughput for each major component—the collimator, f/2 camera, and f/4 camera, based on a $\lesssim 1\%$ loss per surface. Although it was difficult to assess the amount of damage caused by the hydrating of the coatings, we believe this is the principal reason that the throughput is between 85–88% for each of these optical assemblies.

7.4.6. Filters

A wide variety of wideband, narrowband, and order-sorting filters are required for the multiple operating modes of the f/2 and f/4 cameras. Both cameras were designed to use a standard-sized filter ($165\ \mathrm{mm} \times 165\ \mathrm{mm}$). As some of the filters used colored glass substrates with varying indices of refraction, the designs for the filters attempted to maintain a constant optical path length. Even with a best effort in this respect, we found sufficient variation in the optical path length to require a lookup table in which offsets are stored for each filter to correct camera focus. The filter substrates were fabricated and the filter coatings applied by Barr Associates, Inc.,[26] and Custom Scientific.[27]

7.5. Electromechanical Components

When possible, we used commercial motion-control stages for the subsystems of IMACS, including the slit-mask server and filter servers. However, most of the electromechanical systems of IMACS required the custom combination of off-the-shelf actuators and encoders, including the principal and Shack-Hartmann guiders, which travel on curved paths around the science field. Standard THK America, Inc.,[28] rails were available for the required radius of curvature, but the drive required a prototype high-capacity sprocket-and-chain drive that is relatively compact. The disperser server uses a novel combination of four clamps modeled on automobile convertible-top-style latches to grab, pull, and secure heavy grating and grism units on to the optics support structure.

IMACS mechanical devices use a combination of air actuators, stepper motors, and linear motors (for the f/2 and f/4 camera shutters). Air actuators were used when only discrete motions were required, for example, translation between two positions defined by mechanical stops or electrical hard limits, for example, the insertion stages for the mask and filter servers. Continuous or multiposition devices, such as the motion of guider stages, rely on commercial stepper-motor controller units. In our typical application, at the end of travel are two switches that are wired into the device controller. Tripping the first, the soft limit, terminates forward motion, but allows reverse motion to be initiated by software control. Tripping the second, the hard limit, sends a signal to the controller that shuts off power to the drive motor and requires a manual reset on the IMACS electronics rack (on the Nasmyth platform) for continued operation or testing. The soft limit switches are magnetic proximity sensors, while the hard limits are electromechanical microswitches. In the following discussion the term hard stop is reserved for an actual physical stop that prevents motion at the end of travel.

7.5.1. The IMACS Guiders

Unlike the standard guide cameras on Magellan, where a two-camera system is mounted between an instrument and a port rotator, IMACS provides its own internal guide-camera system consisting of three individual camera systems. Each camera is assembled on its own base plate that is, in turn, mounted to the IMACS front-structure disk. The CCD cameras are separable

[24] See http://www.spectrumthinfilms.com.
[25] See http://www.quantumcoating.com.
[26] See http://www.barrassociates.com.
[27] See http://www.customscientific.com.
[28] See http://www.thk.com/us.

from the guider assemblies and can be removed from the instrument without affecting the operation or alignment of the others. This proved to be a useful feature during the test, integration, shipping, and commissioning phases of IMACS, and it continues to be a beneficial feature in operation.

The IMACS guide-camera assemblies were designed to be stiff structures that present pickoff mirrors and their associated optics in the beam to known (encoded) locations in the telescope field of view, at the telescope/instrument focal surface of the west Nasmyth port. The three systems have similar optical trains and they share an electromechanical design philosophy and hardware, as described previously. For direct imaging of the sky (as opposed to the imaging of the Shack-Hartmann multilenslet array), a field of $105'' \times 105''$ is accessed by each camera, at a scale of $\approx 0.20''$ per rebinned pixel.

The CCD camera for each guider is positioned on an optical bench using a three-point set of dowel pins, assuring high repeatability when a camera needs to be removed and reinstalled. The camera is secured with cammed cleat screws to ensure that the mating surfaces are flush and square. Cooling lines employ quick-disconnect fittings at the camera head and guider-unit bulkheads. Power and data lines—also with connections at the camera head and unit bulkhead—run through a cable chain to allow for proper cable play during camera moves and instrument rotations.

High-resolution five-phase DC stepper motors drive and brake all of the motions of the cameras. The motor brakes are engaged with the power off, allowing the motor to be switched off when a desired position is reached, thereby minimizing heat generation in the forward compartment. Renishaw RGH24 Series linear encoders are used to provide precise position feedback at the level of 5 μm. End-of-travel limits are detected using magnetically tripped SUNX GXL Series proximity sensors. In case of proximity sensor failure, subminiature electromechanical switches (Honeywell SM Series) located slightly past the proximity sensors will kill power to the drive motor—these are the soft limits and hard limits described in § 7.5.

The unique details and capabilities of each guider are described next.

7.5.1.1. The Center-Field Guide Camera

The center-field guide camera (CFGC) uses a stiff truss-type structure that, when fully deployed into the beam, is cantilevered from four bearing blocks; two blocks mounted in a THK KR3306B Series LM guide Actuator, two blocks on a THK HSR SeriesLM guide Rail. The rail and actuator are located against dowel pins whose mating holes were machined in one setup; this provides precise parallel alignment for smooth, continuous motion. The bearing blocks of the system are set as far apart as space constraints allow—they provide a wide base from which to cantilever the guider loads. This configuration sufficiently stiff to carry changing load conditions as the instrument rotates during telescope slewing, setting, and tracking. A photo of the forward section of IMACS showing the CFGC and principal guide camera (described subsequently), with engineering drawing of the CFGC, is shown in Figure 24.

Power to the linear actuator is provided by a Mycom PS569AM five-Phase DC Stepper motor with brake. As only three discrete positions are allowed for this camera, a linear encoder is not required. The two end-of-travel limits are set by electromechanical switches, and the intermediate position is reached by counting motor steps back from the in position. Magnetically tripped proximity sensors are used to verify these three positions. The center-field guide camera takes less than 30 s to move radially through its full range of motion.

The truss structure houses a standard Magellan guide camera, a pair of optical barrels, and a set of filters. When fully deployed—the center-field position—the flexure of the system measured at the pickoff mirrors holds to within ± 25 μm for a full instrument rotation. This performance was confirmed from both physical and optical measurements.

The two optical barrels—one for direct imaging, the other for Shack-Hartmann operation—can be changed at the operator's command, as can the filter slide. Both optical barrels are fixed to an extremely stiff Schneeberger NKL3-155 cross-roller linear table that is comfortably rated to handle the changing moment load. Its total run-out is approximately ± 3 μm over the full stroke. The filter assembly is affixed to a THK LS 1077 linear ball slide, as high stiffness and accuracy are not needed to locate the flat filter windows. Both slides are pneumatically actuated with Bimba ISO series air cylinders. Adjustable mechanical hard stops are used to properly locate the optics, and Bimba HSK series band-mounted solid-state Hall-effect sensors provide state feedback.

The direct-imaging barrel houses two achromatic field lenses, an Edmund Optics K45354 and an off-the-shelf Cannon EF50 lens group that allows for simple fine-focus adjustment. This may be required if the optical path length from the telescope focal surface and the guide-camera CCD changes, as sometimes occurs when the entire camera assembly is removed from the instrument, or if the CCD camera is changed. Although the fine focus requires manual adjustment, the process is relatively simple and done quickly. The pickoff mirror for this optical train is a polished square of aluminum into which a stepped slit, a crosshair, and a small circular aperture have been machined. These features allow for multiple viewing options, including quick and simple single-slit and direct standard star observations.

The Shack-Hartmann wavefront-sensing optical train houses an achromatic collimating lens, Edmund Optics K08057, and a small 9×9 lenslet array. These lenses are also fixed in off-the-shelf lens mounts. The pickoff mirror employed here is simply a small front surface mirror ellipse on a glass substrate; the ellipse is sized to act as an aperture stop. With this design most unwanted light passes through the glass without reflecting up to the CCD.

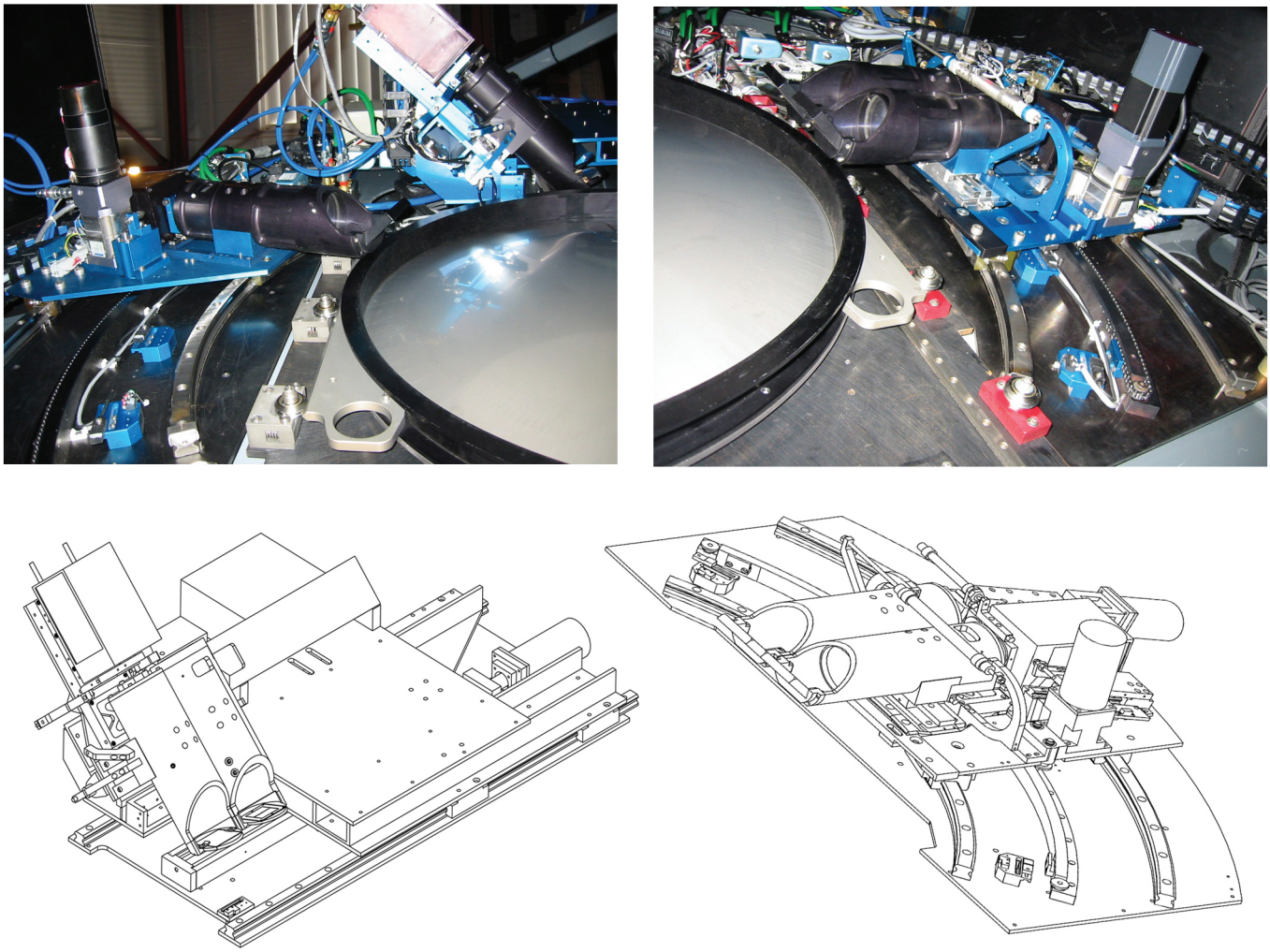

FIG. 24.—The three IMACS guiders. *Left*: Principal guider and center-field guider (*background*), with illustration beneath. *Right*: Shack-Hartmann guider, with illustration beneath. The components of have been rotated by 90° for clarity—the telescope beam, coming from the top in this orientation, is, of course, horizontal.

The filter stage assembly, located between the barrels and CCD, is a simple housing for two flat filter windows, one a neutral-density and the other a red filter that can be used to increase contrast against moonlight background. The filters are potted in off-the-shelf lens rings that mount in a larger housing.

7.5.1.2. The Off-Axis Guide Cameras

IMACS employs two similar off-axis guide cameras, referred to as the principal and Shack-Hartmann guide cameras (PGC and SHGC, respectively). These cameras sweep through an arc segment of approximately 40°. They are mounted at opposing locations at the edge of the field of view of the telescope plus ADC corrector, at a radius of 15′. The Shack-Hartmann guide camera also moves radially from 14.5′ to 16.0′ to allow for centering a star in the aperture of the Shack-Hartmann optical train.

The radial motion of the SHGC adds another complication, as the telescope focal surface is approximately spherical. The radial motion is linear and, therefore, set such that a line representing the center of the pickoff mirror cuts the focal surface twice as to keep the camera as close to focus as possible. Because the SHGC requires motion in two dimensions, extra attention to stiffness was necessary to ensure that total flexure would not be significant.

The PGC and SHGC utilize curvilinear rails, THK HCK 25 series, to achieve high stiffness and smooth motion over the required range. The rail systems are sized to ensure adequate moment capacities; they provide an axial and radial run-out of ± 3 μm over the range of motion. As with the CFGC, careful alignment of the rails against pins was accomplished by machining the alignment holes in a single setup to ensure accurate, smooth motion. The dimensions of the selected rails and blocks also provide sufficient undercarriage space to allow

for convenient placement of the drive and encoder hardware. A photo and engineering drawing of the SHGC are shown in Figure 24.

Because the PGC operates with only one degree of freedom—azimuthal motion—a simple configuration of three bearing blocks provides a sufficient base. The blocks are set to form a wide triangular base to which a base plate is fixed. This plate, in turn, holds the optical bench, drive system, and motion encoder. Overall, the motion and mechanics for the SHGC are more complicated and required four blocks. In fact, the pickoff mirror of this system must drop below the plane defined by the top of the blocks. As such a U-shaped plate, with a block in each corner, forms the base plate to which the radial motion system, drive, and encoder hardware are mounted. The decision not to replicate the SHGC design for both guiders was motivated by the desire to have a simple, short load path for the principal guider, in order to guarantee negligible flexure between the IMACS focal surface and the guide-camera focus. This choice was entirely justified in the subsequent operation of the system.

As with many of the other motion stages on IMACS, several systems are employed to detect position and control motion. Each camera has a discrete position sensing system of proximity sensors and mechanical trip switches to flag the physical end-of-motion limit. A high-resolution optical linear encoder is integral to the optomechanics as well. A linear encoder with a 5 μm step resolution allows for precise position control, as required to acquire and track target objects. To increase reliability and stability of the system, commands of less than three encoder pulses are withheld, equivalent to a 15 μm step at the pickoff mirror, or 1 pixel (0.2″) of image motion at the CCD camera. Again, for simplicity of design, the hardware described previously is the same as that employed by the center-field guider.

The prescribed curved motion is achieved through a sprocket-and-chain, an inexpensive and simple way to conform to the curvature while providing an accurate and solid physical drive system. This direct drive system for both cameras provides ample resolution and torque for very fine positioning, and it easily overcomes camera inertia. In fact, a motion of as small as ± 10 μm can theoretically be achieved, although only moves three times that size are ever necessary. The pitch of the sprocket and size of the chain were selected to both exploit the resolution of the drive motor and fit to the physical constraints imparted by the tight volume available, while taking flexure and backlash into consideration. A fully prestretched chain was selected to avert stretching over time by the considerable load. Neither chain stretch nor backlash have proved to be a problem, since we hold the unit at the proper position through feedback from an encoder. Nevertheless, increasing the stiffness and robustness of the system is considered desirable. We are presently considering replacing the current chain with a zero-backlash sprocket-and-chain system.

For both the PGC and SHGC, backlash in the main angular drive system (sprocket and chain) provided an interesting design challenge. Early on, a goal was set of holding either camera to within 25 μm of a commanded position. However, early testing of the system exhibited a motion of nearly 1 mm at the pickoff mirrors as the cameras were rotated about an axis perpendicular to their planar motion. This motion, greatly out of specifications, was primarily due to backlash, driven by the changing gravity vector. The problem was overcome with a software-based solution. The high-resolution linear encoder, polled at a frequency of 0.5 HZ, is used as input to a hunt-and-peck algorithm that corrects the guider position through added motor pulses. This proved to be sufficient to meet the position goal when tracking a field near zenith, which produces the fastest rate of instrument rotation at the Nasmyth focus.

The only function of the principal guide camera is guiding. As such this camera is equipped with a simple optical train consisting of a CCD camera, a filter slide, and a direct-imaging optical barrel including: a pickoff mirror, a field lens, and a Canon EF50 lens. For simplicity, these components are exactly the same as all other direct imaging trains on the other two guider cameras. The barrel is referenced to and fixed on the main optical bench and located to present the pickoff mirror at the edge of the field, centered at a radius of 15′, as discussed previously. The CCD camera and filter assembly are the same as those of the CFGC. The mounting schemes are the same here as well. Overall flexure of the system is held to less then 25 μm for a full instrument rotation.

The design and function of the optical hardware for the off-axis Shack-Hartmann guide camera are the same as that of the CFGC. The same mounting hardware is used and similar locating schemes are employed. This camera also has the addition of radial motion between 14.5′ and 16′. To accommodate this axis of motion the main optical platform is mounted onto the main assembly base plate with a combination of short linear rails and a linear actuator. As with the angular motion, four blocks are separated as far as physical constraints allow, providing a rigid mounting configuration. The added complexity with its higher mass resulted in larger flexure of the structure for the SHGC, but it remained within the goal of under ± 25 μm through a full instrument rotation. The combination of linear encoders and high-resolution DC stepper motors provide accurate and repeatable positioning, ± 3 μm per step. The full range of radial motion is traversed in less then 30 s.

7.5.2. The Mask Server

The IMACS mask server system (MSS) is a jukebox-style mechanism designed to house, transfer, and locate slit masks and a complement of other focal-plane masks and devices at the telescope/instrument focal surface. The jukebox-style design was a functional choice, driven primarily by the large field area provided by the telescope, which made the use of a typical wheel-style changer infeasible. The jukebox-style design is by nature compact; it makes efficient use of the limited volume available for this system.

The primary function of the MSS is to insert masks for multi-object spectroscopy into the telescope beam from the ADC/corrector that feeds IMACS. slitmasks start as 0.010 inch stainless steel sheets cut to 668 mm (26.3 inch) diameter circles. These are hydroformed to approximate the radius of curvature (1492 mm) of the focal surface of the telescope; the process leaves a flat flange of 21 mm that is used to clamp the mask into a slit-mask frame. The shape of the formed slit mask matches the telescope focal surface to better than a millimeter, which means that there are at worst slight focus variations over the field, but some significant position offsets (see § 6.3). All features cut into a mask—not only the slits and star-alignment boxes but also mounting slots and clearance holes—are done with a Convergent Prima Gemini laser system with a Coherent, Inc., 50 W CO_2 laser. There are slight ripples at the mask edge from the forming process that sometimes confuse the autofocus function of the laser, which requires an operator restart to continue the cutting process.

A slit-mask assembly consists of a flanged hoop and two thin wings mounted on the hoop 180° from each other. The slit mask itself is centered and clocked in the ring against dowel pins and clamped down to the flange of the ring. The wings provide the interface between the v-groove rollers (described subsequently) and the ring, and they provide multiple hard points, mounting for sensor magnets, a cutout with which a clamp engages (upper wing) and a key profile for the insertion device (lower wing).

Figure 25 shows the mask server assembly in the design development phase. The MSS consists of two main subassemblies, the base, insertion, and clamp subassembly, and the cassette and motion stage subassembly.

The base, insertion, and clamp subassembly provides: the mounting plate interface, which mates to a machined surface on the instrument FOSS disk; the v-groove rollers that guide and locate masks to-and-from the in-beam position; the mounting (and location) for a pneumatic linear actuator that moves masks between the cassette box and the beam; and the mounting location for the mask clamp mechanism.

The main component of the base subassembly is a steel rectangular base plate approximately 31×36 inches. The base plate was shimmed and pinned to the machined mounting surface on the FOSS after being precisely located to ensure that a slit mask would be on-axis with the instrument rotation axis and the mosaic CCD detector. This positioning was accomplished with an autocollimating telescope mounted along the optical axis as far forward as possible and sighting in a wire crosshair fixed at the vertex of the primary instrument focal surface.

Figure 26 shows a photo and engineering drawing of the MSS. The base plate is populated with 10 v-groove-style rollers in two parallel lines that guide a slit-mask assembly from the cassette, where they are stored to the active position. A long-stroke pneumatic cylinder draws the slit-mask assembly into the beam, locating it against three hard points—two fixed rollers on the bottom track and a button screw at the end of travel. State feedback for the pneumatic cylinder (open/closed) is provided by Hall-effect sensors mounted to the body of the actuator that are tripped by a magnet imbedded in the cylinder piston. In-beam confirmation of a slit-mask assembly is provided by a magnetic proximity sensor.

On the top track the last three rollers are spring-loaded to force the slit-mask assembly against the two fixed rollers of the bottom track. In both the bottom and top track the intermediate rollers have cams to adjust for close contact with the v-shaped edges of a wings of a slit-mask assembly. The two fixed rollers and button screw approximate a kinematic mount with three degrees of freedom, but the triangular configuration is a shallow one and forces are relatively high. A complicating issue is the fact that the slit-mask frames are neither identical nor perfectly round. The result is that, in operation, insertion of a slit mask assembly often led to a small gap (a few thousandths of an inch) at the hard points, which translated into a motion of the slit mask of fractions of an arcecond as the instrument rotated—a serious problem. Small gaps also made it difficult to reposition a slit-mask position to the desired accuracy of less than 0.2″. Larger gaps were found when inserting GISMO and the Durham IFU, units also carried by the slit-mask server that were developed after the initial design. These units proved to be too heavy to be held rigidly in position by the pneumatic cylinder and spring-loaded rollers.

For these reasons, an additional active holding force provided by a clamping mechanism was added in 2007 to ensure proper contact of the mask frame assembly to the hard points. The clamp mechanism is a latch-style device that engages a pocket cut into the mask frame once the mask is detected to be in position. This device pulls the unit up against an additional fixed hard point to ensure contact at any gravity angle. This clamp, acting with the pneumatic cylinder, is strong enough to compensate for the small differences of the different mask frame assemblies and to handle the much greater weights of GISMO and the IFU.

Shuttling a slit-mask assembly from the storage cassette into the beam is accomplished by an assembly that includes the pneumatic linear actuator, a linear guide rail and bearing block, and a key for grabbing a slit-mask assembly, as described subsequently. The key and linear actuator mount to the body, which is mounted, in turn, to the linear bearing block. The assembly is oriented parallel to, but above the lower row of v-groove rollers.

The stage and cassette subassembly completes the mask server system. This system can be further broken down again into three assemblies; the stage assembly, the cassette assembly, and the latch assembly.

The motion stage is the base of this subsystem. It is a Daedal linear motion stage comprised of a large table mounted on two linear rails fitted with two bearing blocks each. The table is driven by a DC stepper motor and a ballscrew. This component is extremely rigid and robust, substantially overrated for moving the required loads. The stroke of the stage is limited

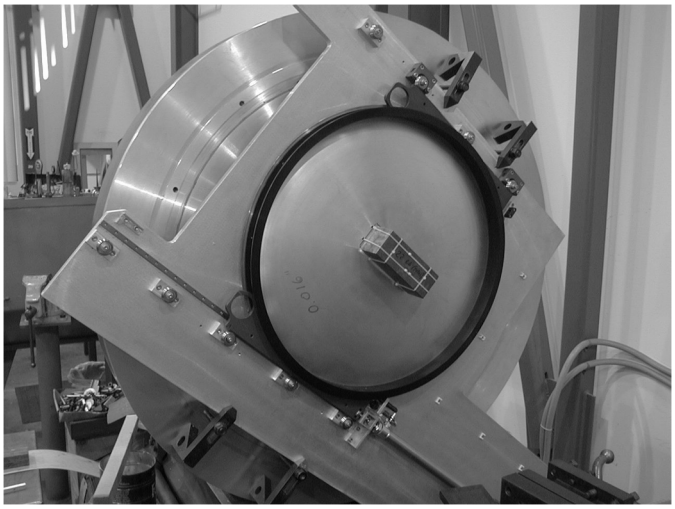

FIG. 25.—Mask server, early in the design development phase. The mask assembly consists of a C-channel hoop that holds the mask and two opposing wings that attach to the hoop. The beveled straight edge on each wing engages with the V-roller wheels to guide the mask assembly between the mask cassette and the in-beam position. In the lower half of the image, the air-cylinder insertion actuator and linear bearing guide are visible. This picture shows the testing of the mechanism under varying gravity orientations, using a gap bed lathe in the Carnegie shop to rotate the unit (this test was done prior to the assembly of the main structure and carriage). The large weight at the center of the mask simulated the estimated mass and center of gravity of the Durham IFU, which was much heavier than a single multislit-mask assembly.

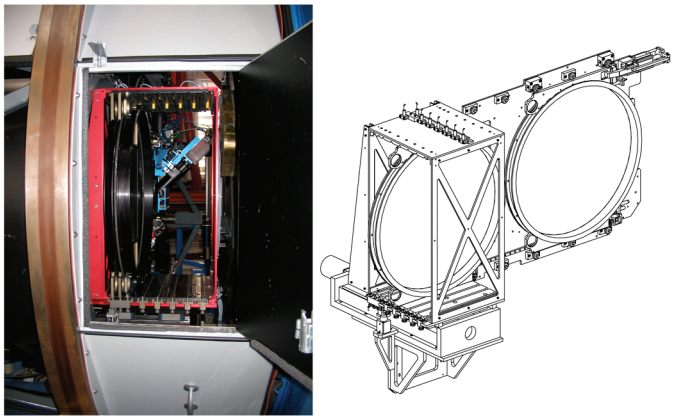

FIG. 26.—*Left*: The MSS installed in the IMACS forward compartment, as it is seen (but through a door in one of the enclosure panels) when a mask is about to be loaded. *Right*: Engineering drawing of the complete assembly, showing the pneumatically activated insertion system that loads one mask into the telescope focal surface, just ahead of the IMACS field lens. The slit mask is pushed against a hard stop by a pneumatic actuator (*bottom*), and a clamp on top grabs the slit mask through a small pocket in the upper wing.

by electromechanical microswitches wired in a fail-safe configuration such that power to the circuit is cut if a normally closed switch is tripped or the circuit is somehow broken, for example, a continuity break. The stage is equipped with an optical linear encoder with high accuracy and repeatability, essential requirements for correct, trouble-free operation of the stage. The stage mounts to a trussed frame that is fixed to the FOSS disk. Its motion is parallel to the optical axis and therefore always perpendicular to the gravity vector.

The cassette is a four-sided open-frame box that is fixed to the stage table. It is outfitted on its inside top and bottom faces with Delrin slide plates into which eight v-groove slots are machined. These groove pairs (one each on the top and bottom plates) provide six positions for stowing multislit masks supplied by the IMACS user. The remaining two slots are dedicated to baffles, one that defines the f/4 field. and another for using the center-field guider in slit-viewing mode. Population of the cassette box is monitored via magnetic proximity sensors (occupied/open), using small magnetically permeable tabs that have been epoxied the mask frames.

The slots are oriented parallel to the v-groove rollers: that is, perpendicular to the optical axis and the axis of stage motion. Each slit mask or baffle is held in place with a latch pin that is spring-loaded in the closed position. The pins hold slit-mask assemblies and baffles in the cassette as the instrument rotates. The latch pin must be retracted in order to allow the insert mechanism to move a mask, baffle, or device from the cassette into the beam, but only after the key at the end of the pneumatic actuator engages the keyway in the top wing. A simple two-position air cylinder retracts the latch pin to release a mask assembly from its stowed location. The latch assembly is fixed to the stage mount, but a keyway is mounted to the air cylinder, which allows the knob on each pin to pass through as the cassette moves to a selected position. The state feedback (open/closed) for this air cylinder provided by Hall-effect sensors.

To transfer a slit-mask assembly from the cassette, the cassette is moved so that the keyway in a mask frame aligns with the grab key of the insertion actuator. Table stiffness and encoder accuracy makes this a precise and repeatable action. The latch is toggled to the open position to unlock the mask from the cassette. The pneumatic linear actuator pulls the slit mask from the box along the v grooves and then onto the roller-defined tracks into the beam. Once the mask is detected to be in position the mask clamp is activated, firmly latching the slit-mask assembly against the hard points that define the in-beam location.

Due to the nature of the multicomponent system, proper alignment of the individually mounted subassemblies turned out to be a challenge. Early in instrument commissioning, slight misalignment of these components resulted in mask insertion malfunctions that were not recoverable from control room commands. These misalignments were found to be the result of small rotations and/or flexure between the various components with the changing gravity vector of instrument rotation.

Even though the instrument was exercised in a lab environment, it was not possible to test every configuration and operating condition. This was especially true for the Durham IFU and for GISMO, which was first installed in IMACS at

the telescope. Once flexure issues were better understood, a systematic approach to achieving and holding proper alignment was developed, including deriving an order in which alignment processes are carried out. In time we were able to improve reliability to the point that intervals of trouble-free operation are measured in months or years.

7.5.3. The Filter Servers

Like the mask server system, the IMACS filter server system (FSS) is a jukebox-style mechanism, similar in both design and function. The purpose of the FSS is to house, transfer, and position filters in the beam at a location just before the last optical element of the camera. There are two identical units, one for each optical channel.

The cassette-style design is a natural complement and extension of the MSS design. In fact, these mechanisms were designed in tandem and share many common features and functions. The cassette server-style design was a functional choice, driven primarily by desire to provide the user with large complement of filters (15 for each channel) during a night. Because of size of the IMACS filters (165 mm $\times$ 165 mm) the customary filter wheel design was not feasible for such a large filter complement.

The FSS is a multicomponent device comprised of three main subassemblies; the cassette and stage subassembly (which includes the filter assemblies), the insertion arm assembly, and a rail assembly.

The stage is the base of the main subsystem. It is an off-the-shelf linear motion stage assembly (Parker Daedal linear positioning stage, 4060400XR) comprised of a linear table element mounted on two linear rails that are fitted with two bearing blocks each. The table is driven with a ball lead screw and nut system powered by a NYDEN Mycom PS596AM five-phase DC stepper brake motor, running in half-step mode (0.36° or 1000 steps per revolution). This system is very rigid and robust; it is substantially overrated for moving the required loads. As with the guiders, the stroke of each filter server stage is limited by electromechanical microswitches wired in a fail-safe configuration such that power to the circuit is cut if a normally closed switch is tripped or the circuit is somehow broken, for example, a continuity break.

The stage is fitted with a linear encoder that is both accurate and repeatable to ± 1 μm. The combination of high-resolution encoder, stepper motor, and lead screw results in a step resolution of ± 10 μm per motor step; however, moves less then ± 30 μm are never executed. These are basic requirements for correct, trouble-free operation of the system.

Figure 27 shows a photo of one of the FSS and an engineering drawing.

For each optical channel the mechanical components of the filter server are mounted to the instrument itself—not directly to the camera barrels, except for the disconnected rail subassembly that carries the filter into the beam (upper left of the FSS drawing in Figure 27). In this way, the load path is such that potentially deforming forces of the stage mass are carried by the main instrument structure and not the barrels. This feature was considered essential to minimize flexure in the spectrograph. This requires that the stages for both cameras mount to beam members cantilevered from the MOSS box. The f/4 camera required an additional load bearing member to keep alignment issues between separated components in check.

Even with such preparations, great care and effort was required to ensure that the physically separate components of the FSS maintained alignment. Because the instrument rotates, the effective gravity vector seen by the hardware continually changes, causing very slight misalignments that—if alignments were not optimal—resulted in poor system performance at best (sticking) and, at worst, serious malfunction (jamming).

Like the mask cassette box of the MSS, the filter cassette box is an open-frame-style four-sided box that is fixed to the stage table. Slide plates, fabricated from Delrin, into which 15 v-groove-style slots are machined are fitted on the inside top and bottom faces, providing the positions to stow the filters in their aluminum mounting frames. The slots are oriented parallel to the rail assembly (which is perpendicular to the axis of stage motion). Filters are held in the box with magnets mounted in pivoting access latch arms, one at each position, and retained on the other (camera) side with a rail. The population configuration of the filter box is recorded in software but not actively monitored.

The rail subassembly is a lightweight rail system designed to carry filters from the cassette into the beam. The rail assembly employs both fixed and spring-loaded v-groove rollers, Bishop-Wisecarver Dual V-Roller W1SXX, assembled to a frame that penetrates a slot cut into the camera barrel. This assembly is the only component of the filter server system that is fixed directly to the camera barrel; that is, it is a separated (yet integral) component of the FSS.

Filter frame assemblies are the interface for the large filters, 165 mm $\times$ 165 mm, required in IMACS. The frame includes features machined into the aluminum body that mate with the v-groove rollers. Filters are potted into frames and a baffle is employed as a secondary restraint. A handle is integrated into the frame, as are locations for hard points, magnets, and a keyway. The magnets are used, in part, to hold a filter in place both either in the beam or in the cassette box. The keyway allows the cassette box to move laterally with respect to a key on the insertion assembly.

The insertion subassembly, comprised of a Bimba rodless linear slide, UGSM-1462, a THK RSR 12VM linear bearing, and a Bimba EM series air cylinder (EM-10-150-J), is the device that moves a filter between the cassette and beam. The linear slide is the base of the system and mounts to the MOSS box. The air cylinder is mounted in a bracket and fixed to the block of the pneumatic linear slide, and together they comprise the retractable extension arm that feeds a filter into the barrel via

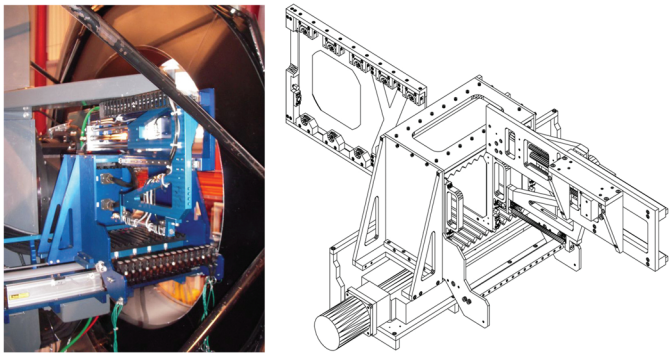

FIG. 27.—*Left*: The f/2 FSS installed in the IMACS aft compartment. The unit is accessible for installing filters (as shown) by removing at least two of the conical enclosure panels. *Right*: Engineering drawing of the complete assembly, showing the motion stage, the filter cassette box, the double-pneumatic-actuator insertion arm, and the system of guide wheels that carry a filter into the converging beam of the f/2 or f/4 camera.

the rail assembly. Magnetic reed switches are mounted on both pneumatic air devices and provide state feedback (filter in/out).

Inserting a filter is a simple process. The stage is moved to position the requested filter at the rail assembly so that the grooves in the box, filter and rail are all in-line. Next, the pneumatic actuators are activated and provide enough force to over come the holding force of the magnet, the spring-loaded rollers, and gravity. The filter frame assembly moves along the v-groove rollers and the hard point on the frame until forced against the hard point on the rail assembly. Filter changes are rapid and occur in less then 30 s. The system is robust and reliable and has been operating as expected.

One unexpected problem incurred by the use of so many strong rare earth magnets was that any extraneous metal, such as orphan screws or nuts, that comes near a filter server has a good chance of attaching to one of the magnets, either on the filter frame or on the rail assembly in the camera barrel. This has resulted in some serious malfunctions because of the close tolerances of the device. We have found that in an instrument as complex as IMACS, the presence of loose fasteners is a frequent occurrence.

One interesting design aspect of note was the difficulties associated with proper assembly and alignment of the multicomponent systems that comprise the FSS. These problems are similar to those experienced with the MSS; however, the FSS assembly has the added complication that each component of the FSS system mounts to an unique base, which is, in turn, movable. In fact, during the infancy of the life of IMACS many of the aforementioned components were frequently moved as the instrument was worked on during the testing and commissioning phases of the project. The result of constant assembly/disassembly was that alignment stack-up errors, however slight, would sometimes result in performance issues for the FSS. The tricky part was that the system would flex slightly as the instrument rotated, so that misalignments were not always obvious nor immediately evident.

7.5.4. The Disperser Server

The disperser server system (DSS) is a turret/wheel-style device that houses and delivers one of many possible dispersing elements to the beam on request. The wheel has five positions that can be populated with a disperser or filter element. In addition, two positions are dedicated to direct imaging—an unpopulated open position for imaging with the f/2 camera and a permanently mounted fold mirror needed for imaging with the f/4 camera. The system is remarkably versatile and yet easily configurable for use of both the f/2 and f/4 channels during the same night. Changes between dispersing elements are simple and virtually transparent to the observer; a change takes less than 60 s.

In addition to standard grisms for the f/2 channel and gratings for the f/4, a holder is available to place a standard IMACS filter in the beam, which is important for narrowband filters that perform best in a nonconverging optical path. A recent project used another type of mounting to place a filter in front of a grism, in order to enable a special type of spectroscopic blind search limited to a narrow wavelength band. The desire to take this narrowband capability to even smaller bandpass led to the tunable filter (MMTF), a high performance Fabry-Perot that is unique on a 6 m or larger telescope. The echelle unit, MOE, allows for multiobject spectroscopy at high spectral resolution over the f/4 field of $15' \times 15'$—another unique capability. The broad range of options available to an observer, and the ability to configure the DSS to cover a wide range of programs, using both the f/2 and f/4 channels, was a design goal for IMACS that has many-times-over rewarded the great effort that was required in its design and construction—from a functional and operational perspective, the DSS is the heart of IMACS.

The DSS is comprised of three smaller subsystems; the wheel subassembly, the clamping subassembly, and the drive subassembly.

7.5.4.1. The Wheel

The large (52 inch diameter) wheel component of the system is fitted with seven positions that house the various dispersing devices and optical elements used with IMACS. A wheel this size is necessary to house the large diameter disperser units for the 6.5 inch collimated beam, which are both large (~15 inches) and heavy (up to 45 lb). The locations of the device positions on the wheel are such that the wheel is approximately balanced without the adding extra mass, which allows for great flexibility in populating the DSS. The residual imbalances are well within the capacity of the drive components.

The wheel is an aluminum weldment complete with a hub and chain groove; the wheel is reinforced with gussets to provide added lateral stiffness. Disperser assemblies are mounted

close to the edge of the wheel and their centers of mass are forward of the wheel itself. This wheel subassembly is fitted with a large, industrial-grade, preloaded precision ball bearing (Kaydon, MTO-210) that is mounted to a turret axle. The axle, in turn, is mounted and fixed to a machined surface on the MOSS disk. Because the mounting surface and attachment points were machined concurrently with other important mounting surfaces on the instrument, the initial location of important fiducials of the system are well known. Angular position feedback of the wheel is provided by a Renishaw RGH25 series linear encoder system with 5 μm resolution, with tape applied to the axle and head fixed to the wheel. This configuration provides ample resolution to allow for precise, accurate, and repeatable positioning of any of the devices. The linear encoder system is not absolute, therefore a homing procedure is required immediately after power-up. Utilizing a linear encoder on a curved surface proved to be difficult. Application of the tape to the axel and alignment and positioning of the read head to the wheel are all extremely sensitive variables. As such, several revisions of a read head mount were required to achieve a system that would function both properly and consistently.

Figure 28 shows a photo of one view of the DSS and an engineering drawing.

Each position on the wheel is equipped with a set of four mechanical switches, mounted on taper pin base blocks (discussed subsequently) and wired in series, employed to detect the presence of a device on the wheel. The wheel will not move unless the configuration of the wheel is as expected by the software.

7.5.4.2. Taper Pins and Blocks

Each dispersing device is fitted with four slide blocks that are used to fix the disperser unit to the wheel via a set of four tapered pins and springs. The pins are fixed to the wheel with the taper pointing axially away from the wheel, such that springs are necessary to hold the device on the pins. In essence, the tapered pins and blocks (blocks mounted on the dispersing units) form a planar bearing. When a requested device is rotated to the correct location for installation, a clamping system (detailed subsequently) engages with the unit and pulls the device off the wheel and on to the MOSS box. The clamping forces are enough to overcome the spring (return) forces and hold the device firmly in position.

The pins and blocks have tapered features that allow for the unit to become physically uncoupled from the wheel as it is moved to the final clamped position. This was considered of critical importance to minimizing flexure in the spectrograph. The greatest sensitivity in the optical train is for elements in the spectrograph beam, therefore, changing moments and stresses on gratings and grisms result in large, unpredictable motions of the spectrum on the detector. We designed the system to enable a disperser to be properly (and freely) clamped in place, with no loads passed from the wheel to the spectrograph. Designing a system that moved a sizable bulk and mass from the wheel to the MOSS box perpendicular to gravity was a significant challenge.

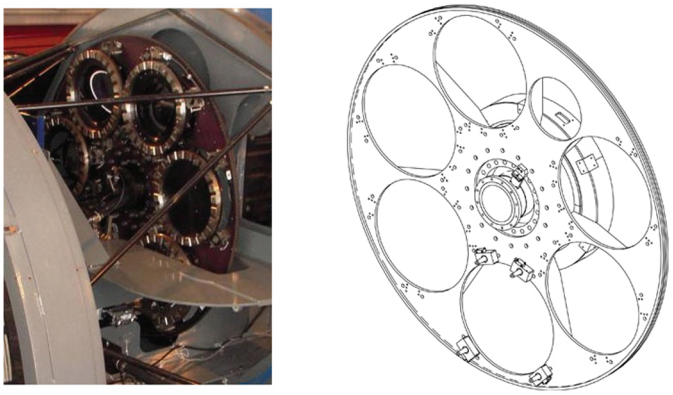

FIG. 28.—The DSS wheel that carries the gratings, grisms, filters, MOE, and MMTF. *Left*: The DSS wheel is seen loaded with disperser devices, which are seen from the back (the index rings); the optical elements face forward toward the telescope, to the right in this picture. *Right*: The engineering drawing shows the bare structure of the wheel, the central bearing, and the taper pins and blocks that allow the GTMs or other optical components in their cells to slide off the wheel and be captured by the index ring attached the MOSS, the spectrograph bench to which the collimator and f/2 and f/4 cameras are attached.

7.5.4.3. Clamping System

There are four clamps used to properly fix a dispersing unit in place during an observation. The clamps are located at approximately orthogonal positions, although two are offset slightly as required by hardware clearances.

Figure 29 shows a photo of one of the disperser server clamping system and solid models of the components. The clamps employed with the DSS were inspired from the design of an automobile convertible-roof–top latch. Basically, the unit is a simple two-position latch that is pneumatically actuated. The clamp latch is attached to an articulating arm, which is fixed to the end of the air-cylinder piston rod. The base of the assembly contains a slot for the clamp latch and two guideways for join and pivot pins. The guideways are cut with a profile that defines the motion of the clamp arm and sets the stroke limit of the actuator. State feedback of each clamp mechanism is provided by Hall-effect sensors mounted on the body of the air cylinder.

Once a dispersing unit is rotated into position the clamp mechanism is activated. The clamp latches move and engage with the base of the dispersing unit and pull with sufficient force to move the unit off the wheel, working against the spring load. The unit moves down the tapered pins until it engages with fingers that guide the unit into position. At this point mating index rings join together and properly constrain the device in all degrees of freedom. The tapered pins are a key component of properly returning the component to the disperser wheel.

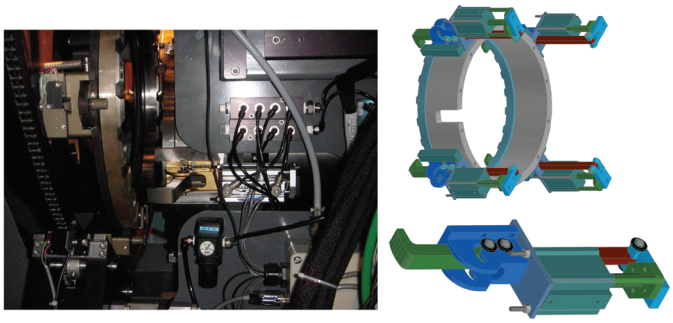

FIG. 29.—The clamping mechanism of the disperser server system. The photo shows, on the far left, the motor and drive train for the DSS wheel. Left of center, in the foreground, is an index ring mounted to the back of a GTM—this unit is one position off in rotation from the receiving ring in the pupil (*background*). One of the clamps is seen in the open receiving position. The solid models on the right show the detail of one clamp and the arrangements of all four clamps that allow IMACS to pull a disperser unit free of the DSS wheel and clamp it to the MOSS structure.

The most interesting component of the clamping system are the mating rings, which are a matched set of slightly modified index rings, fabricated from steel. These are manufactured by Matrix International (Scotland) for use in the heavy equipment industry. One ring is located and fixed to a machined surface on the MOSS box. Again, because this surface was fabricated with the other important mounting surfaces, the relative positions are well known, thereby providing a reliable mechanical fiducial. The other (mating) ring is mounted to the dispersing element or optical device, one for each unit.

Each ring has 12 flat teeth, and each set provides 24 mating flats (chamfered edges of the flat teeth). Essentially, these short, wide flats provide for an overconstrained mating of the ring pairs—this might normally be considered detrimental. However, due to the rotating nature of the instrument with its constantly changing mate-up orientations, overconstraint proves to be very helpful, specifically, because the mating procedure can happen at any rotational orientation of the instrument and because the units do not always move from the wheel to the fixed mating ring along the axis of the rings. It was thought that because the heavy units move in this way, a truly three-point kinematic system might not provide highly repeatable performance or, worse, there might be physical situations where proper clamping might not occur at all. Regardless, the mating performance of the index rings has proven successful: clamping has been measured to repeat to the level of ~10 pixels (for gratings; much better for grisms), even when a device has been removed from the active position, the instrument rotated to a different gravity angle, and the device reinserted back into the beam.

7.5.4.4. Drive System

The disperser wheel is driven by a chain drive system. A chain sits in a groove wrapped around the circumference of the wheel and runs through the motor subassembly, which is mounted on a wing of the MOSS box. The motor subassembly consists of a Mycom PS569AM high-torque five-phase DC stepper motor with brake, two idler gears, a chain tensioning device, rotation-limit hardstops and proximity sensor mounting points. Large metal chain clasps are mounted in the groove on the wheel to serve as chain blocks, physical hard stops, and trips for the proximity sensors. The brake on the motor is on when powered off for safety purposes; i.e., the brake is engaged if the system loses power. As many of the elements and devices mounted on the disperser server themselves require power, the rotation of the wheel is limited to approximately 355°, allowing for a relatively simple cabling solution.

7.5.4.5. Dispersing Units and Optical Devices

The full complement of devices that can be used with IMACS include: for use with the f/2 camera—grisms, prisms, filters, and a tunable filter (MMTF); for the f/4 camera—fold mirror, reflection gratings with adjustable tilt angle (discussed subsequently), and an echelle unit (MOE).

7.5.4.6. The Grating Tilt Mechanisms

The grating tilt mechanisms (GTMs) allow for absolutely rigid support of a grating during instrument rotation and also have the important feature of tilting a grating through its full operating range, remotely commanded from the IMACS control computer. Furthermore, grating angles are preserved during mounting and dismounting of a GTM from the disperser wheel, allowing the observer to retain setups while changing observations to another disperser or different device. There are four working tilt mechanisms available, into which any grating can be mounted. However, because GTMs require power, and power is only provided to three positions on the DSS wheel, a maximum of three GTMs can be installed at any one time.

IMACS uses reflecting gratings from Richardson Gratings (Newport Corporation[29]). These are standard rulings from the catalog that have been replicated onto 205 mm × 165 mm × 35 mm substrates. The gratings are mounted quasi-kinematically into aluminum cells that are, in turn, mounted on the tiltable yoke of the mechanism using precise position-locating buttons and bushings. The yoke is fitted with a pair of SKF Group[30] angular contact bearings on either side. The bearings are pressed into mechanically stiff uprights that are fixed to the mechanism base plate. The high-precision angular contact bearings are situated in a face-to-face configuration and are preloaded when properly mounted, providing a very solid, precise axis through which the yoke pivots.

The tilt drive is a steel cable and capstan system, where a cable is fixed to an arc mounted on the yoke, and the capstan

[29] See http://gratings.newport.com/home.asp.
[30] See http://www.skf.com.

is fixed to the output shaft of a Mycom 20:1 cycloidal ball reducer, which is driven by a Mycom PS566 five-phase DC stepper motor with a 1000-step-per-revolution (half-step mode) resolution. Both the cable arc and capstan are fabricated from titanium. The custom drive cable is fabricated from a high-tension prestretched steel aircraft cable; it does not require any tensioning device. This cable-drive approach has the great advantage of being backlash-free (without requiring an external brake)—this is an essential property of a good grating tilt mechanism that makes the angle settings of the GTM reproducible to $\lesssim 0.002°$, equivalent to a few pixels on the detector (typically 1–2 Å).

Figure 30 shows a photo of one of the GTMs and an engineering drawing.

Combined with a 1 μm resolution linear encoder, the step resolution of the device is less than 0.0001° per step; however, for practical purposes, the angular resolution of the tilt is approximately 0.002°. The allowable range of tilt angles is 19.5° through 34.5°. Although any grating can be installed into any GTM, one GTM has been modified to allow for a slightly higher amount of tilt, up to 35.5° to accommodate operation of the 1200 liters mm^{-1} grating in second order in the blue.

As previously mentioned, position feedback is provided by a linear encoder, a Renishaw RGH25 series linear encoder system with 1 μm resolution, with tape applied to a separate arc intended for the tape alone and the read head fixed to a bracket mounted to the unit base plate. This configuration provides ample resolution to allow for precise, accurate and repeatable positioning of any of the devices. Again, as the linear encoder system is not absolute, a homing procedure is required immediately after power-up. As with the DSS encoder system, utilizing a linear encoder on a curved surface proved to be difficult. Application of the tape to the arc and alignment and positioning of the read head from the base to the arc are all extremely sensitive variables. As such, significant time was required to achieve a procedure that would result in a setup that would function both properly and consistently.

Proximity sensors serve as soft limits and electromechanical microswitches serve as hard limits, as described in § 7.5. As these sensors are normally closed, tilt adjustments are not possible if wires to these switches are shorted or cut.

The load path, from the grating through to the index ring, is as short as the mechanics allow. In fact, a physical hard stop is required to prevent the cell from being tilted into the first element of the f/2 camera. One of the most difficult yet most satisfying achievements of engineering IMACS came in achieving the extremely tight spec that grating flexure contribute less than a few pixels of image motion as IMACS rotates.

Accomplishing this goal was not a simple task. Preliminary image testing with original hardware provided confusing results and clearly showed that revisions to the GTM design or hardware would be necessary. Further investigations revealed that although the angular contact bearings performed as expected, the stiffness of both the originally designed yoke and uprights—the bearing pillow blocks—were insufficient to support the load when the grating was turned on its side, that is, when the bearing blocks were in line with the gravity vector (one above the other), despite use of finite element analysis. Further study and detailed investigation of the finite element analysis results revealed important flexure modes that led to revisions of both the yoke (adding material at strategic locations) and the uprights (adding to the footprint and adding gussets): both needed to bring the GTM performance to design specifications.

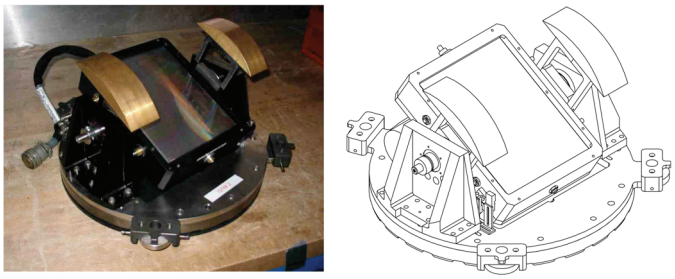

FIG. 30.—*Left*: The GTM is built on an index ring whose teeth mate with another ring firmly attached to the MOSS. Attached to the ring are the blocks, which slide on fixed taper pins. Also clearly visible in the picture are the brass counterweights, the yoke supports and bearings, and the grating itself. *Right*: The engineering drawing makes more obvious the proportions of the yoke supports that are key element of the remarkable stiffness of the unit. The cable-drive system and motor are behind the grating cell.

Since the entire flexure of the f/4 system is only 3×4 pixels at the detector for full rotation, it is difficult to know how much of this to attribute the GTM, but the fact that imaging with the f/4 fold mirror—a much lighter, stiffer structure without bearings—exhibits the same flexure suggests that the GTM's contribution is negligible.

Final adjustments for tilt and yaw are made by adjusting contact points of the grating in its cell (adjustable screws and spring-loaded contacts). The adjustment for roll had been accomplished by simply placing shims between the grating cell and grating itself. Utilizing hard plastic shims in this manner had proven unsatisfactory due to an unfortunate tendency for the shims to work their way out, be it from shake, vibration, or temperature cycling. The new shim scheme involves utilizing compliant rubber shim stock in place of the hard plastic material.

Although the GTMs are heavy and consequently cumbersome to install and remove from the wheel, the performance of this subsystem—indeed, of the entire disperser server—is among the most satisfying accomplishments of the IMACS project. The unprecedented versatility afforded by nearly instant access to many spectroscopic and imaging options is a principal reason for the considerable success of IMACS on Magellan.

7.5.5. The Shutters

The IMACS shutters are novel, relatively simple dual blade-style mechanisms designed to allow for highly uniform

exposures of the CCDs down to very short exposure times. The design goal for the IMACS shutters was a ~1% exposure linearity across the mosaic CCD array for a 1 s. exposure. The necessity of placing the shutter in a tight space close to the camera focus eliminated off-the-shelf solutions. Furthermore, as we were unable to find any commercially available product that shuttered an approximately 7×7 inch area, designing and building a custom shutter for IMACS was unavoidable.

An IMACS shutter is comprised of three subassemblies—the main body of the shutter and two motor assemblies. One motor/blade assembly is located at each end of the body, along the long axis of the shutter (perpendicular to the optical axis). Each shutter mounts to its camera through a slot in its camera barrel, located as close to focus as possible, just before the filter and dewar window.[31]

The design of the IMACS shutter started with an investigation of previous generations of blade-style shutters, which were often pneumatically actuated. The main problem with pneumatic-style shutters is that the blades are propelled across the aperture in a basically uncontrolled manner, which makes linearity of a short exposure almost impossible to achieve. Furthermore, these shutters were also prone to frequent mechanical failure, due to the shock of blade decelerations, and a tendency to exhibit different performance characteristics when used at considerably different temperatures.

Figure 31 shows a photo of one of the shutters in the design development phase.

The system is configured such that the blades run in a common channel/slot but move independently: one blade must be moved to open the shutter before the next blade can be moved to close it, which closes it. These blade motions are driven by Linmot P01-37 $\times$ 120 linear DC servo motors. They are not only powerful but also provide programmed, feedback-controlled velocity profiles that are both accurate and repeatable. In this application the motion profile is such that each blade edge (and hence the full blade) moves across the aperture with constant velocity for most of its stroke, bounded by smaller intervals of acceleration and deceleration. Very uniform exposures can be achieved by matching the full opening and closing profile so that each part of the detector is exposed for the same amount of time.

The choice of using linear electric motors was judged to offer distinct advantages over other options. Because of the smooth, controlled motion over the full length of travel, mechanical wear, malfunction, and other failure modes are all greatly reduced. This same feature of programmed motion-control was paramount in allowing the original design goal, ~1% exposure linearity in a one second exposure, to be easily met (something that was certainly out of reach with the basically uncontrolled motion of a pneumatically driven system). This performance was verified through flat-field tests of long and short exposures performed at the telescope.

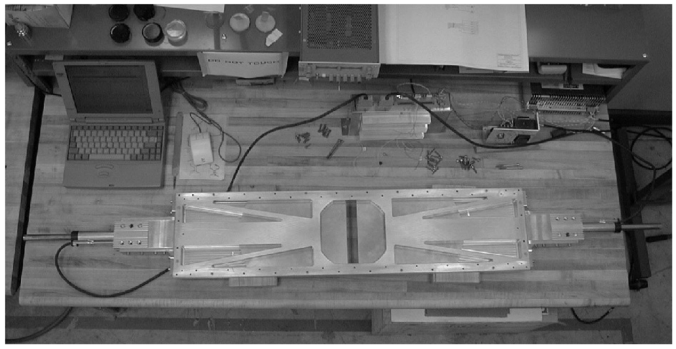

FIG. 31.—One of the two shutter assemblies during fabrication. The linear motors are seen extending to each side, each pushing or pulling a blade that can be seen in the center aperture. The web structure used for lightweighting is visible.

While using linear motors in the shutters was considered essential to achieve such performance characteristics; they did, however, present several interesting design challenges. First, the size of the linear motors selected for the speed and power required for a one second exposure with ~1% exposure linearity required that the motors be mounted to a solid body of significant thickness. This was not optimal given the tight space constraints at the mounting location (especially when considering the f/4 camera), and it also ran counter to our plan to avoid fixing any significant mass directly to the camera barrels. Although the final design for the shutters yielded a body that was large and heavy, approximately 30 lb, even after significant material removal for lightweighting, the mass does not seem to adversely affect image quality or image motion. The symmetric design—balanced across the camera barrels—certainly mitigates this problem.

Another issue of concern was heat generation and dissipation. The design of the linear motors requires that they be constantly powered up to hold a constant position; this results in the motor stator (which is essentially the outer body of the motor) becoming hot to the touch. To overcome this problem we embedded magnets in physical hardstops at the end of travel and in the slider/blade guide block to hold each blade in either the open or closed position. This allows the motors to be turned off after opening or moving the blades, greatly reducing the amount of heat released into the core of IMACS.

A further design issue that caused significant problems was misalignment sensitivity. Ideally, the slider of the linear motor should be allowed to float freely—unconstrained—through its full range of motion. This proved to be a difficult to achieve given the tight space constraints and the need to firmly affix the blade to the slider, which was accomplished through a guide block. The requirement to solidly attach the blade to the slider came from studying the problems of previous generations of

[31] Although the dewar window is separated from the optics in each camera barrel, the window has power, so it is—essentially—the final element in the f/2 and f/4 optical trains.

pneumatically actuated blade-style shutters. A common problem with these shutters was that screws used to fix the blade to the air-cylinder piston would work loose—likely due to the large shock forces attending sudden acceleration and deceleration. (The blade could actually shear off the exposed screw heads.) Our wish to avoid such problems led us to a solid attachment scheme and a well-controlled motion profile. However, the result of constraining the slider was that slight misalignments of attaching the linear motors to the body resulted in motor failure. Not only are the linear motors sensitive to position, they are sensitive to force feedback. Slight misalignments resulted in increased friction in the motion, causing current spikes, resulting in motion profile feedback errors that would cause the system to shut down. Modifications to the original mounting hardware, specifically ensuring proper squareness of the mounting hardware and parallelism of the slider and guide block to the guideway, has resulted in virtually trouble-free shutter operation. Another promising approach that was not explored would have involved a redesign of the slider/blade guide block to allow for some flexibility in noncritical degrees of freedom.

With these issues satisfied the performance of the shutters has been solid—they are now considered very successful mechanisms.

7.6. Motion-Control System

The motion-control system design philosophy was to use as many off-the-shelf items as possible and maintain a commonality of spares and experience with components currently used on both Magellan telescopes. The electronics control racks were physically placed outside of the instrument to remove them as a source of heat contamination. Two liquid-cooled heat exchangers are used to remove the heat generated by the electronics (about 700 W) to help equalize the internal temperature of the racks to the ambient temperature within the dome. Power and data signals are passed through a 35 ft long bundle of cables routed through a flexible IGUS cable chain. A single-point ground return was used throughout to prevent the occurrence of ground loops. It was found necessary to design and build a custom digital filter to eliminate false triggering of the hard limit.

Electronic components of the motion-control system include: 16 stepper motors; four linear motors; piezo transducers; air actuators; Renishaw encoders; and 272 digital optically isolated input/output lines. The latter are used to monitor soft and hard limits and in-position sensors, and for controlling brakes, calibration lamps, and air flow. A data-acquisition unit is used to monitor temperatures, voltages, coolant and air pressure. Motor control within the instrument is mostly done by a garden-variety single-board-computer running DOS on a 15-slot ISA backplane. The linear shutter motors and Physik Instrumente piezo stages have their own dedicated controllers.

The role of hard-limit microswitches is described in § 7.5. Custom-designed hard-limit logic boards are included in each chassis to shut down affected subsystems. Intervention by a technician or night assistant is required before resumption of normal operation. A digital filter was programmed to eliminate false triggering of the hard limits. Soft limit sensors are input directly into the MCS computer and the user GUI.

7.7. Control Firmware and Software

The IMACS control system is responsible for controlling the instrument. It constitutes the interface between the user and all IMACS-related hardware (science arrays, motion controllers, and sensors).

7.7.1. Design Philosophy

All code for the *IMACS* control system was written in C and runs under Linux (RedHat/Fedora), Solaris, and Mac OS-X (10.4–10.6). All graphical components make use of the X11 libraries without any third-party extensions to ensure high flexibility and compatibility over various platforms. The communication with all hardware components utilizes TCP/IP to serial converters; this allows any computer on the local network to control IMACS and avoids the need for special drivers.

The IMACS control system was designed from the top down. This allowed the coding of the user interface and high level control functions during the design and construction phases, during which there was only limited access to the actual hardware—the mask server, the filter servers, etc. IMACS software also can be run entirely, or in part, in simulator mode, by disabling individual components at startup of the software. This allowed for testing of the software before the actual hardware was built. It also allows the continuing operation of IMACS if a noncritical component fails, by restarting the software with that particular component in simulator mode.

The IMACS software modules (GUIs) store their status in a database. This database allows each module to retrieve status information about other modules, but keeps interfaces between modules as simple as possible. Communication between all IMACS control system modules is done over TCP/IP sockets. This allows for maximum flexibility and compatibility between operating systems.

Figure 32 shows an overview of the entire IMACS control system. The user interface runs on the Observer Workstation (Mac OS-X) in the control room. It communicates via ethernet (TCP/IP) with the hardware controllers in the electronics rack on the Nasmyth platform and two Linux computers in the utility room that are connected to the CCD controllers (DSP) via optical fibers.

7.7.2. Mechanical Control

The mechanical control GUIs follow a three tier design strategy: (1) testing individual components (construction);

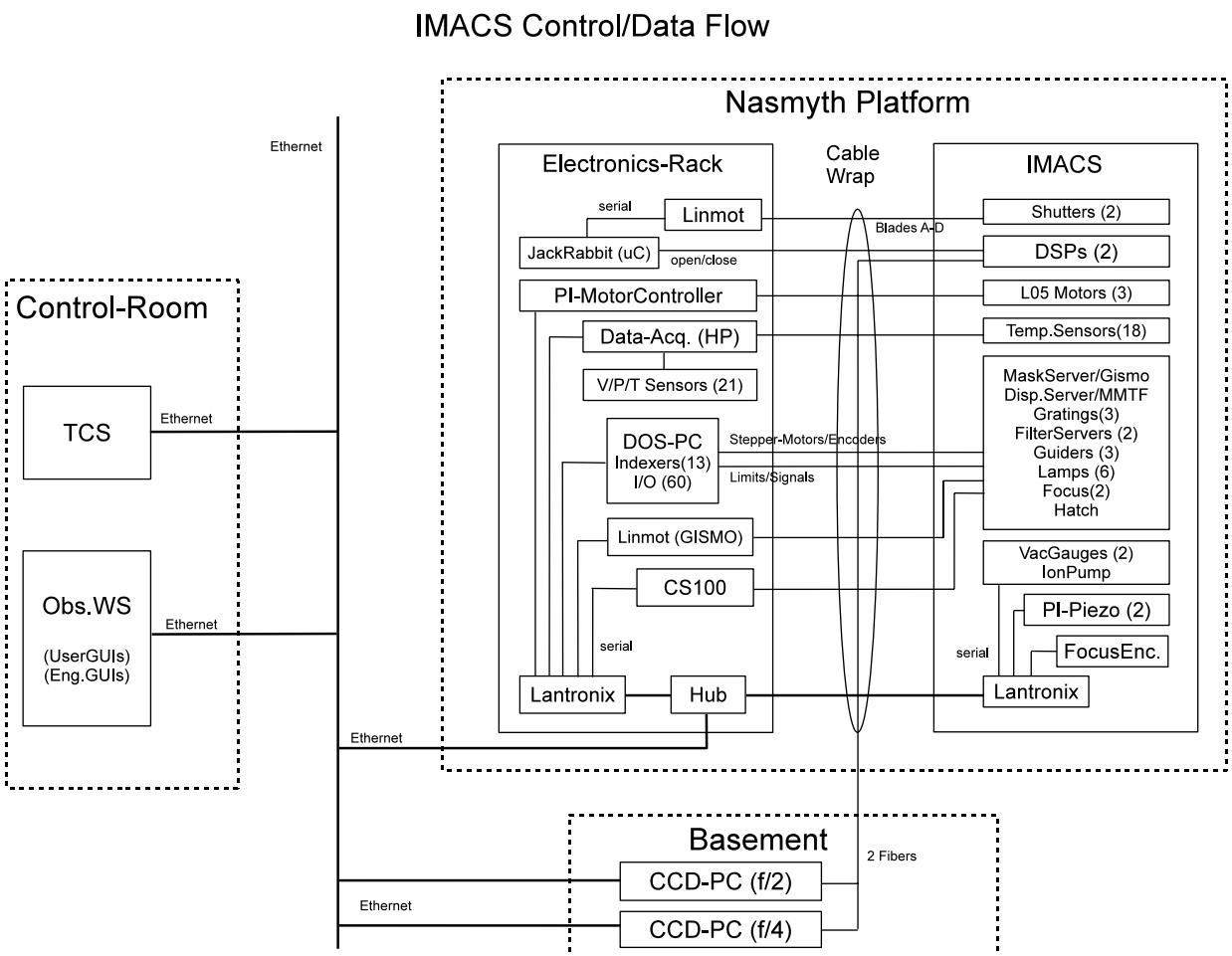

FIG. 32.—IMACS control diagram.

(2) integration testing (system troubleshooting); and (3) user level control (operation).

7.7.2.1. Individual Component Testing: Device GUIs

There is one GUI for each component (e.g., the mask server, shown in Fig. 33), that shows the component's status in complete detail. Every limit switch, position sensor, brake, etc., is displayed. The parameters are in native units, for example, numbers of motor steps, encoder pulses, and the states of limit switches. Movements are controlled by commanding a given number of steps, allowing them to be moved even without an encoder and independently of soft limits. Each air cylinder or actuator may be moved independently with only minimal checks for interference. These device GUIs were used during the construction phase of to test and verify the performance of each subcomponent. For maintenance and repair, they are used to recover from hardware failures where some part of a component is broken or a faulty sensor prohibits the higher-level software from moving that particular subcomponent.

Figure 33 shows an example of a device GUI, the one for the mask server.

7.7.2.2. Integration Testing: The EngGUI

The EngGUI shows the full range of IMACS hardware. It was used during construction phase to integrate components

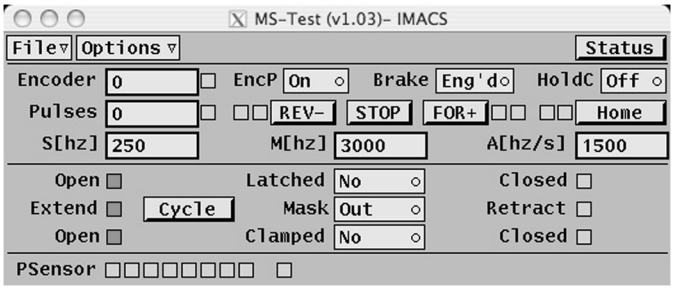

FIG. 33.—GUI used for testing the mask server at the level of individual components.

and perform engineering tests and is used at the telescope mostly as a troubleshooting tool. Because the detailed status of all subcomponents and sensors are displayed, the EngGUI is the normal place to start when there is an instrument malfunction. The EngGUI is shown in Figure 34.

Like the individual component control GUIs, the EngGUI displays the state of all sensors, but it differs from the individual component GUIs by allowing the user to engage different functions, for example, inserting a slit mask. In the case of binary operations, a simple command is sufficient, but with continuous motion devices, actions are initiated by entering a desired encoder position.

7.7.2.3. User-Level Control

The operator or observer interacts with IMACS through the IMACS GUI (shown earlier, see § 4). This GUI abstracts each component and hides all subcomponents (e.g., two air cylinders, motor, encoder, and position sensors of the filter server) into a single control element. This GUI is used by the astronomer to select the appropriate instrument status for the current observation.

7.7.3. Data Acquisition

The data-acquisition software consists of three programs. The ccdserver, running on the CCD-PC (see Fig. 32), controls the data-acquisition hardware (DSP) via a fiber optics interface that allows for rapid real-time data transfer. It buffers the CCD data until the user level software (CamGUI) copies it via a TCP/IP (ethernet) connection to the observer workstation. This program is invisible to the observer. The CamGUI (shown in § 4) is the interface for the observer, the place where the astronomer sets exposure parameters: exposure time, readout mode, etc. The CamGUI sends the exposure parameters to the ccdserver, initiates transfer of the CCD data into a buffer shared by the QuickLook Tool (shown in § 4) and eventually writes the data to disk as FITS files. The CamGUI has two separate parts, f/2 and f/4, for the two mosaic CCD cameras. The f/2-version has a scripting feature that enables sequences of images with the MMTF.

8. THE MOSAIC CCD CAMERAS

Each of the two IMACS detector systems consists of eight back-illuminated $2\mathrm{K} \times 4\mathrm{K}$ 15 μm pixel devices mounted as a 4×2 array on a single baseplate (see Fig. 35).

The original IMACS detector system used an array of SITe ST-002a devices. In 2007–2008, an array of E2V deep-depletion CCD48-84 was obtained through a 2006 NSF TSIP award. A second dewar, Mosaic-2, was constructed for this higher performance array. Since its completion in March 2008, Mosaic-2 has been dedicated to the f/2 focus, while Mosaic-1 has been dedicated to the f/4 focus. The original SITe devices had been chosen as part of a joint acquisition with

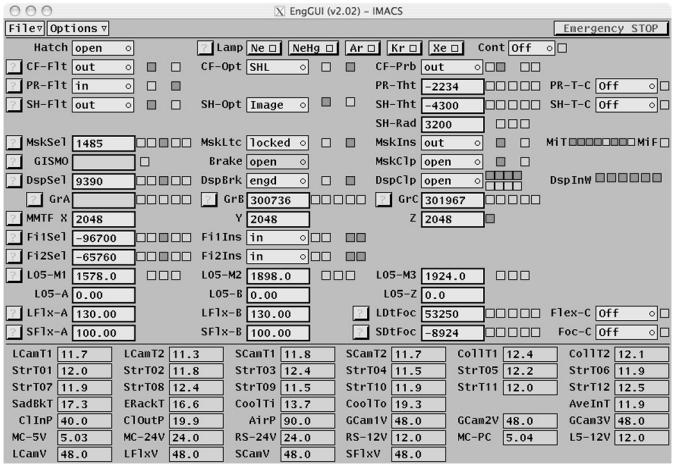

FIG. 34.—EngGUI shows the status of all subcomponents in detail. It is also used to command functions, for example, directing a stage to move to a desired encoder position In operation, the EngGUI is used as a first step to troubleshoot a malfunction.

NOAO and were among the best available at the time with high sensitivity and low read noise. The E2V detectors were chosen for their enhanced red sensitivity and very low read noise. As discussed in the preceding science examples, the E2V detectors have provided gains in sensitivity of 50–100%, compared with the SITe CCDs. In 2009 a second TSIP award was made to replace the original SITe detectors with E2V detectors, reusing the Mosaic-1 dewar and hardware to create Mosaic3, to be available in late 2011.

Except for the detectors, Mosaic-1 and Mosaic-2 use the same components and are almost the same mechanically. The primary difference is that the Mosaic-1 CCD array is flanked on two sides by 2680×512 pixel wing CCDs. These were provided as image motion sensors for a future, closed-loop flexure control system involving the internal piezo stage. In practice, flexure in IMACS proved to be very small and an open-loop control of the piezo stage worked more than well enough to correct it—the wing chips were not needed. They were not included in Mosaic-2. Figure 35 shows Mosaic-2 in the assembly phase.

The IMACS detectors are operated by a custom-designed set of CCD-controller electronics.[32] The BASE system for IMACS consists of an electronics box housing one DSP board, four dual-channel clock driver boards, four dual-channel signal processing boards, a power conversion board, and a backplane board. Four dual preamplifier boards reside inside the dewar. Read noise is limited by the detectors; readout speed is 10 μs pixel^{-1}. The mounting scheme for the detectors is another significant difference. The newer E2V detectors are delivered from the fabricator preflattened; that is, the detector packaging is customized at the factory to remove tip/tilt. Simply

[32] See http://obs.carnegiescience.edu/instrumentation/ccd/base/base.html.

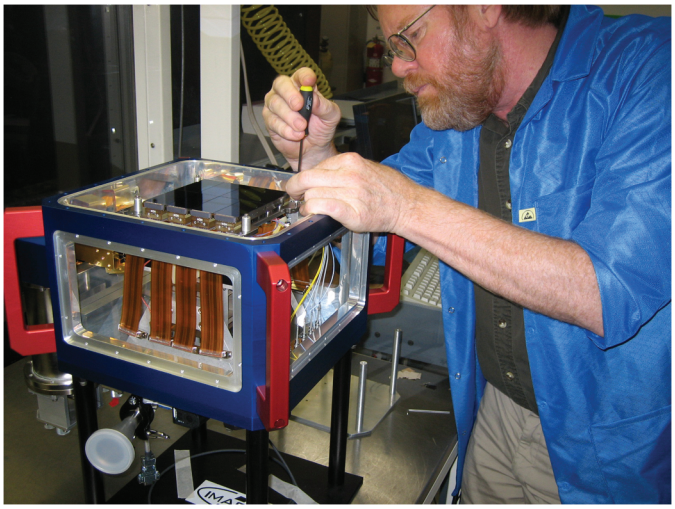

FIG. 35.—Ian Thompson and the Mosaic-2 camera in late assembly. The wiring harnesses for the eight CCDs are seen hanging down, disconnected from the side panels that carry signals out to the readout electronics. The mounting platen and mosaic CCD array are clearly visible at the top of the dewar.

fastening the detectors to a platen that had been machined and ground flat resulted in an array with all detector coplanar to ± 20 μm. The older SITe detectors were delivered with a built-in tip-tilt of up to ~ 100 μm, corner to corner. We flattened them by mounting each on a three-point support block, which we ground to remove the overall tilt, and set the CCD imaging surface at the same height for all devices. Mounting the blocks on a machined and ground platen produced an array with all detectors coplanar to ± 40 μm.

Inside the dewar, the CCD platen is supported by a G10 truss that is mounted on a Physik Instrumente (X,Y) piezo-actuated stage. The stage is specified for a ± 100 μm dynamic range at room temperature. It is used with an open-loop, lookup table scheme for flexure compensation. In practice, it was necessary to shield the stage from the cold CCD platen directly above it to prevent it from becoming too cold to operate properly. Even so, at a measured operating temperature of -20 C, the control electronics for Mosaic-1 needed to be carefully retuned to prevent the stage from oscillating. The stage is operated vertically with a constantly rotating gravity vector: both conditions are a nonstandard application for this device. The principle change required was to greatly decrease the bandwidth; corrections more rapid than 0.1 Hz are not needed in this application. Our experience with the second piezo stage for Mosaic-2 was even more difficult, as we could not find a consistent, stable set of hardware feedback settings that prevented occasional oscillations at some angles. In 2010 we decided to bypass the hardware control system provided by PI and use the stage in external-control mode, writing our own feedback loop into the software control. This appears to have completely eliminated the problem.

Each CCD array is housed in a vacuum vessel and cooled to cryogenic temperatures. Two Cryotiger closed-cycle coolers are mounted on the side of each dewar to cool the detector arrays. The cold ends of the CryoTiger systems are connected to the CCD platen using copper straps. Each of two cold heads are operated by its own compressor; these can be mounted up to 45 m away from the cold ends.

The original specs for the dewar allowed for the use of a large liquid nitrogen tank for cooling the chips. But due to the large size of the LN2 tank, the expected thermal loads, and the desire to minimize daytime maintenance, closed-cycle coolers were always considered the first choice. The CryoTiger systems use PT-13 gas. With no load, the cold head reaches approximately -160°C. With the fully loaded CCD mosaic, the two coolers bring the chips to -100°C in approximately 5 hr. The cold head temperatures stabilize at -150°C, while the temperatures of the eight CCDs stabilize between -110°C and -120°C, slightly different for each detector.

Obviously, a closed-loop refrigeration system offers many operational advantages over liquid nitrogen cooling. However, it was soon discovered that to prevent water/ice condensation in the cooling lines, the cold head should not be disconnected from the compressor until the compressor is switched off and the pressure has returned to its nominal value (or the head warms to room temperature). Our tests indicated that equalizing the pressure takes several hours; unfortunately, this operation was very common during the early years of IMACS when we had only the Mosaic-1 detector system. The necessity to move a single camera back and forth between and f/2 and f/4 was eliminated with the installation of Mosaic-2, so the contamination of cooling lines caused in this operation has been eliminated, and there is no half-day or more cycle of the system that must be undertaken on a regular basis.

Nevertheless, the system is not particularly robust: compressors need to be cycled back to the manufacture for service on an approximately yearly basis, and cryogen lines remain susceptible to ice plugs, even though the number of disconnects has been greatly reduced. As of 2010, these problems have been an unwanted complication, although manageable, and the time lost to observers is still measured in hours, but we continue to work on procedures in the hope of making the cryogenic system more trouble-free.

A more complete description of the Mosaic-1 detector system can be found in Bigelow et al.(2003).

9. LAB TESTING

9.1. Thermal Testing

As described previously, the nominal temperature range at Magellan extends from below freezing to above room temperature; we anticipated that IMACS might experience an even wider spread in temperature during shipping. To test both component survival and operational performance, thermal testing of

the assembled instrument was incorporated into the final integration phase in Pasadena. To create a thermal testing environment, we purchased a commercial Bally modular refrigerator with a large chiller unit capable of cooling the entire instrument mass and volume to -5°C. The enclosure was assembled in place around the instrument: the modules of interlocking wall and ceiling panels were set directly on the concrete slab floor of the OCIW instrument assembly lab. Figure 36 shows the freezer just after assembly in Pasadena.

Once the installation of the thermal enclosure was complete, the instrument was operated over the full range of expected temperatures, over all field rotation angles and possible rotation speeds. These tests used essentially final versions of the instrument control software and electronics. The instrument was slowly cooled to -5°C and back to room temperature through multiple cycles. In general, we found that the optical and electro/mechanical systems performed as designed throughout the temperature range, with a few important exceptions.

One unexpected problem was thickening of internal lubricants in some of the air-powered motion stages. Commercial air cylinders are typically delivered prelubricated with a light oil. In some cases, for the smallest air cylinders, we found that the normal shop air pressure (100 PSI) was insufficient to operate the cylinders at the lowest temperatures. In these cases, the air cylinders were removed from the instrument, the oil-based lubricants were cleaned out, and low-temperature compatible lubricants were applied. Lighter lubricants and slightly higher operating pressures fully restored the operation of the problematic actuators.

Another problem, immediately obvious in retrospect, was control of humidity inside the thermal enclosure. During cool-down, the chiller unit itself was sufficient to remove and vent the moisture from the air in the enclosure. Passage of people in and out of the cold chamber was minimized in order to limit additional moisture from human respiration and from air exchange through the door of the enclosure. However, in contrast to such careful procedures, the chiller unit (and its dehumidifier), was simply switched off during the first warm-up cycle instead of slowly bringing the chamber back to room temperature. A consequence of the rapid warm-up that ensued was that the high-heat-capacity optics remained well below the dew point, while the air and metal instrument structures returned much more quickly to room temperature. This thermal time lag in the optics led to a serious condensation event that damaged some of the water-sensitive antireflection coatings. After the initial condensation experience we added a standalone dehumidifier and used the chiller to slowly return the instrument to room temperature. If this refrigeration system were to be used again, a high-capacity dehumidifier would be added and warm-up cycles would be carefully controlled, to keep the instrument mass above the dew point temperature.

FIG. 36.—A commercial freezer enclosure was erected around IMACS for thermal testing in the lab in Pasadena. The Bally freezer came with a refrigeration unit with dehumidifier; an independent dehumidifier was added to keep humidity low during warm-up.

10. SHIPPING, INSTALLATION, AND OPERATION

The shipping plan for IMACS was presented at the final (preshipment) project review and, with few exceptions, was executed as described. The IMACS structure and subsystems were to be shipped, by trucks pulling air-ride trailers, from the Observatories facilities in Pasadena to the port of Long Beach, California. From Long Beach, the two shipping containers ($8' \times 8' \times 20'$ and $8' \times 10' \times 40'$) were to be loaded below deck on a container ship and then carried to the port of San Antonio, just west of Santiago, Chile. The final leg of the trip would again be via trucks with air-ride trailers, from the port at San Antonio, to the Magellan Observatory at Las Campanas. For the most part, IMACS project personnel were not allowed in the dock area during the loading of the containers and, in any case, the containers were scheduled to be unloaded and reloaded en route. After the fact, it was clear during unloading in San Antonio that the containers had been carried above deck (with potentially catastrophic consequences), indeed, near the top layer of exterior stacks of containers. Fortunately, in our case, there were no negative consequences of this breach of the transport contract.

Immediately following the preshipment review, the instrument was disassembled and broken down into shipping units organized by subassembly. Most parts of the instrument were wrapped in sealed plastic bags, packed into boxes, and loaded into foam-padded wooden crates. Desiccant packets were placed in the bags with the subsystems and then sealed inside the plastic liners. The main optical subassemblies (collimator, f/2 camera, and f/4 camera) were packed in standard-sized Hardigg blow-molded plastic shipping boxes with cut-to-fit foam liners. The water-tight and vented Hardigg cases were also packed with desiccant bags, then loaded together in a single wooden crate. The field lens was repacked in the original shipping crate provided by Cleveland Crystals. Additional wooden crates were built to fit the remaining subsystems in a variety of shapes and sizes. The four bottom corners of each crate were fitted with compliant plastic feet to provide additional shock absorption. The crates were then packed into the shipping

containers and secured to the floor, walls, and—in some cases—to each other.

Subsequent instrument shipments to Magellan have included logging accelerometers to measure shock loads throughout the shipping process. Expensive items are occasionally shipped with internal GPS tracking systems, to enable continuous world-wide location tracking of the crate. However, neither accelerometers or GPS trackers were used in the IMACS shipping containers. Inspections during unloading and unpacking at Magellan and subsequent reassembly of the instrument on the telescope revealed no transport (or other) damage to any IMACS parts or subsystems.

Immediately upon arrival of the IMACS shipping containers at the Magellan telescopes in 2003 August, the containers were unloaded and the instrument components stored at various locations at the observatory. The reassembly and installation process was carried out in an intense two week session, followed by a second one-week session to install the f/2 camera systems in 2003 September. Figure 37 shows the lifting of the IMACS main structure into the Magellan enclosure and subsequent positioning on the west Nasmyth platform.

The instrument carriage and structure were hoisted by crane directly through the dome slit and stored on the top-level dome floor. The remaining optics and motion stage crates were stored in the Magellan Auxiliary building, between the enclosures for Magellan-Baade and Magellan-Clay. The Mosaic-1 CCD detector system was reassembled in a clean room at the Astronomer's Support Building. The auxiliary building was used as the main staging area, where most of the subsystems were reassembled and checked for damage, prior to reinstallation on the instrument.

The initial installation steps were carried out in parallel. The IMACS subsystems were reassembled in the Auxiliary building, and the instrument carriage, structure, and electronics cabinets were installed on the Nasmyth platform. Installation of the instrument carriage required welding of bolting pads on to the floor of the Nasmyth platform. The entire Nasmyth platform was tented and the surrounding telescope systems (including the Nasmyth instrument rotator) were masked off and sealed to prevent contamination by grinding debris and welding fumes. Locations for the bolting pads were surveyed in place by the Observatory staff and then welded in. The pad locations were rechecked after welding, and then the instrument carriage was lifted from the floor and guided into position on the pads. Next, the IMACS main structure was hoisted into position above the carriage, before being carefully lowered on to the four carriage roller assemblies. Alignment fixtures on the Baade Nasmyth rotator and the IMACS MOSS were used with an autocollimator to align the IMACS rotational axis with the Baade Nasmyth axis. It was during this process that we discovered an assembly error between the MOSS and MOSS disk that caused the instrument optical axis to orbit the Nasmyth axis. In a difficult on-site repair, the MOSS, which had been pinned in place on the MOSS disk at Martinez & Turek, was unbolted and reshimmed in order to bring the instrument and telescope optical axes into concentric alignment. The carriage and structure in place, the large IGUS[33] utility wrap was attached to the fixed and rotating portions of the instrument, respectively.

FIG. 37.—*Left*: In 2003 August, IMACS is raised from a palette outside the Magellan enclosure by the dome crane and lifted through the dome slit. *Right*: IMACS is positioned on the west Nasmyth platform.

Once the structure was properly located with respect to the carriage and the telescope, reassembly of the instrument subsystems continued in a serial fashion, generally working from the center of the instrument outwards. The disperser server was installed on the MOSS first, followed by the collimator and f/4 camera. Once the camera was in place, the f/4 filter server, shutter, and mosaic detector system were mounted. At the front of the instrument, the field lens was installed first, followed by the mask server, the guider and wavefront sensor cameras, and the calibration sources. Once all the internal subsystems were in place, the front, center, and rear sets of enclosure panels were installed, completing the reassembly process.

An unfortunate consequence of the timing of the delivery of IMACS was that the ADC/corrector for the Baade telescope had not yet been completed. In fact, IMACS had to be commissioned and operated for almost a year before this crucial component arrived. This made commissioning the wide field of IMACS difficult, not only its performance as a wide-field imaging spectrograph, but also linking to the Magellan TCS through the onboard IMACS Shack-Hartmann and principal guiders (guiding and telescope active optics), which did not function well with the uncorrected, poor image quality far from the field center. Even after the delivery of the ADC/Corrector there continued to be problems with achieving the same high-quality imaging for the full IMACS field that had been accomplished in the smaller field instruments. By this point, of course, the commissioning team for the MagellanTelescopes had finished their work and were not available to trouble shoot the problem, which was instead attributed to some alignment or manufacturing problem in IMACS. It was almost two years before it was discovered that the ADC/corrector had been set improperly to feed the telescope beam to IMACS, with a ~1°

[33] See http://www.igus.com.

alignment error that delivered a badly tilted focal surface. Once remedied, the image quality and active optics functions improved to original expectations, except for smaller but still troublesome aberrations in the f/2 camera (discussed previously). In retrospect, the late arrival of the ADC/Corrector had prevented a thorough commissioning of the wide-field of the Nasmyth port by the Magellan Project Team, an important lesson, we think, for interfacing large wide-field instruments on large-aperture telescopes.

With the exception of this ADC/corrector issue, the work of the Magellan technical group—led for many years by site director Frank Perez—in the installation, commissioning, and maintenance of IMACS, was exceptional. The IMACS team is especially grateful to the staff at Las Campanas and at the Observatories headquarters in La Serena for their dedication and unfailing support since 2003. An instrument like IMACS simply cannot succeed without the contributions of many talented people beyond the instrument team.

The authors acknowledge the generous support of the Inamori Foundation, the National Science Foundation (NSF) Advanced Technologies and Instrumentation program through NSF grants AST-9618875 and AST-0352960, and the NSF Telescope System Instrumentation Program through a grant in 2006. Over the years, the following people have made major contributions to the construction, commissioning, and operation of the Inamori-Magellan Areal Camera (IMACS): Joe Asa, Tim Bond, Dave Carr, Jersson Castillo, Matt Johns, Vince Kowal, Jeanette Stone, Robert Storts, Joe Appels, and the Technical Support Group of the Magellan Observatories. The IMACS team also thanks Carnegie Observatories Director Wendy Freedman and Associate Director Mark Phillips and former Carnegie Institution President Maxine Singer for their crucial, unwavering support.

REFERENCES

Abraham, R. G., et al. 2004, AJ, 127, 2455
Allington-Smith, J. R., Murray, G. J., Content, R., Dodsworth, G. N., Davies, R., Miller, B. W., Jorgensen, I., Hook, I., et al. 2002, PASP, 114, 892
Bigelow, B. C., & Dressler, A. 2003, Proc. SPIE, 4841, 1727
Bigelow, B. C., Lupino, G. A., Burley, G. S., & Thompson, I. B. 2003, Proc. SPIE, 4841, 727
Bigelow, B. C., Dressler, A., Shectman, S. A., & Epps, H. W. 1998, Proc. SPIE, 3355, 225
Bolton, A. S., Burles, S., Koopmans, L. V. E., Treu, T., & Moustakas, L. A. 2006, ApJ, 638, 703
Dressler, A., Hare, T., Bigelow, B. C., & Osip, D. J. 2006, Proc. SPIE, 6269, 13
Epps, H. W., & Sutin, B. M. 2003, Proc. SPIE, 4841, 612
Glazebrook, C., & Bland-Hawthorn, J. 2001, PASP, 113, 197
Hook, I. M., Jargensen, I., Allington-Smith, J. R., Davies, R. L., Metcalfe, N., Murowinski, R. G., & Crampton, D. 2003, PASP, 110, 1216
Kelson, D. 2003, PASP, 115, 688
McDonald, M., Veilleux, S., Rupke, D. S. N., & Mushotzky, R. 2010, ApJ, 172, 1262
Osip, D. J., Phillips, M. M., Bernstein, R., Burley, G., Dressler, A., Elliot, J. L., Persson, E., Shectman, S. A., & Thompson, I. 2004, Proc. SPIE, 5492, 490
Papovich, C., et al. 2010, ApJ, 716, 1503
Schmoll, J., Dodsworth, G. N., Content, R., & Allington-Smith, J. R. 2004, Proc. SPIE, 5492, 624
Sutin, B. M., & McWilliam, A. 2003, Proc. SPIE, 4841, 1357
Veilleux, S., et al. 2010, AJ, 139, 145